INVESTIGATION OF THE IMBRICATED SYSTEM ALONG THE MUROTO TRANSECT AND ITS RELATIONSHIP TO THE SUBDUCTING MUROTO SEAMOUNT

A Thesis

Presented to

the Department of Earth and Atmospheric Sciences

University of Houston

In Partial Fulfillment

of the Requirements for the Degree

Master of Science

---

by

Kenan Yazan

May, 2014

INVESTIGATION OF THE IMBRICATED SYSTEM ALONG THE MUROTO TRANSECT AND ITS RELATIONSHIP TO THE SUBDUCTING MUROTO SEAMOUNT

Kenan Yazan

APPROVED:

Dr. John F. Casey, Chairman

Dr. Michael A. Murphy, Member

Dr. Pete Emmet, Member

Dean, College of Natural Sciences and Mathematics

Acknowledgements

I am very pleased to people who supported, and believed in me throughout my academic education at the University of Houston.

I would like to express my gratitude to my advisor, Dr. John F. Casey, for his valuable guidance during my research. Extended special thanks are given to committee members, Dr. Michael Murphy and Dr. Pete Emmet, for their worthwhile support to completion of this thesis.

I would like to show my appreciation to Alex Barnard, for his excellent help to complete the bathymetry of the Muroto Transect.

I would like to thank the Marine Geosciences Data System (MGDS) for their generous donation of the seismic and well log data. I would like to thank Turkish Petroleum Corporation (TPAO) for their financial support. I would like to thank my roommates, Sercan Pisen, Omer Akbas, Gokhan Alkir, and my classmates, Ozbil Yapar and Selin Deniz Akhun and to all my friends in the Department of Earth and Atmospheric Sciences at University of Houston for their friendship and positive criticism.

I wish to express my appreciation to my mother, Fatma Yazan, my father, Mehmet Yazan, my sister, Aysegul Curel, and all my family for their support.

Finally, I want to dedicate this thesis to my newborn nephew, Egemen, who was born before I finished my master's education in the United States.

INVESTIGATION OF THE IMBRICATED SYSTEM ALONG THE MUROTO TRANSECT AND ITS RELATIONSHIP TO THE SUBDUCTING MUROTO SEAMOUNT

An Abstract of a Thesis

Presented to

the Faculty of the Department of Earth and Atmospheric Sciences

University of Houston

In Partial Fulfillment

of the Requirements for the Degree

Master of Science

By

Kenan Yazan

May 2014

Abstract

This thesis investigates a series of seismic reflection lines across the Nankai Trough called the Muroto Transect. The 3D pre-stack depth-migrated data were acquired off Shikoku Island, Japan and covers the seaward portion of the Nankai Trough accretionary prism. Determination of shortening and implications of Coulomb Wedge Theory were evaluated.

The lines provides an opportunity to study deformation effects, structures, and extent of shortening of sediments being subducted-accreted to the hanging wall as well as along strike variations and influences of the subducting seamount deformation in the accretionary prism. Shortening was measured across 3 lines and was estimated to vary between 20 and 25.6 percent. The coulomb wedge taper varied from 3.4° and 3.9°. These values of taper show that the Nankai accretionary prism at the Muroto Transect lies on the weak décollement zone.

Based on the percentage of shortening amount in distance of three lines, the percentage of shortening in distance of the prism increase in the direction of southwest to northeast. The angle of surface slope and dip of décollement are determined for five lines. The tapers of the lines increase in the direction of southwest to northeast (3.4-3.9). The internal friction (μ) and internal effective friction (μ_{beff}) coefficients calculated decrease in the direction of southwest to northeast from 0.25 to 0.176 and 0.07 to 0.054 respectively.

Detailed investigation over the imbricate system of the Muroto Transect suggests that there is a little to no effects presented by the subducting Muroto Seamount. Based on the seismic interpretation, the contact between the seamount and the accretionary prism was illustrated below the interpreted subduction channel, and the imbricate thrust system detached to the décollement without any impact of the seamount in the down-going plate. Based on the result of structural restoration and Coulomb Wedge Theory, the present imbricate system has developed with no apparent inherited or lingering effect from the seamount subduction, as the seamount upper contact lie below the subduction channel as interpreted, and wedge strength indicates very little change from the interpreted transect along strike outside the zone of seamount subduction.

Table of Contents

List of Figures

List of Tables

Chapter 1: Introduction

1-1. Introduction

Because of seismic investigation, both the understanding of subduction zone evolution and the classification of the convergent margins have been advanced during the last three decades (Moore et al., 2001). In this study, I have investigated a three-dimensional seismic reflection volume that was acquired along the Muroto Transect of the Nankai subduction zone. The data were made available by Marine Geoscience Data System during the Ewing 9907/9908 cruise. The transect is located south of Shikoku Island (Fig. 1-1) (Moore et al., 2001). Historically, the Nankai Trough has been partly studied for 1300 years because this region has had many great earthquakes. Because of the scientific innovations in geophysics during the last century, the region has been investigated in detail. This is because large earthquakes, such as the 1944 Tonankai (M_w 8.1) and 1946 Nankaido (M_w 8.2) earthquakes, have occurred in the region (Ando, 1975).

The accretionary prism, along the Muroto Transect (Fig. 1-1), is divided into: 1) the undeformed Shikoku Basin and overlying trench fill in the Nankai Trough, 2) the proto-thrust zone, 3) the imbricate thrust zone, and 4) an out-of-sequence thrust zone based at the margin to the margin transition (Moore et al., 2001). The imbricate thrust zone involves a series of well-develop, landward-dipping imbricate thrusts. Imbricate thrust sheets are spaced several kilometers apart. The initial imbricate thrust system is marked at the frontal out-of-sequence thrust (Fig. 1-1). The out-of-sequence thrust zone includes many splay faults. Probably these thrust faults initially imbricated the thick sediment packages of the Shikoku basin (Moore et al., 2001).

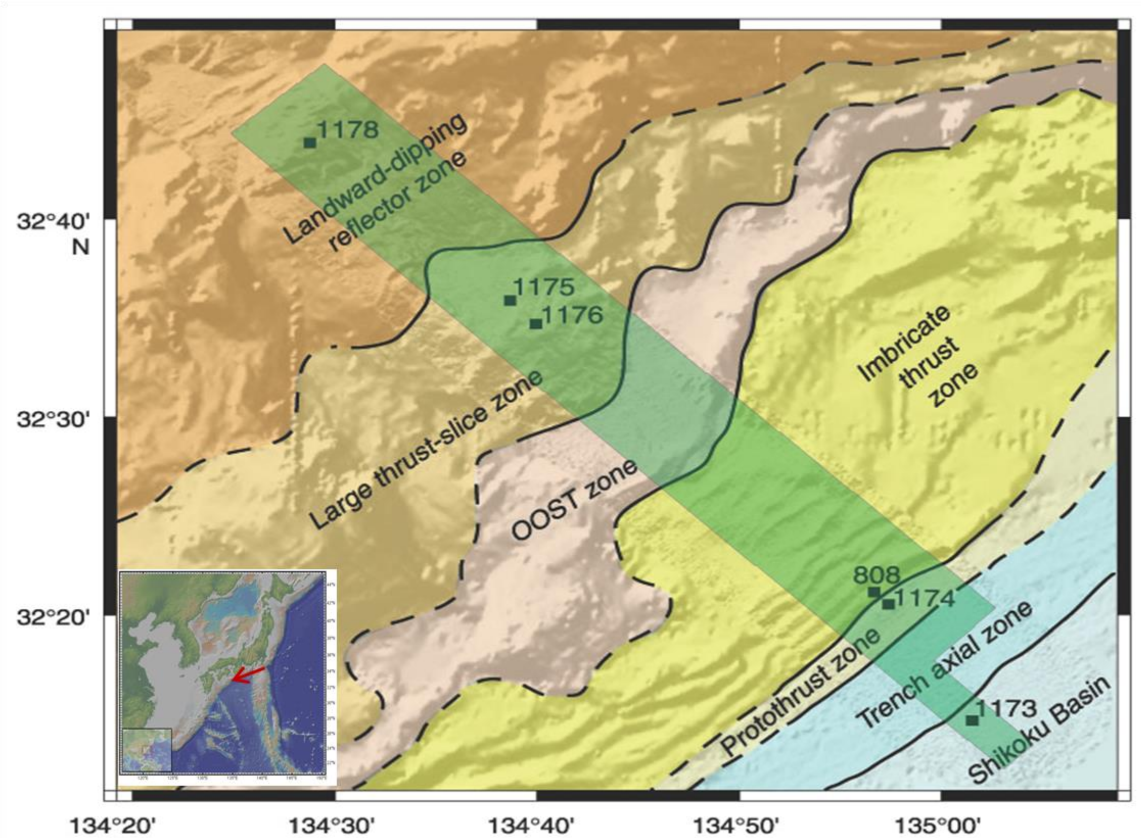

Figure 1-1. Map of tectonic structural domains in the Muroto Transect region interpreted from bathymetry and seismic reflection data. Legs 131 and 190 sites are shown by squares. OOST zone represent out-of-sequence thrust zone. Adopted from Moore et al., (2001).

Evolution of the accretionary prism involved subducted seamounts, and they are important in order to understand how the seamounts affect the prism. The 3D seismic record along the Muroto Transect imaged a seamount beneath the out-of-sequence thrust zone. Based on the interpretations, the height of the seamount is almost determined 1 km.

The goal of this study is to better understand the relationship between the seamount and imbricated thrust system of the accretionary prism. In order to reach this goal, I constructed the sequential restorations along the imbricated system. In addition, I applied the Coulomb Wedge Theory to the toe of the Muroto Transect. Based on these results, I investigated the relation between the subducted seamount and the toe and imbricated system of the Muroto Transect.

1-2. Data set

The 3-D seismic reflection volume was acquired through the corridor which is named the Muroto Transect (Moore et al., 2001). The data set was obtained by the Ocean Drilling Program in 1999 on the R/V *Maurice Ewing* Legs 7 (EW9907) which is produced by the collaboration of UTIG, University of Hawaii, University of California, Santa Cruz, University of Tokyo, Japanese Geological Survey, and STA JAMSTEC (Fig. 1-2). In this survey, the acquisition parameters include a single 6 km streamer with 160 channels, 14 tuned air guns with total volume of 4276 cu. in., and a shot spacing of 50 m. During the acquisition process, 81 individual lines were shot. As a result, the width of the seismic volume is 8 km, and the length of the seismic volume is 80 km. The seismic survey consists of 151,061 shots and 500 Gbytes of seismic data (Fig. 1-2.). (Gulick et al., 2004). In order to enhance seismic images and eliminate smearing, the bin size was set at 25 m in the inline direction and 50 m in the cross-line direction, the inline numbers range from 180 to 360 and cross-line numbers from 1 to 3710.

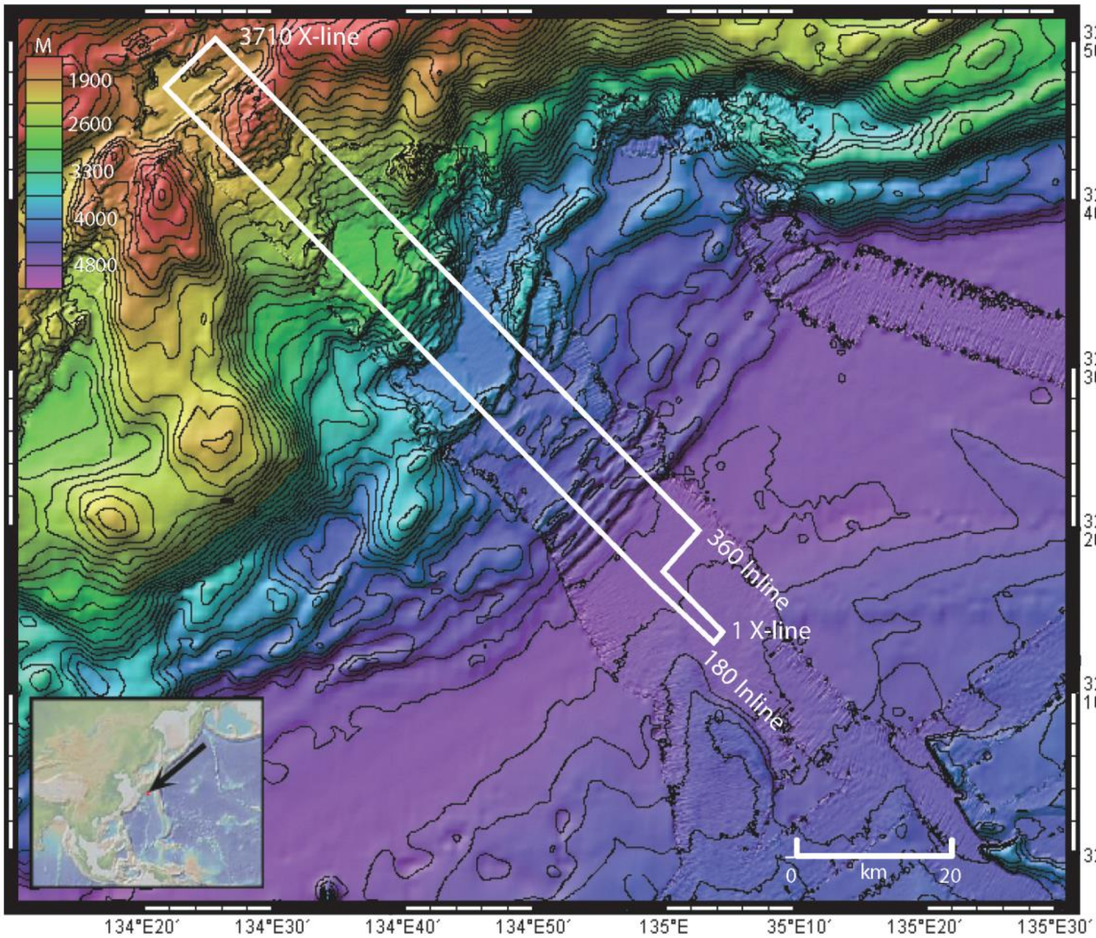

Figure 1-2. The bathymetry map which shows detailed study area and location of the seismic volume (white box).

Chapter 2: Geological Settings

2-1. General Geology of Japan

The arc systems (Fig.2-1) in the northwest Pacific include the Kuril Arc, Hidaka Axial Zone, northeast Honshu Arc, southwest Japan Arc, Izu-Ogasawara Arc, and Ryukyu Arc, and are referred to as the Japanese Island Arc Systems (Niitsuma, 2004). As shown on Figure 2-1, the Japanese Island Arc System's trenches bound the edges of the Pacific Plate, Philippine Sea Plate, Okhotsk Plate, and Eurasian Plate.

The Pacific Plate subducts beneath the Okhotsk Plate along the Kuril and Japan Trenches at the rate of ~8-9 cm/year (Nanayama et al., 2003). Additionally, the Pacific Plate is subducting under the Philippine Sea Plate along the Izu-Ogasawara Trench at the rate of ~10 cm/year (Fig. 2-1) (Miller et al., 2004). The Philippine Sea Plate is also subducting under the Eurasia Plate along the Nankai Trough, Sagami Trench, and Ryukyu Trench at the rate of 4 cm/year (Fig. 2-1). The Boso trench-trench-trench triple junction has links with the Izu-Ogasawara Trench, Japan Trench, and Sagami - Nankai Trough (Soh et al., 1988). The Japan Trench is located along the eastern coastline of the Honshu Island where the Pacific Plate subducts under the Eurasia Plate (Deyhle et al., 2004). This area is defined as an active seismic area based on earthquakes, some of which are >7M_w, which have occurred as shallow as 5000 m beneath the seafloor (Sacks et al., 2000). The northeastern part of the Japan Trench is convex landward, and the southwestern part is concave landward. These features of the Japan Trench form the characteristics of the Northeast Honshu Arc (Niitsuma, 2004). Niitsuma (2004) suggested that the Boso Triple Trench has evolved from the interaction of these arc systems since ~7 Ma. In addition, the similarity of tectonic structures to the shape of the Japan Trench suggests that they are genetically related to the subducting Pacific Plate.

The convergence of the Izu Arc, the northward bend of the median tectonic line, and the uniform east–west compressional stress field, coupled with active strike–slip faults in central Japan is constrained by the Philippine Sea Plate and the Boso Triple Trench junction. The longest exposed land fault is the MTL (Fig. 2-1), which has been active since early Cretaceous (Wibberly and Shimamoto, 2003).

The evolution of the Japan Sea started with rifting and crustal thinning in the northeastern Japan Basin due to subduction of Pacific Plate beneath the Eurasian Plate (Tamaki et al., 1992). After rifting, seafloor spreading developed in the Late Oligocene. During the seafloor spreading in the Japan Basin, the southern part of the Japan Sea began to extend; this extension caused the Yamato and Ulleung Basins to form (Lee et al., 2011). Because of subduction along the Nankai Trough and Japan Trench, and changing motion of the plates, the back-arc started to close, and this closure is still continuing today (Lee et al., 2001). The Japan Sea is located between the Japanese Arc Systems and the Eurasia Plate, and is located on the southeastern part of the North Eurasia Plate. The Japan Sea is composed of three deep basins; these are the Japan, Yamato, and Ulleung Basins (Fig. 2-1). These basins are divided by continental remnants (the Korea Plateau, Oki Bank, and Yamato Ridge) (Lee et al., 2011).

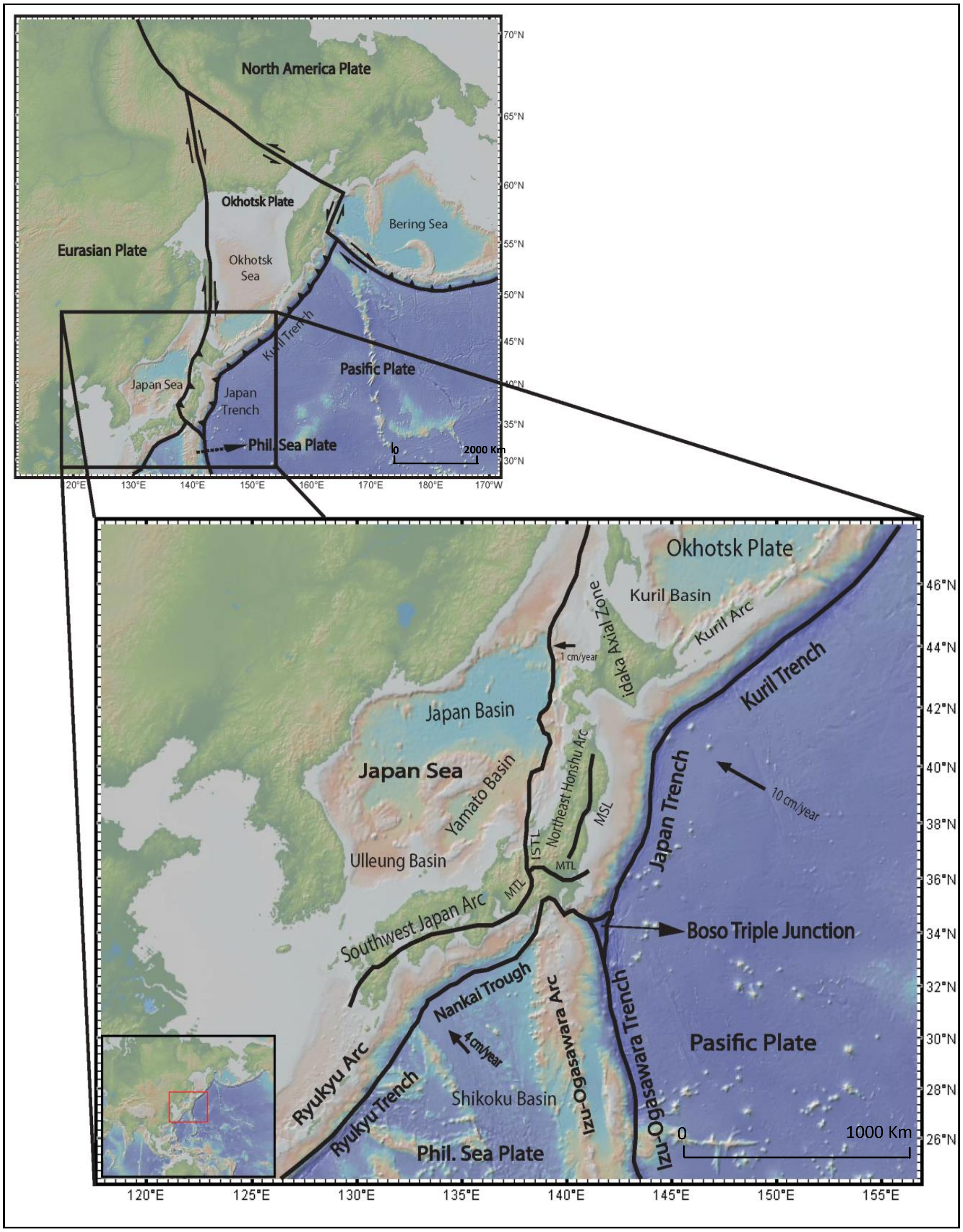

Figure 2-1. Plate tectonic framework of the Japanese Island Arcs. ISLT represents Itoigawa Shizuoka Tectonic Line; MSL represents Morioka-Shirakawa Line; MTL represents Median Tectonic Line. Adopted from Niitsuma, (2004).

2-2. Large Scale Characteristics of the Nankai Trough

Over the past two decades, the Nankai Trough of the southwest Japan region has been studied extensively with many geophysical surveys and conventional coring transects (Underwood et al., 1993). Significant tectonic activity of Japan has been ongoing for more than 20 Ma. The recent tectonic activities across the boundary have included the evolution of the fundamental collision zone in between the Honshu Arc – Japan Trench, the Ryuku - Nankai Arc Trench, and the Izu-Bonin Arc Trench (Fergusson, 2003). Before seafloor spreading initiated in the Japan Sea back arc basin at 15-16 Ma, Japan was a part of the Eurasian plate (Fergusson, 2003).

According to Taire et al. (1988), subduction began in southwest Japan during the Cretaceous and early Cenozoic. This process eventually led to the formation of the subduction complex comprised of Miocene-age rocks on Cape Muroto that is called the Shimanto Belt. During the evolution of the Nankai Trough accretionary prism, the Philippine Sea Plate continued to subduct under the Eurasian Plate at a rate of 4 cm/year (Seno et al., 1993) (Fig 2-2). The accretionary prism is exposed throughout Shikoku Island.

Additionally, rocks which belong to an older accretionary prism have been recognized on Shikoku Island (Fig. 2-2). Because of the tectonic activities of Japan during the Mesozoic and the Cenozoic, deformation has formed numerous faults that bound belts of different ages based on metamorphic grade of the rocks (Needham, 1988). Several belts of accreted rocks have been mapped and shown in figure 2-2. These belts are Sambagawa, Chichibu, Cretaceous Shimanto, and Tertiary Shimanto. The Sambagawa Belt extends over 800 km along the southwest margin of Japan (Utsunomiya et al., 2011). The maximum width of the belt is approximately 50 km in the Shikoku Island (Kouketsu and Enami, 2010). The Median Tectonic Line (MTL) separates the Sambagawa Belt from the Ryoku Belt at the north. The Ryoku Belt contains high-temperature and low-pressure metamorphic rocks of Cretaceous age (Utsunamiya et al., 2011). The Sambagawa Belt consists of high-pressure metamorphic rocks of Cretaceous age (Arai et al., 2009). The Chichibu Belt is located at the south end of the Sambagawa Belt. The belt includes the Mesozoic strata, which consist of sandstone, mudstone, and limestone (Arai et al., 2009).

In addition, one of the belts is the Shimanto Belt (Fig 2-2), which is the closest belt to the recent active margin. The Shimanto Belt is exposed on the Kii Peninsula of Honshu and the Islands of Shikoku and Kyushu (Needham, 1988). Taira (1985) states that rocks of Late Cretaceous to Late Miocene age are exposed along the Shimanto Belt. Taira et al. (1988) have recognized an imbricated thrust zone which is part of the Cretaceous and Tertiary Shimanto Belt. It consists of trench turbidites and mélange, which includes basalt and pelagic limestone radiolarian, and chert, and hemipelagic shale. The Shimanto Belt is generally interpreted as an ancient analog for the modern Nankai Trough Prism (Taira et al., 1982; Ohmori et al., 1997).

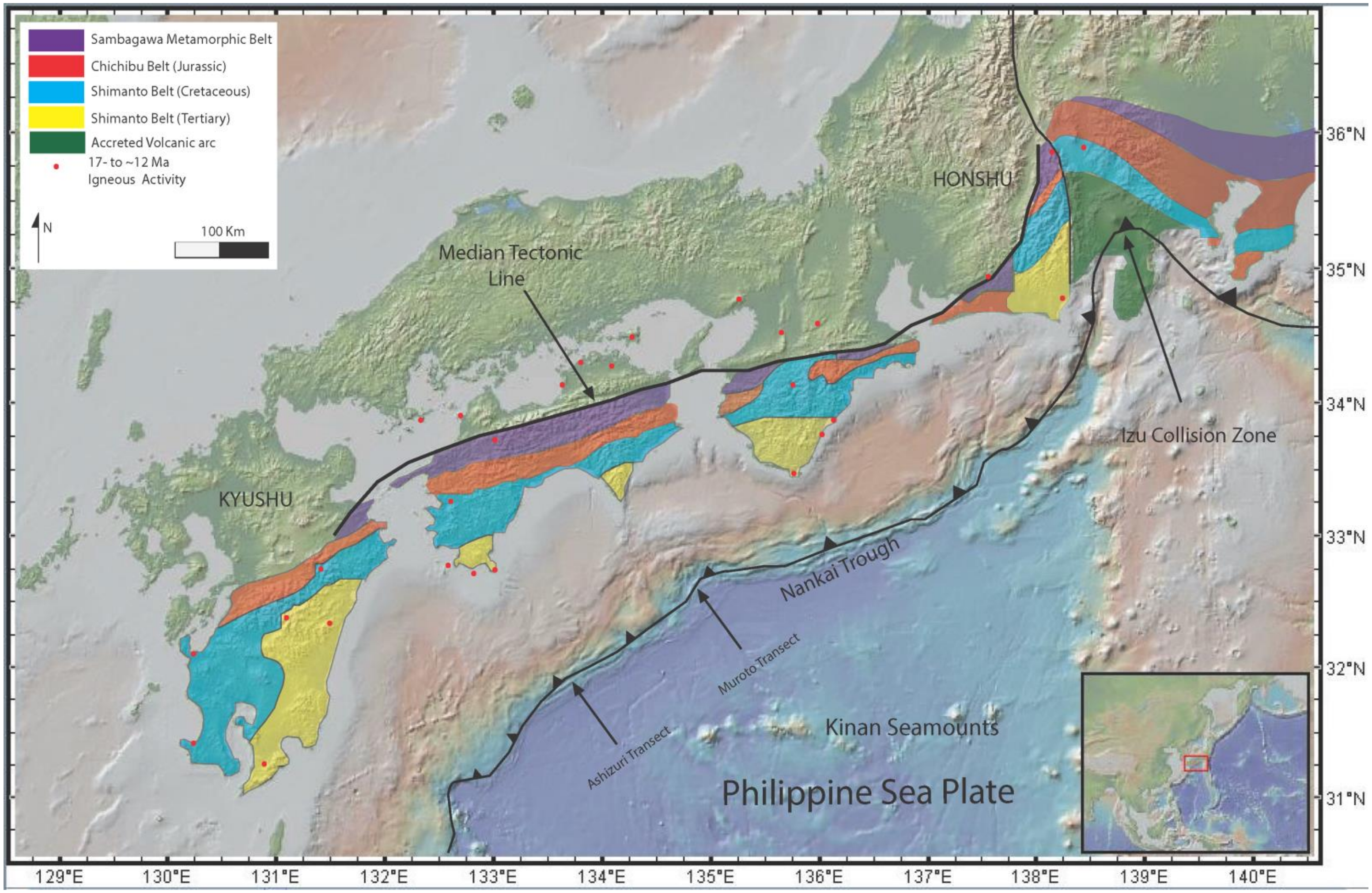

Figure 2-2. Simplified geological map of southwest and central Japan with the major accretionary units of the outer zone of southwest Japan depicted. The map is adopted from Moore et al., (2001). The belts are Sambagawa, Chichibu, K-Shimanto, and Tertiary Shimanto in sequence. Red spots are described as areas of igneous activity.

There is some debate in the literature about the subduction history of the Philippine Sea Plate during the Neogene. For instance, Niitsuma (1988) stated that the Philippine Sea Plate has been subducting for only the past 7 Ma. On the other hand, Maruyama (1997) has proposed that the subduction of the Philippine Sea Plate has continued throughout the Neogene.

Based on Arai et al. (2009), an arc-arc collision zone happened in the north part of the Izu Bonin Arc which is located south of Honshu. The northeastward motion of the subduction of Philippine Sea Plate and the back-arc seafloor spreading in Japan Sea caused the Izu Bonin Arc to collide with the Honshu Island in the Middle Miocene (Arai et al., 2009). After the collision, wide intra-arc deformation developed in the Izu Bonin Collision Zone (Yamamoto et al., 2009). The collision caused some structural features, such as the Tanzawa Mountains and Izu peninsula to develop in the Izu Collision Zone (Arai et al., 2009). Based on tectonic activity and thick clastic deposits in and around the Tanzawa Mt., the uplift of Tanzawa Mts. started during the Late Cenozoic (Ito, 1987). The mountains contain volcanic rocks of early Miocene to middle Miocene and Neogene intrusive rocks (Akai et al., 2009).

Additionally, Amano (1991) and Niitsuma (1989) proposed that the collision of Philippine Sea Plate and Eurasian Plate may be divided into four fundamental accretionary events at ~12 Ma, 7-9 Ma, 3-5 Ma, and ~1 Ma. Based on the Sites 1173, 1174, and 808 of ODP Leg 190-196 (Fig. 2-5), sediments of the upper Pleistocene age were deposited along the Nankai Trough during the last accretionary episodic event at ~1 Ma (Amano, 1991; Niitsuma, 1989).

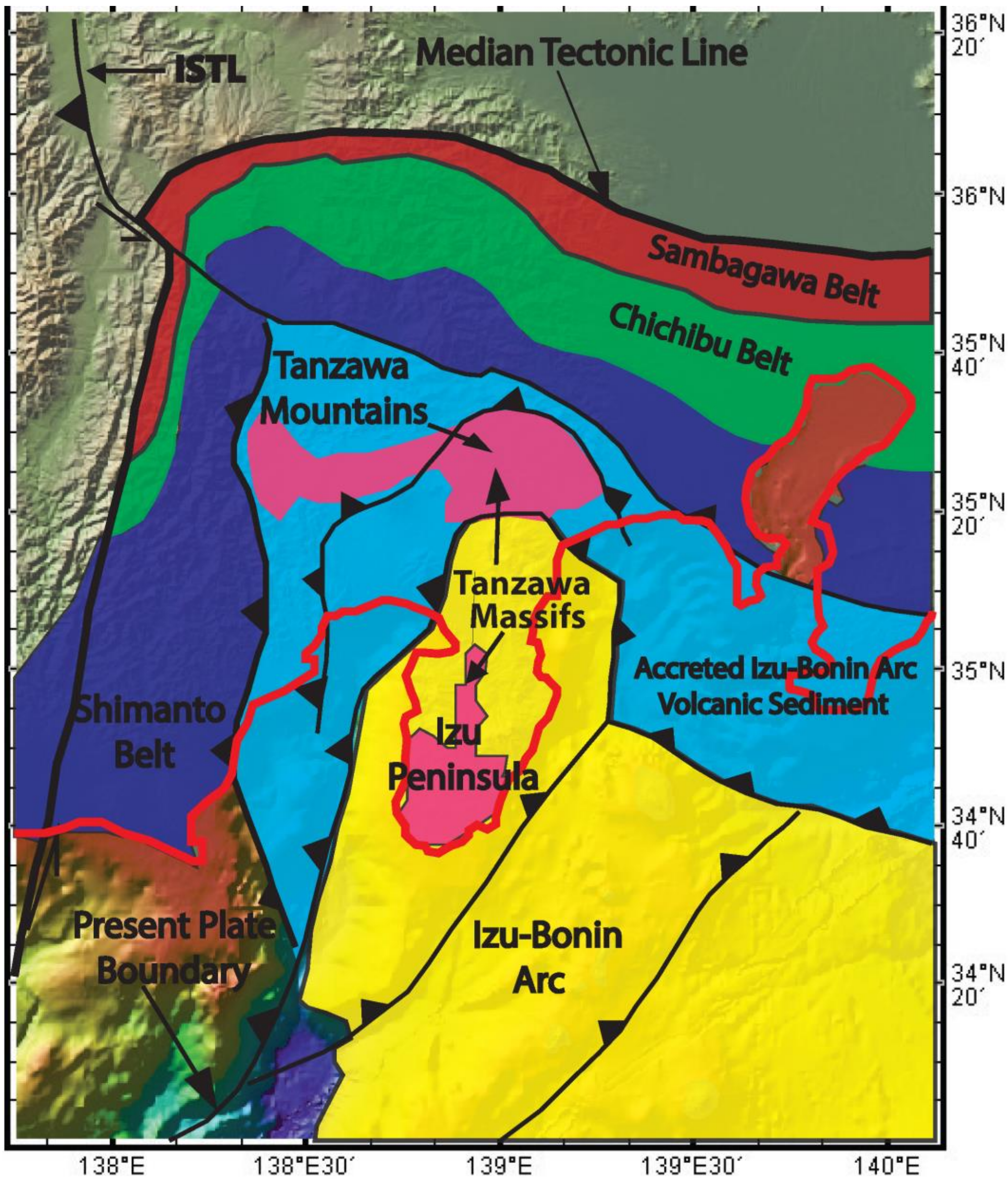

Figure 2-3. Plan view of Izu-collision zone in central Honshu (Modified from Yamamoto et al., 2009). The Izu-Bonin Arc (yellow), Accreted Izu-Bonin Arc volcanic sediment (light blue), Shimanto Belt (dark blue), Chichibu Belt (green), Sambagawa (red), and the Tanzawa Massifs (pink). The coastline is illustrated in red. The map is adopted from Yamamoto et al., (2009). ISTL = Itoigawa-Shizuoka Tectonic Line.

The Shikoku Basin is located behind the Izu-Bonin Ridge, and the basin is classified as back-arc basin. The evolution of the basin is thought to have started in the Late Oligocene to Middle Miocene (Chamont-Rooke, 1987).

The Nankai Trough bounds the Philippine Sea Plate to the east, and is made up of igneous basaltic basement ranging in age from ~15 to ~26 Ma in age. In the Shikoku Basin, volcanic eruptions occurred during the last ~12 Ma on the Kinan Seamounts (Fig 2-5) (Kobayashi, 1984; Kobayashi et al., 1995).

Turbidites, deposited in the trench, have been thickened throughout the deformation front by structural repetition. Based on lithological information from Drilling Site 808, 1174, and 1173 of ODP Leg 190-196, these turbidites are dated at late Pleistocene (Moore et al., 2001). However, Party Scientific Shipboard (1975) stated that early Pleistocene turbidites were documented at Site 298. These turbidites packages contain mafic to intermediate volcanic detritus, quartz, and feldspar, and also small amounts of sedimentary and metamorphic lithic debris (Fergusson, 2003).

The subduction of the Shikoku Basin was triggered by the interarc rifting of the Izu Bonin arc (Fig. 2-1) and its formation as a back-arc basin (Taylor, 1992). Okino et al. (1994) state that the rifting of the Izu Bonin Arc began during the Oligocene, and is related to the Shikoku Basin seafloor spreading event which continued until ~15 Ma.

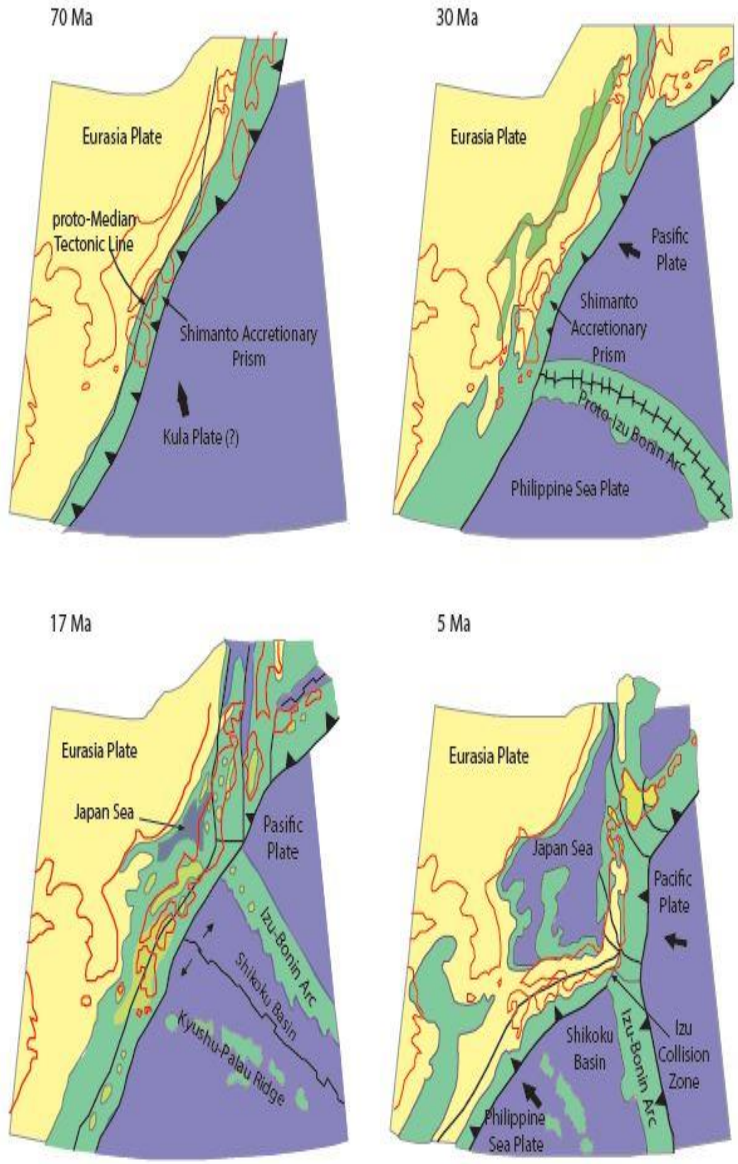

Figure 2-4. Paleogeographic reconstruction of the Shimanto Belt and Nankai forearc evolution (modified after Taira et al., 1989).

Plus, the remnant arc which is called the Kyushu-Palau Ridge was divided from the active Izu Bonin arc by seafloor spreading; as a result, the Shikoku Basin developed (Fig 2-4) (Henry, 2012).

Kano et al. (1991) stated that igneous activity between ~17-12 Ma occurred near the trench. During this period, high Mg andesites erupted behind the Nankai Trough where the spreading center intersected the trench and was subducting (Park et al., 1999).

Kamata and Kodama (1994) stated that volcanic activity started at ~8 Ma in the Southern Kyushu. By ~6 Ma a volcanic front in the southwestern Shikoku Island had begun to form, and the subducting slab had deeply penetrated into the asthenosphere (Moore et al., 2000). Niitsuma (1989) stated the Tanzawa massif (Fig. 2-3) which is a part of the volcanic front of the Izu-Bonin arc, began to accrete onto the Nankai Trough at ~ 8 Ma (Moore et al., 2000). An uplifted collision zone was eroded and the sediment derived from during the erosion of the collision zone accumulated in the axis of the Nankai Trough (Taira et al., 1988 and Niitsuma, 1996).

Throughout the evolution of the Nankai Trough, the accretion of sediment is recorded on the Shikoku Island where ancient accretionary prism rocks have been uncovered. Based on geological investigations in the area, the youngest rocks in the Shimanto belt are early Miocene. Ohmori et al. (1997) claimed that the Shimanto Belt may be considered as an ancient prototype of the Nankai accretionary prism.

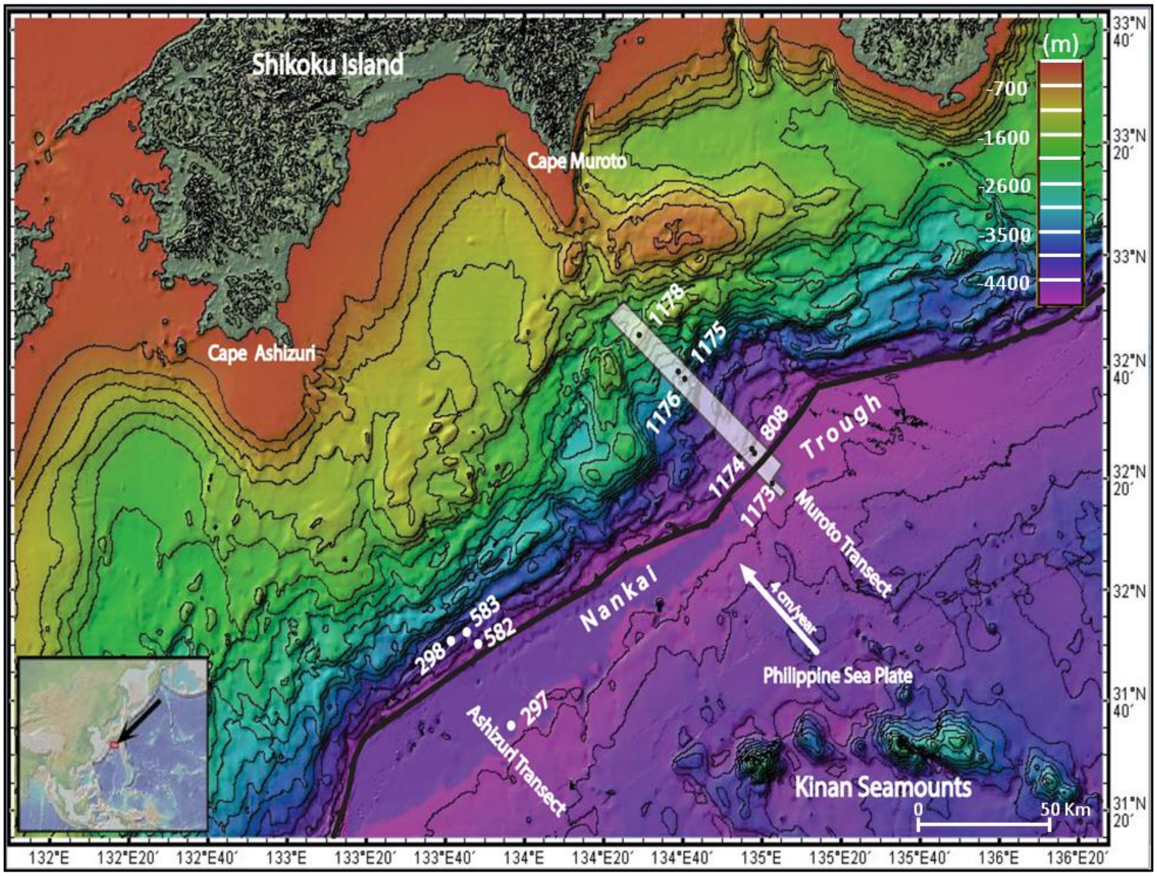

Figure 2-5. The map illustrates the location of the 3-D seismic data and drilling sites of the Leg 131, 190, and 196 along the Muroto Transect .

Chapter 3: Lithostratigraphy of the Toe of the Muroto Transect

3-1. Lithostratigraphy of the Toe of the Muroto Transect

The stratigraphy of the Muroto Transect was investigated using several wells which were drilled in cruises of the ODP Leg 131 in 1989, 190 in 2000, and 196 in 2001. Samples were recovered during Legs 131 and 196 at Site 808, Hole A, B, C, and I, as well as during Leg 190 at Site 1174, Hole B (Fig. 3-1). These drilling sites were targeted to investigate: 1) properties of deformed rocks and related fluids of the plate-boundary thrust fault or décollement, 2) porosity or fluid content of sediments, 3) the relation with porosity and seismic velocity, 4) variation of pore pressure with structure, 5) physical properties of sediments depending on degree of diagenetic alteration, and 6) better understanding the tectonic evolution of the area based on core-log, and seismic-scale data (Taira et al., 1991; Moore et al., 2000; Mikada et al., 2002).

Based on the lithology information from drilling sites, the seismic interpretation has been done by referencing the lithologic units of the Muroto Transect. In order to interpret the imbricated system, I utilized the data from Site 808 and Site 1174. Site 808 from Leg 131 and Leg 196 is located on the frontal thrust fault. Site 1174 from Leg 190 is located on the proto-thrust zone.

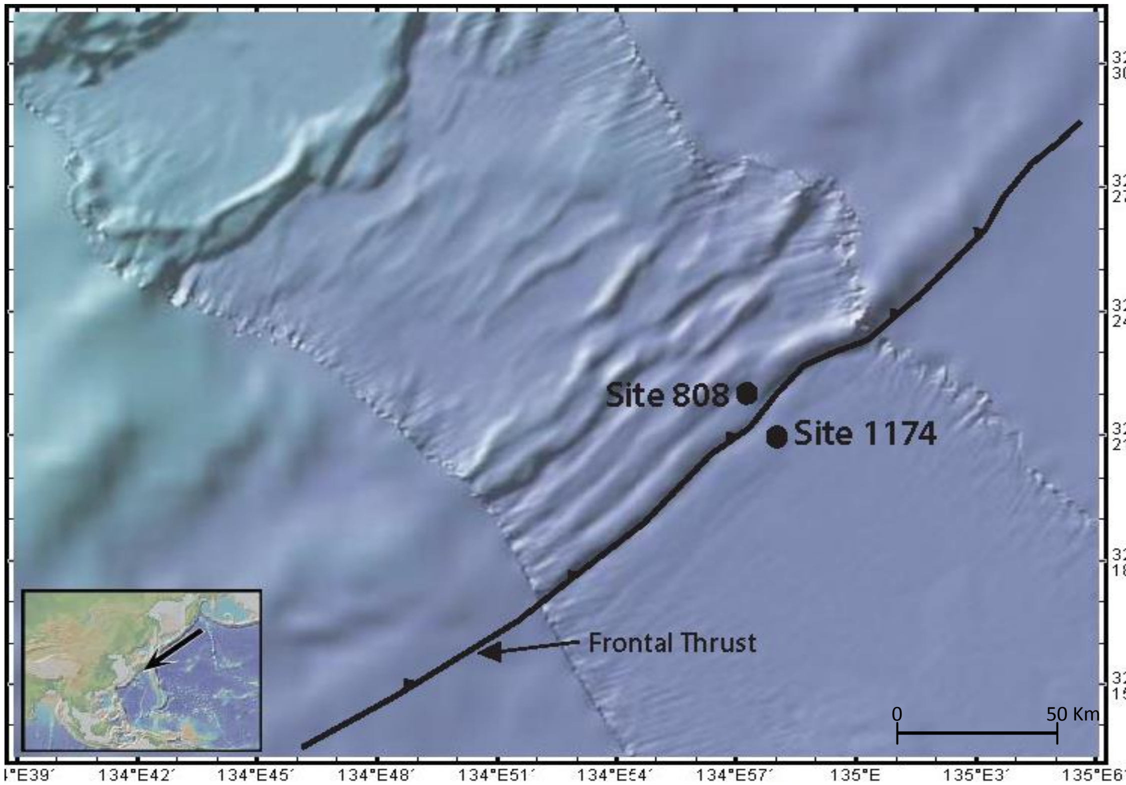

Figure 3-1. The location of the Site which are used for interpreting the Nankai Trench, Proto Thrust Zone and Imbricated Thrust Zone. Based map is high resolution Multi-beam Bathymetric Swath in transect zone.

In Drilling Site 808, Hole A, B, and C from Leg 131, and Hole I from Leg 196, illustrate the lithology of the toe of the Muroto Transect. Site 808 consists of 6 discrete units, two of which includes subunits; the determination of units was based on visual core descriptions, grain size, bed thickness, and mineralogy (Taire et al., 1991). The lithological units below are from top to bottom of Site 808;

1. Unit I : Lower-Slope apron (0-20.55 mbsf)
2. Unit II : Trench-fill deposits (20.55-556.80 mbsf) which is divided into three subunits:

a. Subunit IIa : Upper axial-trench sandy deposits (20.55-120.60 mbsf)
b. Subunit IIb : Lower axial-trench silty deposits (120.60-264.90 mbsf and 365.90-409.54 mbsf)
c. Subunit IIc : Outer marginal-trench silty deposits (264.90-355.50 mbsf and 409.54- 556.80 mbsf)

3. Unit III : Trench to basin transitional deposits (556.80-618.47 mbsf)
4. Unit IV : Shikoku Basin deposits (618.47-1243 mbsf) which is divided into two subunits:

   a. Subunit IVa : Upper Shikoku Basin deposits (618.47-823.74 mbsf)
   b. Subunit IVb : Lower Shikoku Basin deposits (823.74-1243 mbsf)

5. Unit V : Acidic volcaniclastic deposits (1243-1289.9 mbsf)
6. Unit VI : Basaltic Basement (1289-1327 mbsf)

Additionally, Site 1174 was drilled in the proto-thrust zone of Muroto Transect. This site is important because of the structural, stratigraphic, and physical properties of the frontal deformation zone of the accretionary prism. During Leg 190, Holes 1174A and B were drilled at Site 1174. The lithologies recovered in Holes 1174 A, and 1174 B are classified into five lithologic units, one of which is subdivided into three subunits (Moore et al., 2001). The lithologic units are listed from top to bottom of Site 1174:

1. Unit I : Slope-apron deposits (0-4 mbsf)

2. Unit II : Trench-wedge deposits (4-483.23 mbsf). The Unit II is divided into three subunits:

    a. Subunit IIa : Axial trench-wedge deposits (4-314.55 mbsf)
    b. Subunit IIb : Outer trench- wedge deposits (315.55-431.55 mbsf)
    c. Subunit IIc : Trench to basin transition deposits (431.55-483.23 mbsf)

3. Unit III : Upper Shikoku Basin deposits (483.23-660.99 mbsf)
4. Unit IV : Lower Shikoku Basin deposits (660.99-1102.5mbsf)
5. Unit V : Volcaniclastics deposits (1102.5 mbsf)

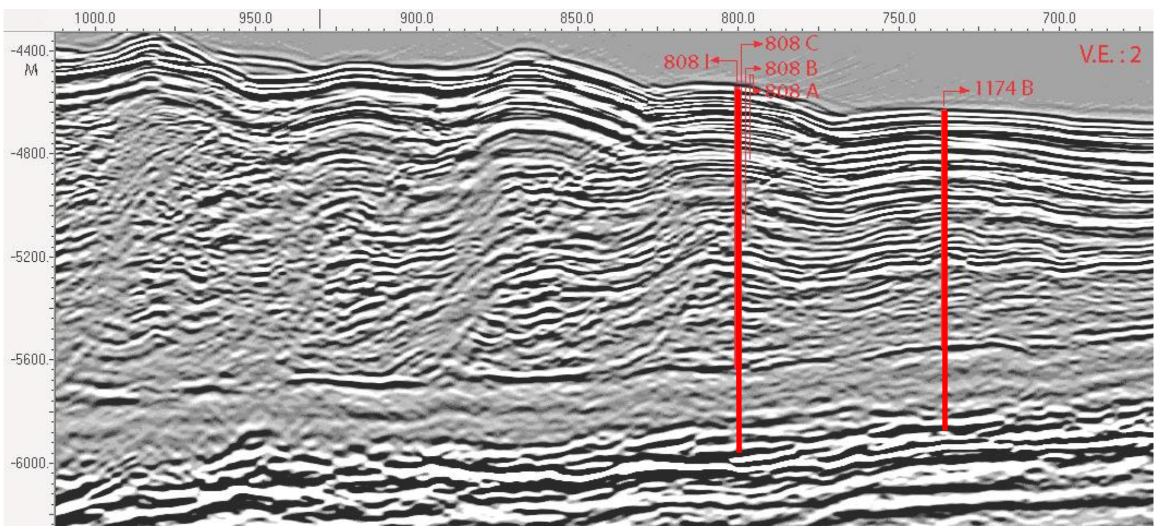

Figure 3-2. The location of the wells that were drilled during the ODP Leg 190 and 196.

The detailed investigations of the sites which were used for interpretation of the Muroto Transect, were defined using the lithologic units below.

3-2. Site 808

Site 808 is located at the toe of the Muroto Transect on the Nankai Trough Accretionary Prism. From this site, six main sedimentary depositions were drilled and evaluated. Their ages are Miocene to Quaternary. These sedimentary units exist in all ~1250 m thick sediment block (Brown et al., 2001). This sediment block is subdivided into four sedimentary units, which were classified as Unit I, II, III, and IV.

3-2-1. Unit I (Lower Slope)

The thickness of the Unit I is 20.5 m, and deposited during the Quaternary. Homogeneous, bioturbated, clayey silt, fine-grained sand, and very thin ash layers make up the Unit I. The unit includes the lower-slope apron, with large-scale down-slope sliding of semi-consolidated sediments (Taira et al., 1991).

3-2-2. Unit II

Unit II lies from 20.5 to 556.8 m and is 536.3 m thick. The unit includes the trench deposits, which are classified as Upper Axial Trench, Lower Axial Trench, Frontal Thrust Zone, Outer Marginal Trench Wedge, and Trench Basin. Based on these facies information, Unit II is divided into three subunits, which are IIa, IIb, and IIc.

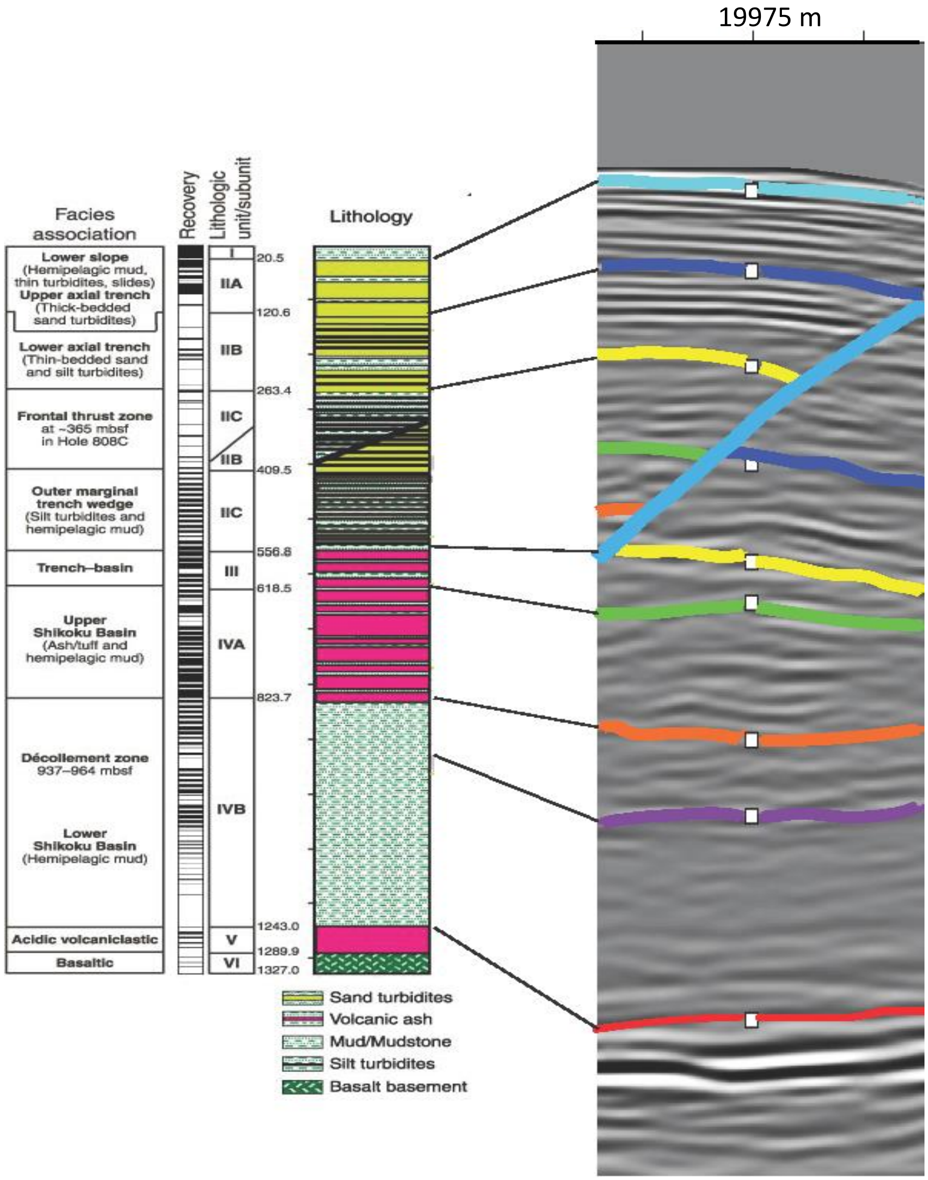

Figure 3-3. Site 808 summary diagram showing combined results of Legs 131(modified from Mikada et al., 2002 and correlated with a seismic section that is from the 3D seismic volume). The column shows the sedimentary units determined from Site 808.

3-2-2-1. Subunit IIa (Upper Axial Trench)

The thickness of Subunit IIa is 100.1 m and it exists in the interval 20.5-120.6 mbsf. Subunit IIa includes axial trench, sandy channel, and non-channel deposits. The unit includes considerably thick packages of coarse-grained sand. In addition, very thin ash layers were observed in this subunit (Mikada et al., 2002).

3-2-2-2. Subunit IIb (Lower Axial Trench)

Based on the well information from Site 808, the thickness of Subunit IIb is 144.9 m within core interval 120.60-264.9 mbsf and 43.64 m in core interval 365.90-409.54 mbsf. This unit includes fine-grained sandstones, laminated till-like conglomeratic mudstone, and thin interbedded siltstones and mudstones. Very thin ash layers can also be observed in the subunit (Mikada et al., 2002).

3-2-2-3. Subunit IIc (Outer Marginal Trench Wedge)

The oldest subunit of the Unit II is Subunit IIC. The measured thickness of subunit IIc is 90.6 m within core interval 264.90-355.50 mbsf, and 147.28 m within core interval 409.54-556.80 mbsf. This subunit consists of a thick tuff which includes mudstone-pebble conglomerate. The Subunit IIc varies from Subunit IIb because Subunit IIb includes very thin sand units (Mikada et al., 2002).

3-2-3. Unit III (Trench-Basin)

The thickness of the Unit III is 61.7 m within the core interval 556.8 and 618.5 mbsf. The unit contains bioturbated siltstone and silty claystone, as well as multiple 25 cm-thick ash and tuff beds. Based on the stratigraphic location of the Unit III, which is placed between trench-fill deposits and the hemipelagic Shikoku Basin deposits, the unit represents trench – basin transition deposits. These deposits contain sediments which were deposited on the outer trench (Mikada et al., 2002).

3-2-4. Unit IV

Unit IV occurs in core at 618.47-1243.00 mbsf. The unit is interpreted as being equivalent to the upper Shikoku Basin. Generally, ash, tuff, and hemipelagic mud are observed in the Unit IV. This unit was investigated by dividing into two subunits which were IVa and IVb (Mikada et al., 2002).

3-2-4-1. Subunit IVa (Upper Shikoku Basin)

The thickness of subunit IVa is 205 m thick in the core interval 618-823 mbsf. Based on the well information, the subunit contains many thin layers of tuff and sandstones which are interbedded with a series of bioturbated mud. Mikada et al. (2002) claimed that this subunit illustrates deposition of the upper Shikoku Basin, and it mostly contains hemipelagic sediments and volcanic layers.

3-2-4-2. Subunit IVb (Lower Shikoku Basin)

The thickness of Subunit IVb is 420 m in the core interval 823-1243 mbsf. The ash and tuff beds are absent at the top of the subunit. In addition, the base of the subunit includes acidic volcaniclastic deposits (Mikada et al., 2002). Bioturbated clayey siltstones and silty claystones which contain prevalent volcanic glass are important portions of the

Subunit IVb. Based on the seismic interpretation, the Subunit IVb corresponds to the location between upper Shikoku Basin and acidic volcaniclastic unit which was deposited on the oceanic crust.

3-3. Site 1174

Site 1174 is located in the proto-thrust zone of the Nankai Accretionary Prism. The site location is ~2 km far from Site 808. The depth of the well is ~1110 mbsf. Site 1174 consists of five stratigraphic packages which include Units I, II, III, IV, and V.

3-3-1. Unit I (Lower Slope)

The thickness of Unit I is 4 m and is exposed at the seafloor. Its age is determined as Quaternary. The unit consists mainly of brownish and grayish muddy beds. A brown glassy ash is also present at ~3 mbsf; its thickness is 22 cm. The mud, which includes less glassy clay minerals, quartz feldspar, siliceous microfossils, and calcareous nanno-fossils, is structureless (Moore et al., 2001).

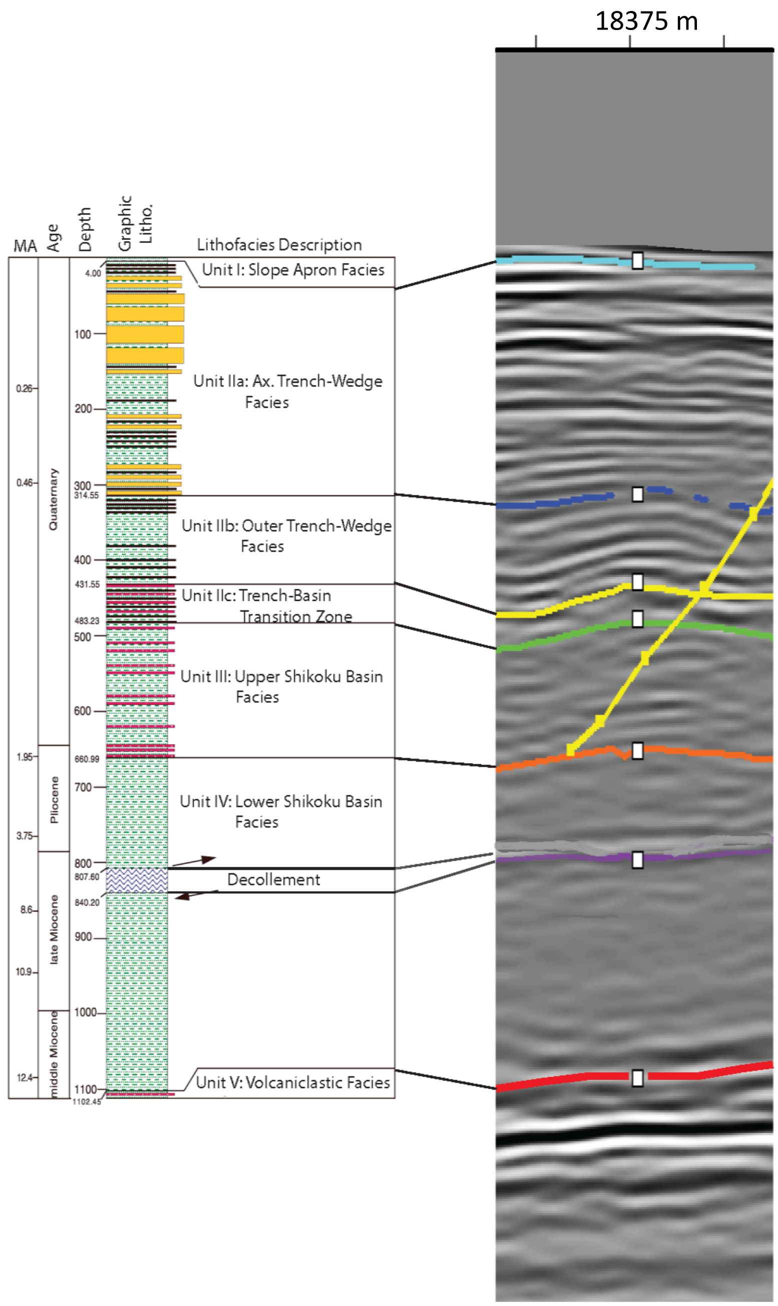

Figure 3-4. Site 1174 summary diagram showing combined results of Legs 196 (adopted from Moore et al., 2001 and modified with a seismic line which is from the 3D seismic volume). The column shows the sedimentary units determined from site 1174; the seismic section is correlated with the stratigraphic column based on the well information.

3-3-2. Unit II

The thickness of Unit II is 479.23 m; age of this unit is also Quaternary. Based on the differences of the facies, the Unit II is classified into three subunits: Subunit IIa, IIb, and IIc.

3-3-2-1. Subunit IIa (Axial Trench-Wedge Facies)

The thickness of Subunit IIa is 310.55 m. Sand, muddy and silty sand, sandy silt, silty clay, and clayey silt occur with the Subunit IIa. Additionally, at 257 mbsf, very thin volcanic ash was discovered (Moore et al., 2001). The sand section occurs between 67.43 and 143.7 mbsf. In Subunit IIa, muddy layers were deposited as hemipelagic sediment and well-developed, grained turbidites. The sandy beds are interpreted as turbidity deposits. According to the seismic interpretation, the axial trench wedge is illustrated with these sandy beds. Party Scientific Shipboard (1991) claimed that the Unit I of Site 808 has similar texture and deposition with 18 m thick of the upper axial trench wedge; on the other hand, bending or reversed layers which are clue of the slump folding are not observed. In the Proto-thrust Zone, ~ 50 m stratigraphic layer was moved over the trench floor due to initial deformation which is observed in the Proto-thrust Zone.

3-3-2-2. Subunit IIb (Outer Trench-Wedge Facies)

The thickness of Subunit IIb is 168.68 m in core interval 314.55 - 483.23 mbsf. This unit was interpreted as turbidite depositions including highly silty clay and clayey silt.

3-3-2-3. Subunit IIc (Trench-Basin Transition Zone)

Subunit IIc is the oldest subunit of Unit II. The thickness of this subunit is 51.68 m in core interval 431.55-483.23 mbsf. Based on the well information, this subunit includes silty turbidites, volcanic ash, and hemipelagic mud. The subunit corresponds to trench-basin transition facies.

3-3-3. Unit III (Upper Shikoku Basin Facies)

The thickness of Unit III is 177.6 m; it ranges in age from Pliocene to Quaternary. This unit mostly includes silty claystone and clayey siltstone with interbedded volcanic ash layers. According to Moore et al. (2001), Subunit IVa at Site 808 has the same characteristics with the Unit III from Site 1174. The base of Unit III is defined by the deepest unequivocal ash bed at 660.99 m.

3-3-4. Unit IV (Lower Shikoku Basin Facies)

The thickness of Unit IV is 441.46 m, it ranges in age from Miocene to Pliocene. This unit includes hemipelagic mudstone, rare siliceous claystone, and rare calcareous claystone. These siliceous claystones are altered ash beds based on particles of cryptoccrytalline silica, smectite, zeolite, and opaque minerals that exist in these claystones (Moore et al., 2001). Therefore, a digenesis has an essential role in the distinction of Units III and IV. The décollement is observed in this unit. The thickness of the décollement is 32.60 m thick in core interval 807.60-840.20 mbsf.

3-3-5. Unit V (Volcaniclastic Facies)

Unit V starts at 1102.45 mbsf and has a thickness of 2 m. This unit includes volcaniclastics and variegated mud stone. The age of Unit V is middle Miocene. Moore et al. (2001) claimed that the hemipelagic claystone is an indicator of same uppermost volcaniclastics facies which are discovered at Site 808, in spite of not being discovered in Site 1174.

Chapter 4: Seismic Interpretation of the Muroto Transect

4-1. Seismic Interpretation of the Muroto Transect

The Nankai Trough is a subduction zone between the subducting Philippine Sea Plate and the overriding Eurasian Plate, which forms the southwest Japan Volcanic Arc. The Philippine Sea Plate, which includes the Shikoku Basin, is being subducted beneath the Eurasian Plate at the rate of ~4 cm/year (Seno, 1993). Taira et al. (1988) studied the core samples of the deep sea sediments which were obtained during ODP Legs 131, 190, and 196. They interpreted the age of the margin of southwestern Japan to be Cretaceous.

Moore et al. (2001) investigated and interpreted the Muroto Transect, which was divided into the undeformed Shikoku Basin, proto-thrust zone (PTZ), imbricated thrust zone (ITZ), frontal out-of-sequence thrust zone, large thrust slice zone, and landward-dipping reflector zone (Fig 4-1) (Moore et al., 2001). In this study, we follow this terminology and structural division of Moore et al. (2001), with the exception of their interpretation of the large thrust slice zone and landward-dipping reflector.

In this study, the high resolution 3-D seismic reflection data are interpreted in order to investigate the structure of the Muroto Transect in detail. For that purpose, the Shikoku Basin, proto-thrust zone (PTZ), imbricated thrust zone (ITZ), and out-of-sequence thrust zone (OOST) are studied in detail. I have interpreted and correlated all in-lines and cross-lines in the 3-D seismic volume; however, in this section, only lines 215, 260, and 284 are shown to illustrate the interpretation of the Muroto Transect.

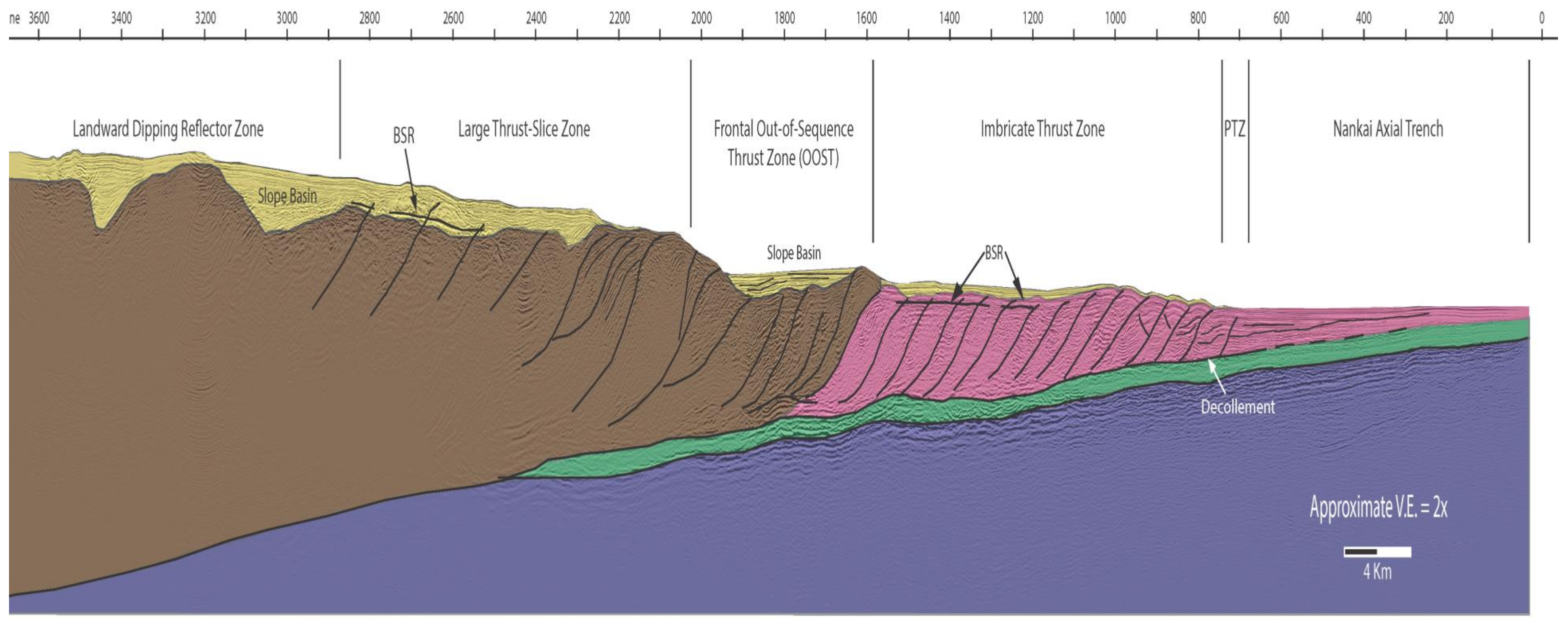

Figure 4-1. Seismic reflection line 284 illustrates the structural subdivision of the MurotoTransect. These structural features are axial-trench zone, proto-thrust zone (PTZ), imbricated thrust-zone (IMT), frontal out-of-sequence thrust zone (OOST), large thrust-slice zone (LTZ), and landward dipping reflector zone (from Moore et al., 2001).

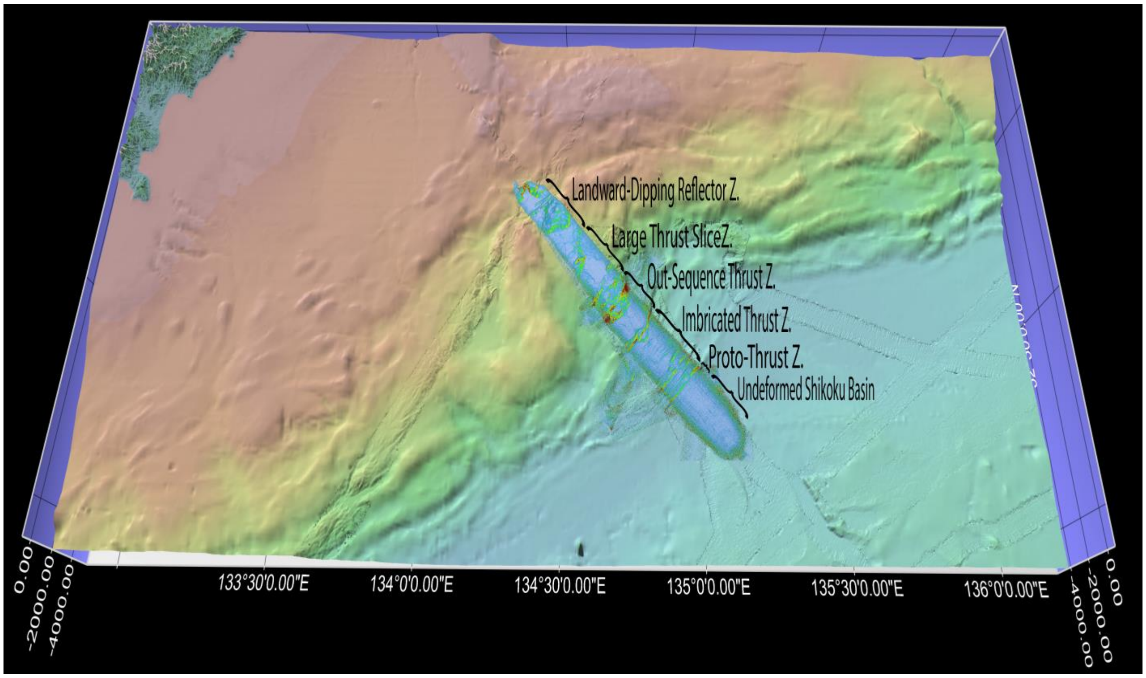

Figure 4-2. A part of the bathymetry of the Nankai Trough (taken from GeoMapApp). The bathymetry illustrates the subdivision of the Muroto Transect with slope angle variation bathymetry (produced with Fledermaus software).

4-2. Multibeam Bathymetry

During ODP Leg 190 in 1999, multibeam bathymetric data were collected using the Maurice Ewing's Hydrosweep system on the Muroto Transect of Nankai Trough in 1999 (Fig 4-2) (Moore et al., 2001). The data set was obtained from the Marine Geoscience Data System (MGDS). The bathymetric data set was processed with Fledermaus bathymetry software. The bathymetric surface map was created using a 50 m grid interval (Fig. 4-3). The bathymetric surface was used to help interpret the Muroto Transect. The structural subdivisions of the Muroto Transect are easily distinguished with the bathymetry of the Muroto Transect.

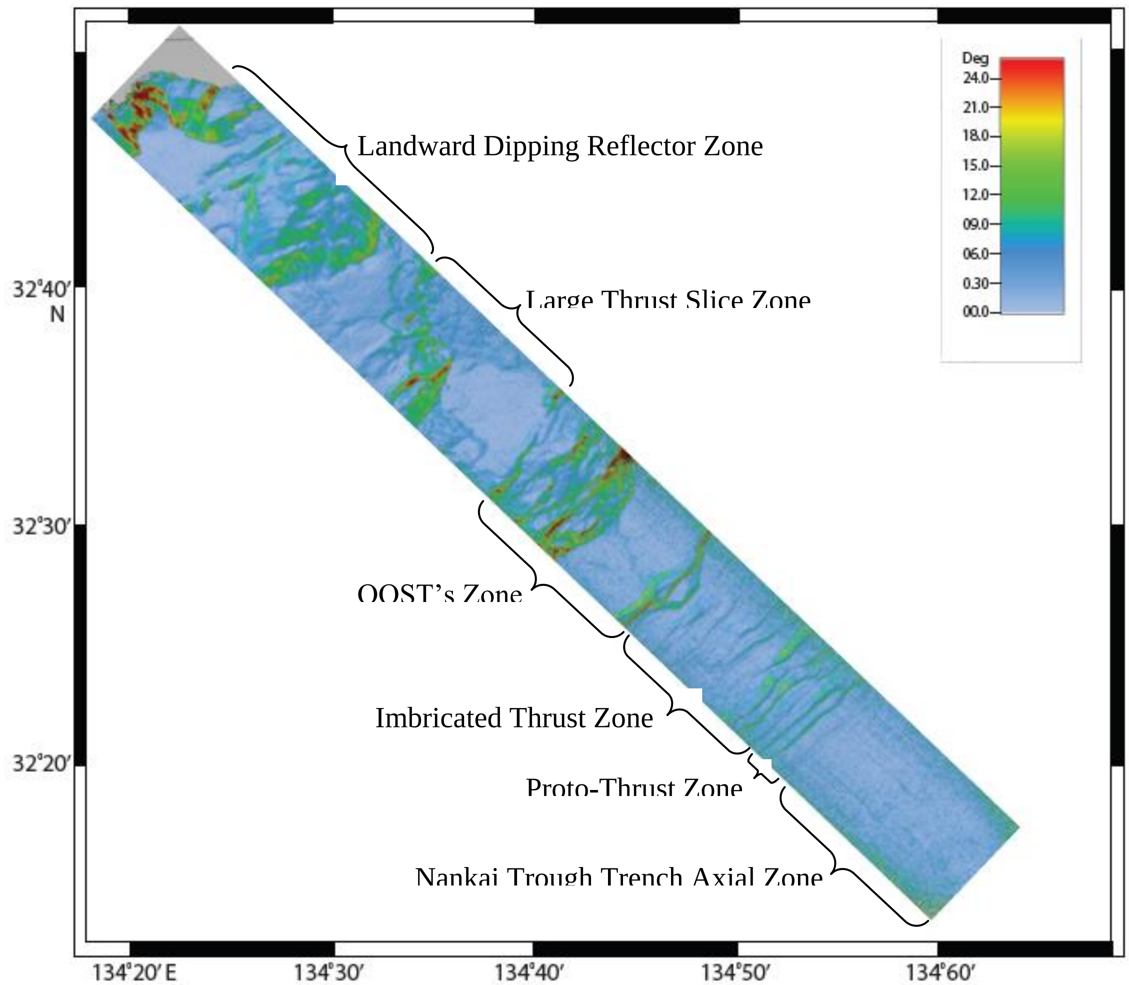

Figure 4-3. The slope angle variation bathymetry of Muroto Transect. The subdivision structures of the Muroto Transect are selected in the bathymetry. The division is based on Moore et al.,(2001)

In order to separate the structural subdivision, calculation of the slope angle from bathymetry data along the transect was carried out using Fledermaus software (Fig. 4-3). The interpretation of faults along the Muroto Transect was based on the bathymetry and seismic data of the transect (Fig. 4-4).

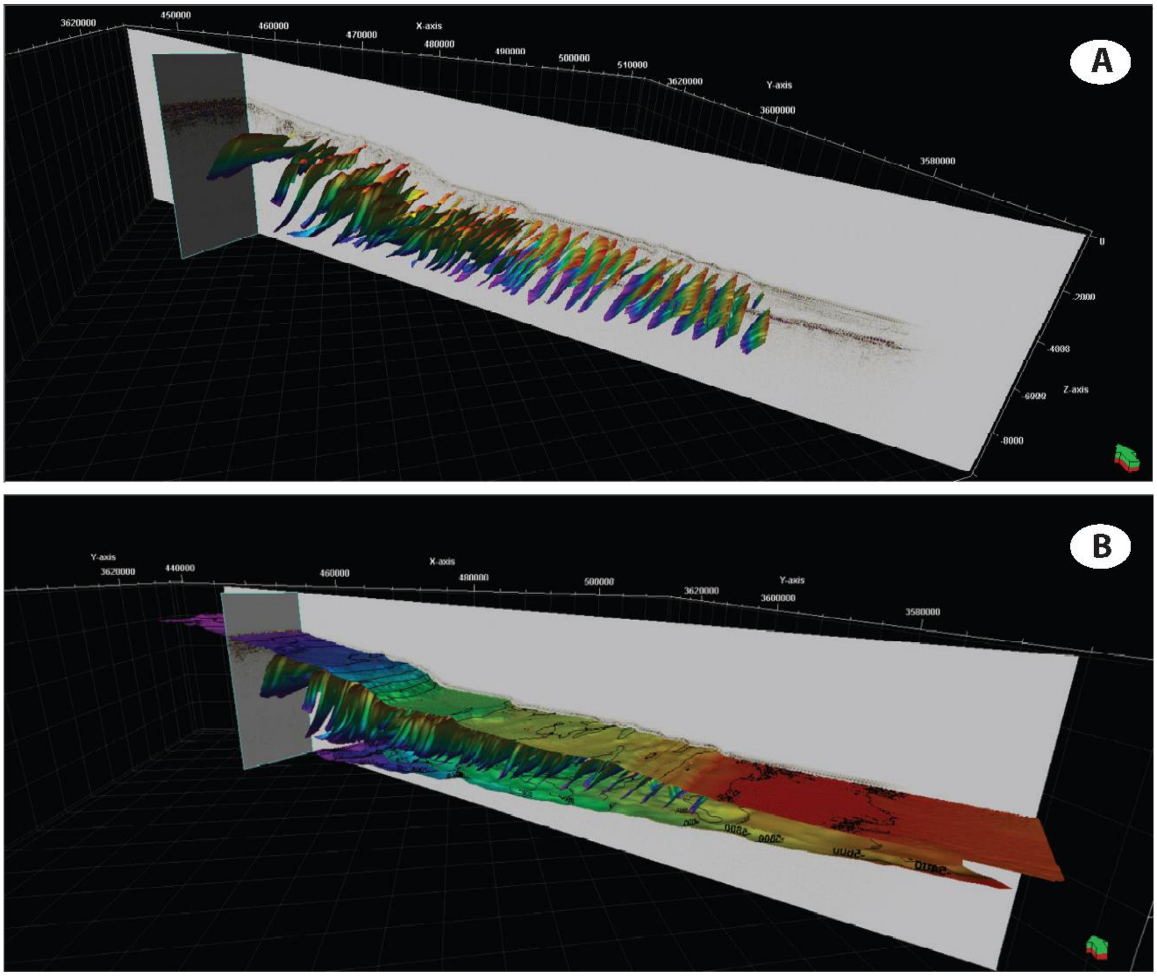

Figure 4-4. 3D interpretation of the Muroto Transect. (A) illustrates the interpretation all of faults along the Muroto Transect. (B) illustrates the interpretation of décollement, oceanic crust, and bathymetry of the Muroto Transect. The bathymetry map is made with Fledermaus software and imported into Petrel interpretation software. V.E.= 1:1

4-3. Décollement of Muroto Transect

The décollement is described as a surface or zone of structural difference which can be generally illustrated along the seismic reflection data (Moore, 1989). According to Tsuji et al. (2008), on seismic, the faults which are parallel to the subduction plate have strong reflectors in the well-developed accretionary prism. Moore et al. (1998) name these kinds of faults 'décollement' (Fig. 4-5). Additionally, these faults are classified as plate boundary faults. On the other hand, in well-developed accretionary prism, the décollement is not observed because the accretionary prism is highly deformed due to subduction (Park et al., 1999).

The décollement of the Muroto Transect is interpreted using the high resolution 3-D seismic data. On the seismic data, the décollement can be seen easily with negative amplitude. Additionally, the décollement clearly shows the deformation difference between the thrusted materials and unthrusted materials throughout the subducting plate.

Moore (1989) claims that the décollement has an effect on the underplate sediments. This effect is changed based on the structural thickness of the duplexes or thrust packages and depth of the underplate sediments.

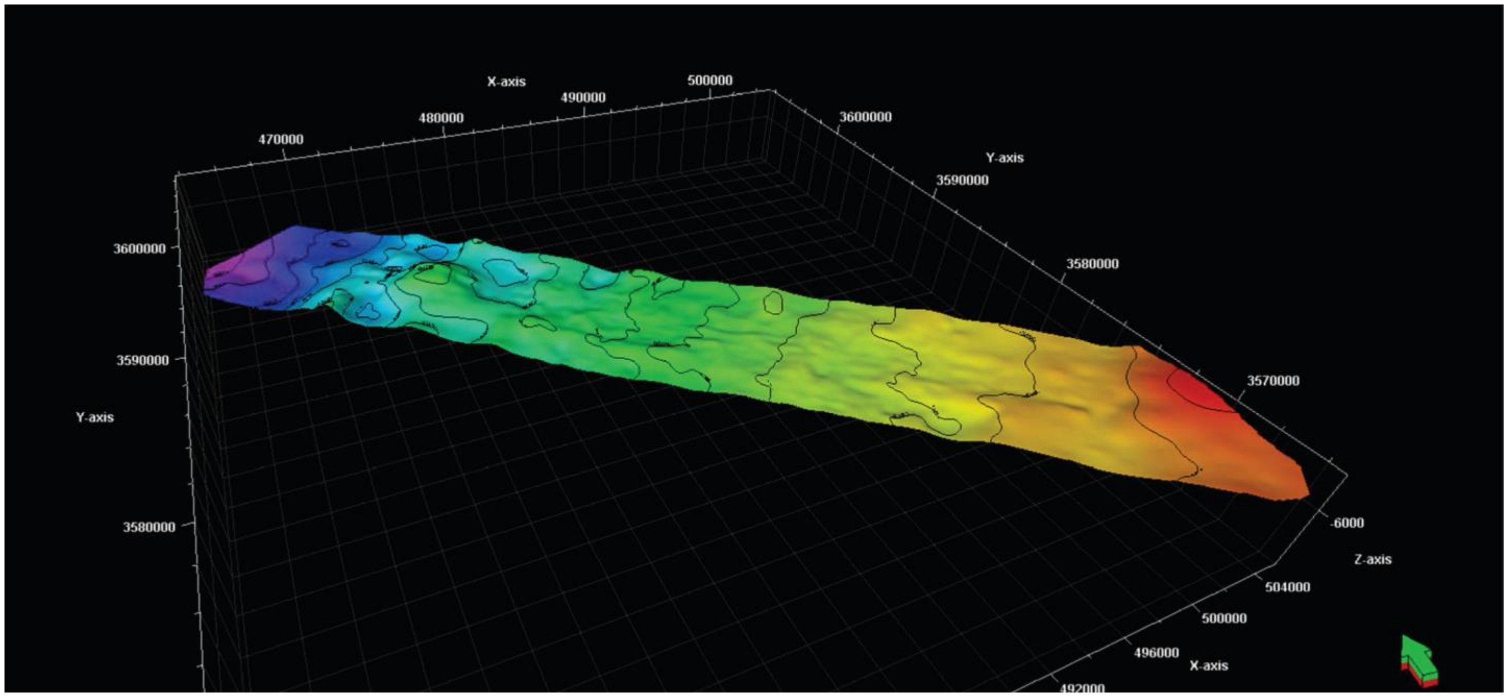

Figure 4-5. The interpretation of décollement of the Muroto Transect. The décollement is interpreted based on the 3D seismic volume along the Muroto Transect. V.E.= 1:1

4-4. Seismic Interpretation of Three In-lines of the Muroto Transect

4-4-1. Line 215

4-4-1-1. Nankai Trough Trench Axial Zone of Line 215

Sediments above the basement reflector of the Nankai trench consist of turbidites overlying oceanic pelagic sediments (Shikoku Basin sequence). While the pelagic sediments are nearly constant in thickness, the overlying turbiditic trench sediments thin seaward. The Shikoku Basin sequence (Moore et al., 2001) is interpreted as the oceanic pelagic sequence above basement formed in the Shikoku trough prior to entering the subduction factory. It is overlain by an arc-derived turbiditic sequence deposited in the morphologic trench. The thickness of the wedge is ~500m landward of the trench axial zone and the thickness gradually decreases to ~100 m through the seaward edge of the trench wedge.

In this zone, the development of new faults is observed on the seismic section. The small, younger faults generally develop in Unit III (Upper Shikoku Basin Facies) and IV (Lower Shikoku Basin Facies), which are right above the décollement. This is an indicator that the initiation of new faults started near the décollement (Fig. 4-7).

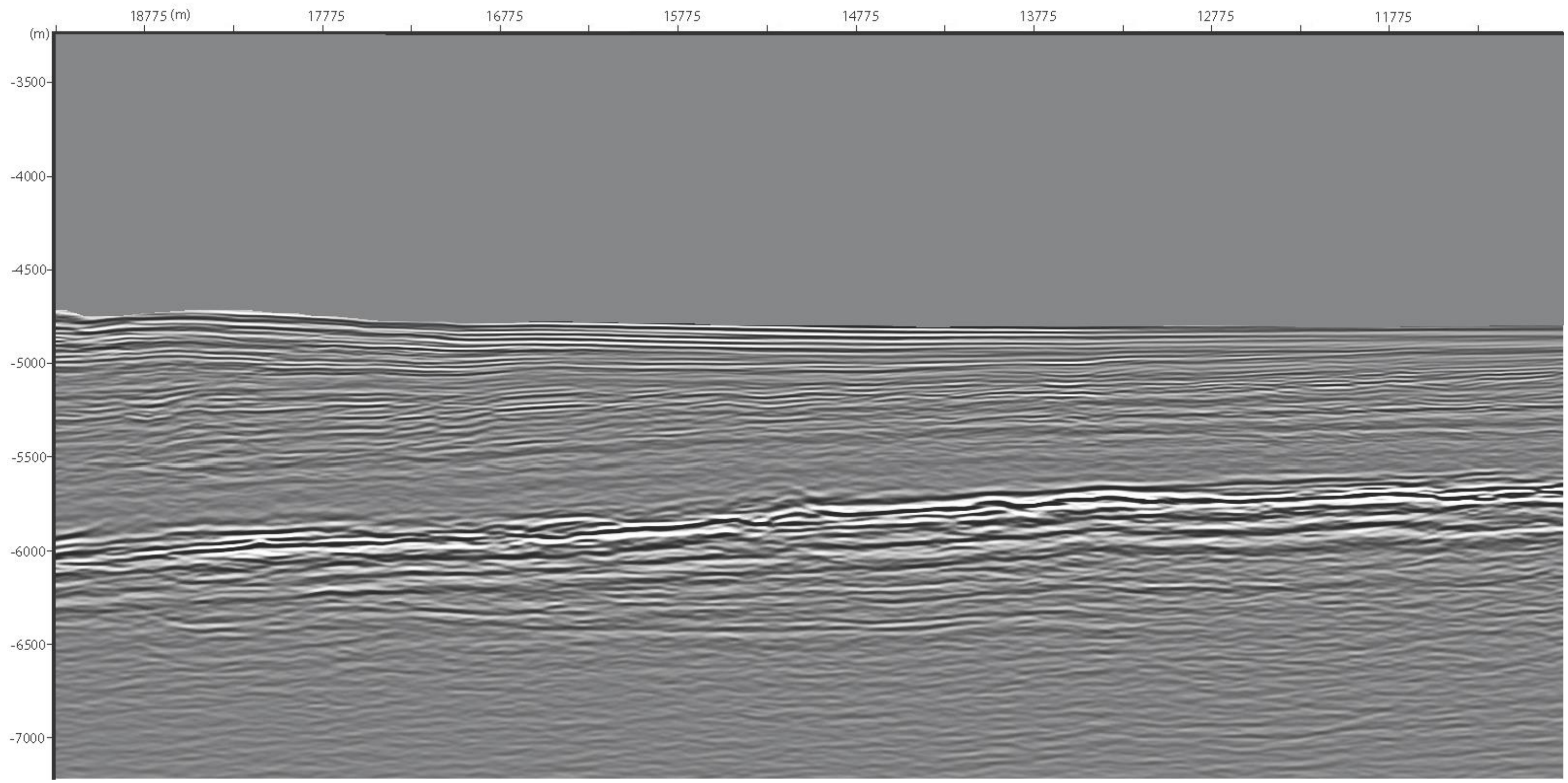

Figure 4-6. Non-interpreted seismic section of the axial-trench zone of the Line 215. This seismic slice illustrates the seaward edge of the trench. V.E. = 1:1

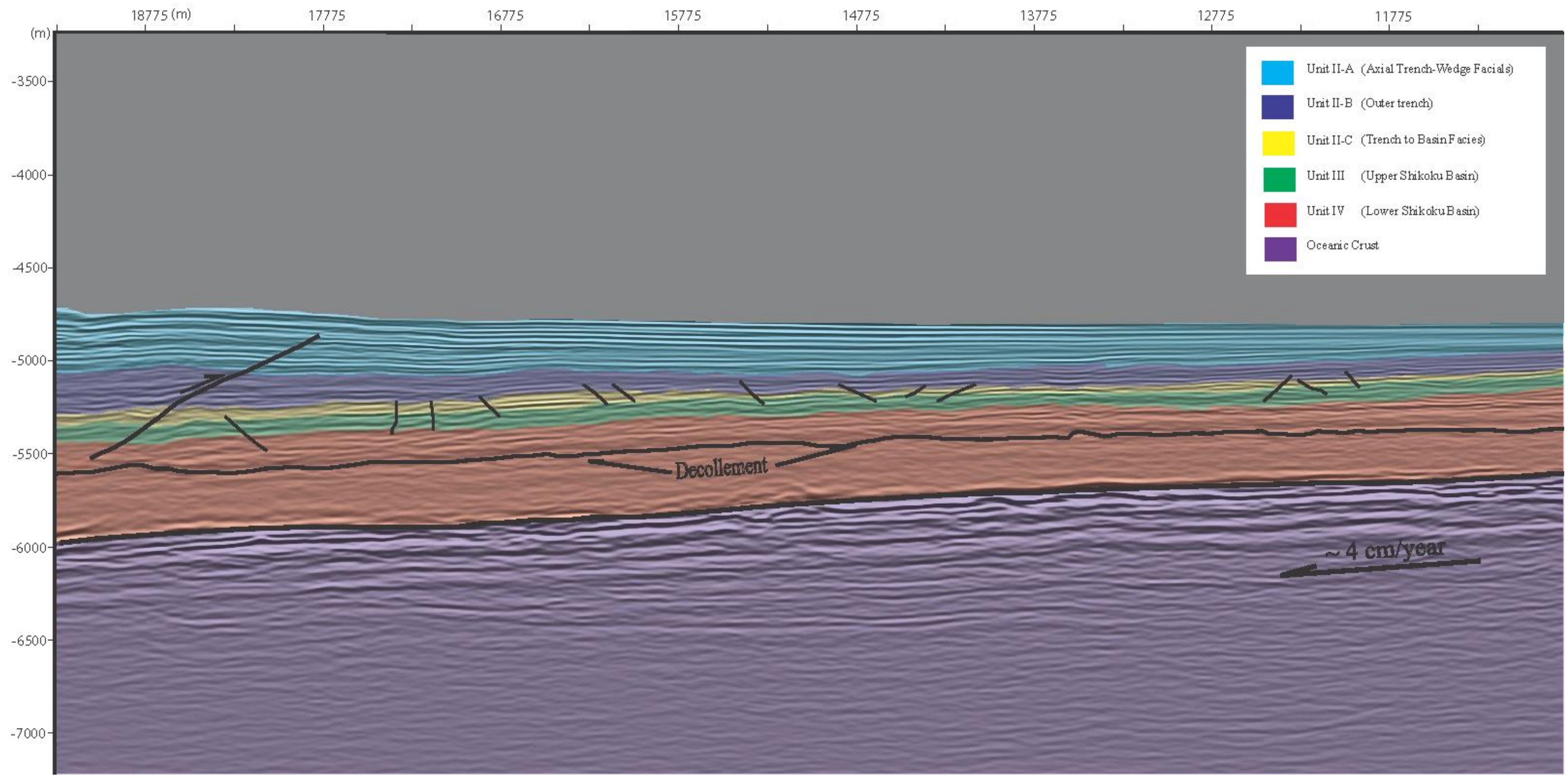

Figure 4-7. Interpreted seismic section of the axial-trench zone and proto-thrust zone of the Line 215. The interpretation of the sequence is done based on the Site 808 and 1174 from ODP Leg 190 and 196. The light blue unit represents Unit II-A (Axial Trench-Wedge Facies). The dark blue unit is Unit II-B (Out Trench Facies). The yellow unit is Unit II-C (Trench-Basin Facies). The green unit is Unit III (Upper Shikoku Basin). The red unit is Unit IV (Lower Shikoku Basin). The purple unit is the oceanic crust. V.E. = 1:1

4-4-1-2. Proto-thrust Zone (PTZ) of Line 215

Because of the subducting oceanic crust, the trench sediment and upper hemipelagic deposits which are overlying on the plate are stripped off and accreted to the overlying plate. The accretionary prism is subdivided into several structural features. One of those features is located between the deformation front and frontal thrust, and is called the proto-thrust zone (PTZ) (Fig. 4-9).

This zone is characterized as a zone where the initial deformation occurs and the décollement can be first seen on the seaward side of the trench. Because of limited tectonic shortening, many small faults and some minor folding deformation are observed in this region. Because of the tectonic shortening, in addition to the landward increase in thickness, structural thickening of the package develops with thrusting, and folding begins in this zone (Morgan and Karig, 1995).

The proto-thrust zone is the zone where the new thrust faults develop. When the trench axial zone is investigated, small-scale thrust faults which are close the décollement are observed. In this case, the fault development starts near the décollement area and it continues through the surface. Depending on the amount of upward progression, some of the faults in this zone are blind faults. Because the blind faults do not offset the surface, they are hard to observe (Dolan et al., 2003).

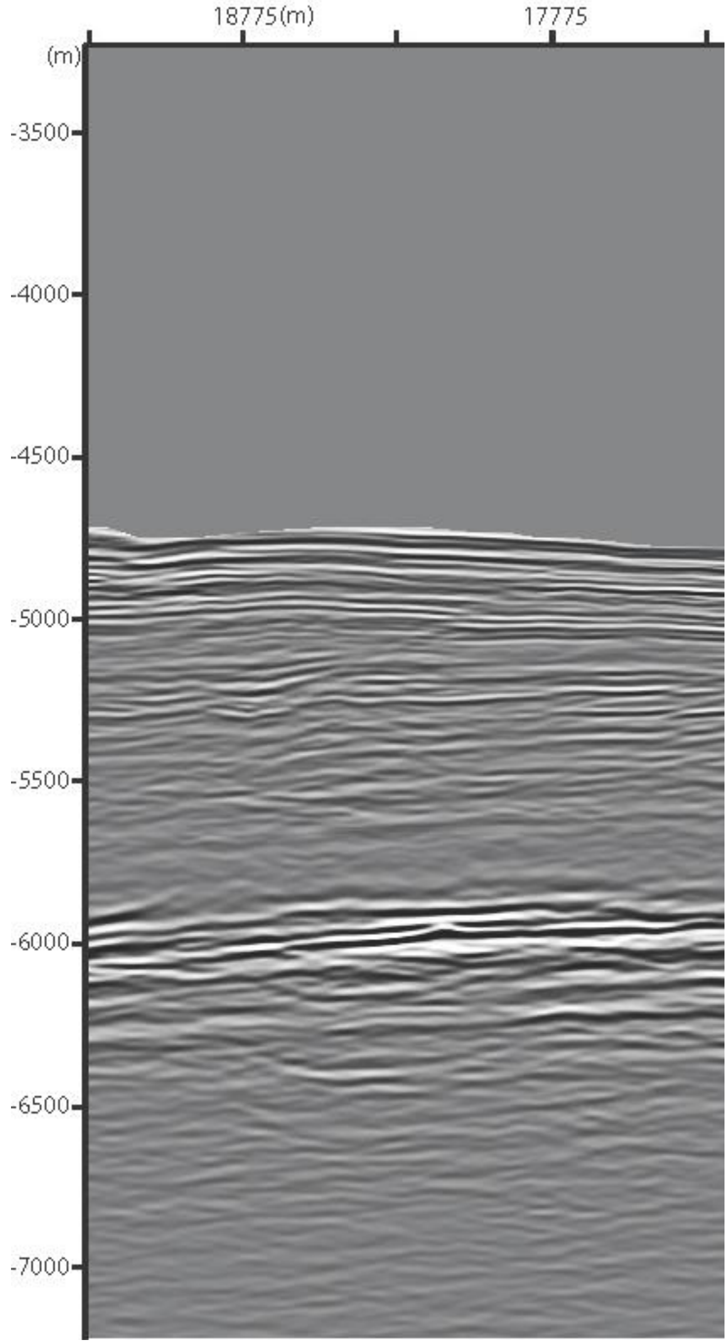

Figure 4-8. Non-interpreted seismic section of proto-thrust zone of the Line 215. V.E. = 1:1

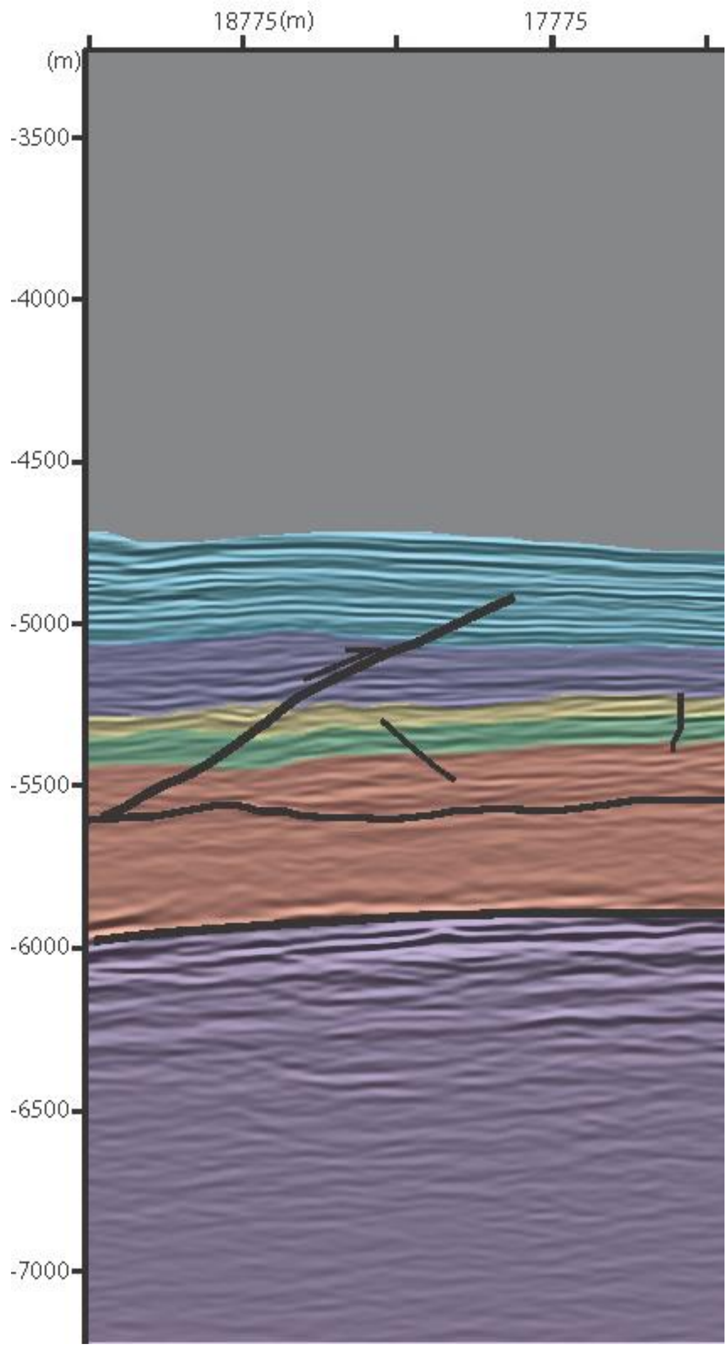

Figure 4-9. Interpreted seismic section of proto-thrust zone of the Line 215. The interpretation of the sequence is done based on the Site 808 and 1174 from ODP Leg 190 and 196. The light blue unit represents Unit II-A (Axial Trench-Wedge Facies). The dark blue unit is Unit II-B (Out Trench Facies). The yellow unit is Unit II-C (Trench- Basin Facies). The green unit is Unit III (Upper Shikoku Basin). The red unit is Unit IV (Lower Shikoku Basin). The purple unit is the Oceanic Crust. V.E.= 1:1

4-4-1-3. Imbricated Thrust Zone of Line 215

A well-formed imbricated thrust zone (ITZ) occurs landward of the PTZ (Fig. 4-12). This zone is ~16 km wide and it consists of 13 thrust blocks, each one of which is dipping ~30° landward. The thicknesses of the blocks vary between ~700-800 m. The most characteristic feature of these thrust packages is a hanging-wall anticline structure (Fig 4-10). This feature is observed through almost every one of the packages. Moreover, these thrust packages detach from the well-defined décollement which is developed ~200-300 m above the oceanic crust. On the seismic data, a well-developed Bottom-Sea-Reflector (BSR) can be observed along the imbricated thrust zone.

According to Suppe (1983), because the fault surfaces are not planar, deformation occurs on at least one of the fault block when they slip past one another; the rocks are not durable enough to fill the large gap. The rocks, which are layered, might fold because of the mechanism of riding over the bend in a fault. The mechanism of folding is called fault-bend folding. This type of mechanism is generally observed in thrust-fold belts and accretionary prisms (Tavani et al., 2006).

Along the ITZ of Line 215, the anticlinal fault-bend folds are observed (Fig. 4-10). This structural feature develops because the hanging-wall of thrust fault moves over the fault surface and the sedimentary sequences of the hanging-wall are bent a fold (Suppe, 1983).

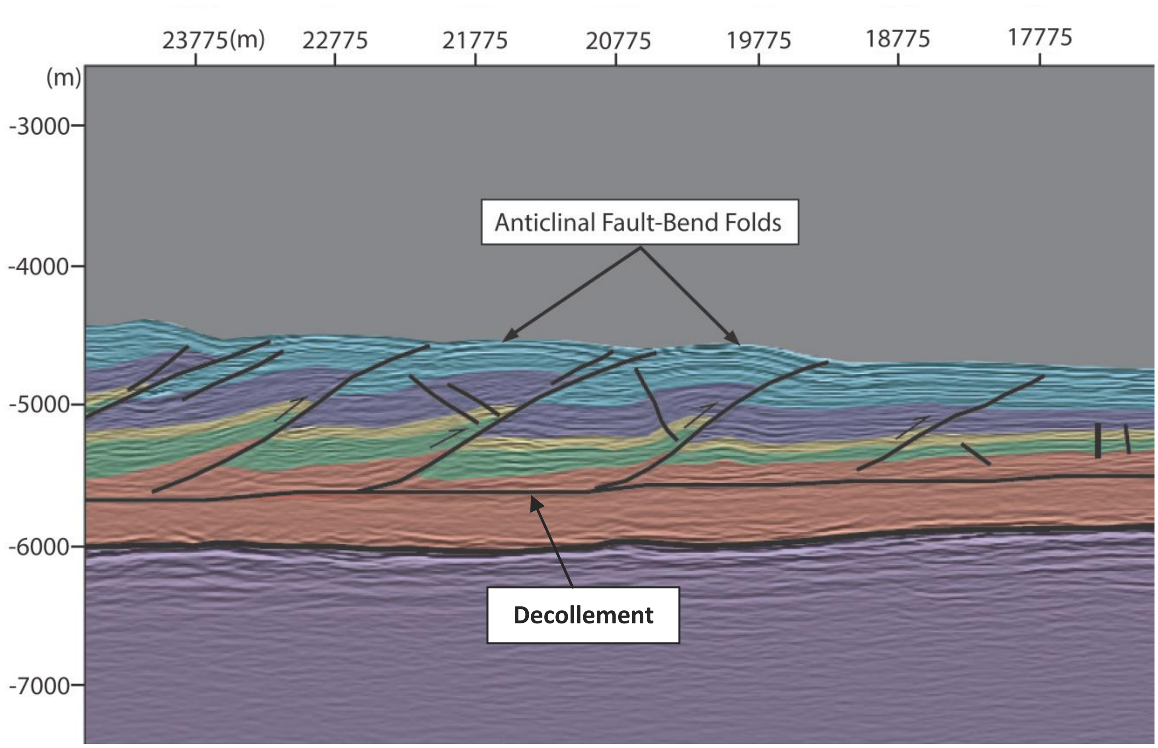

Figure 4-10. This seismic slice is taken from imbricated thrust zone of Line 215. Based on the fault interpretation, well-developed anticlinal fault-bend folds are observed on the seismic slice.

Based on Sites 808 and 1174, the horizons of imbricated thrust zone of Line 215 are interpreted by considering the lithological units described in Chapter 3. This is because the region is geologically very young, and the stratigraphy is known from core samples. Based on the core data obtained from Sites 808 and 1174, the imbricated system of the Muroto Transect developed during the Quaternary.

The uppermost unit of the imbricated thrust zone, which is colored light blue in figure 4-10, is Unit II-A (Axial Trench Wedge Facies). The unit consists of sandy, muddy sandy and silty turbidites, and hemipelagic mud.

The second unit in the system, which is colored dark blue, is Unit II-B which contains silt turbidites and hemipelagic mud interpreted as the Outer Trench Facies. The yellow colored unit is Unit II-C which exists beneath Unit II-B. This unit includes silty turbidites, volcanic ash, and hemipelagic mud interpreted as Trench to Basin Facies. The next unit is Unit III which is illustrated by green color. The unit consists of hemipelagic mudstone and abundant volcanic ash, and is interpreted as Upper Shikoku Basin. Unit IV, shown by red color, is beneath Unit III. Unit IV is interpreted as Lower Shikoku Basin. The décollement surface occurs in this unit. Along the Line 215, the top of the décollement is observed at ~805-920 mbsf and the bottom at ~840-950 mbsf (Fig. 4-12).

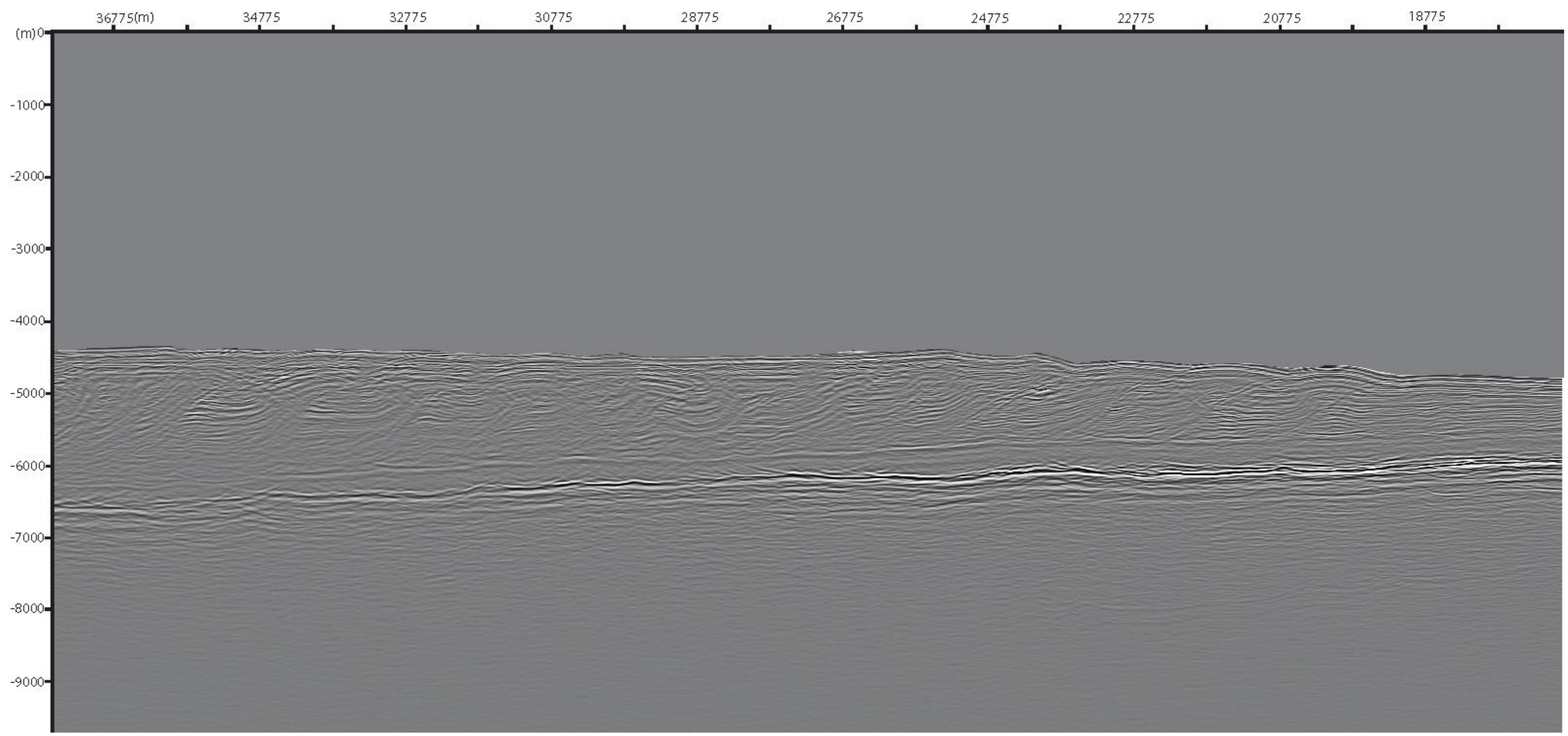

Figure 4-11. Non-Interpreted seismic section of the imbricated thrust zone of the Line 215. V.E. = 1:1

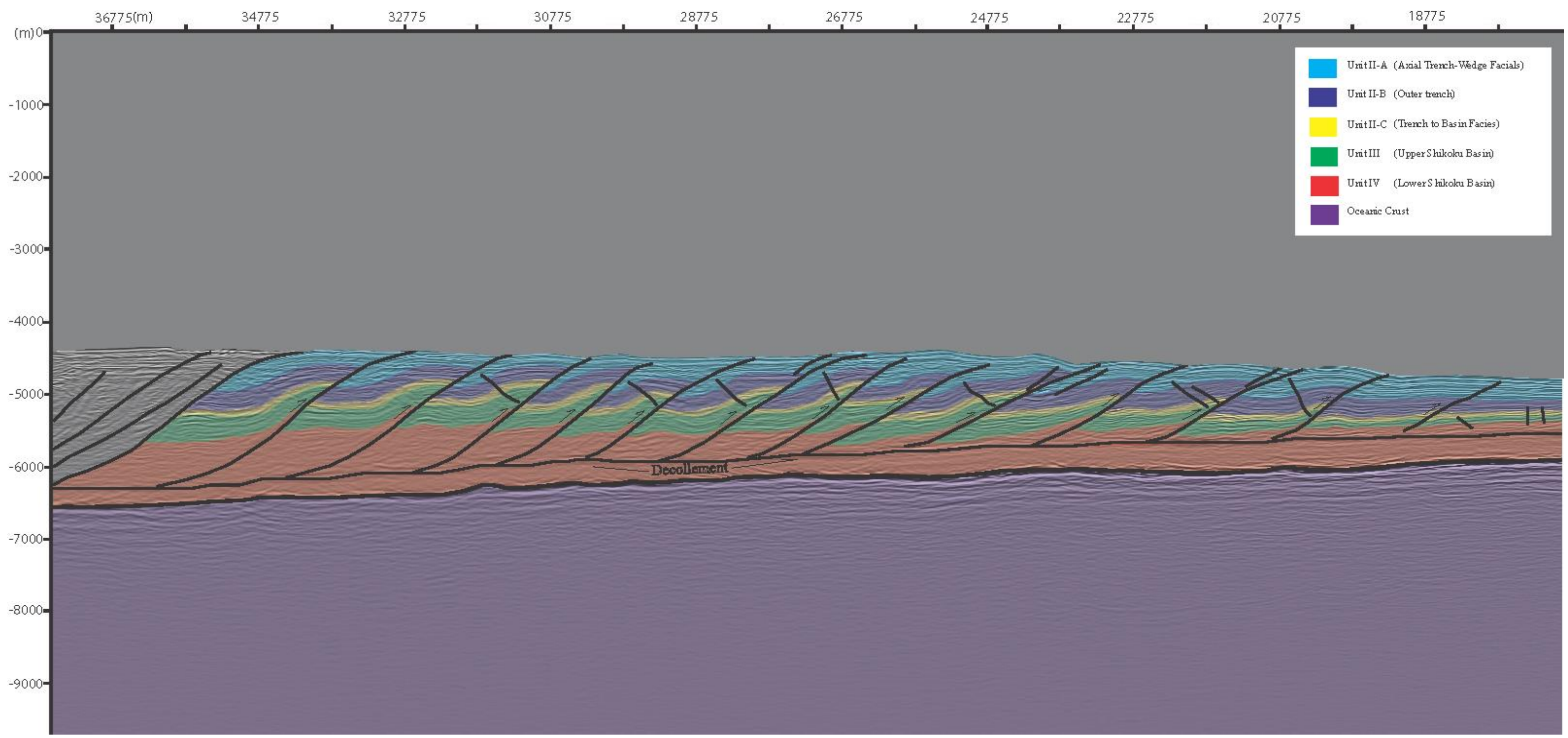

Figure 4-12. Interpreted seismic section of the Imbricated-Thrust-Zone of the Line 215. The interpretation of the sequence is done based on the Site 808 and 1174 from ODP Leg 190 and 196. The light blue unit represents Unit II-A (Axial Trench-Wedge Facies. Dark blue unit is Unit II-B (Out Trench Facies). Yellow unit is Unit II-C (Trench- Basin Facies). Green unit is Unit III (Upper Shikoku Basin). Red unit is Unit IV (Lower Shikoku Basin). Purple unit is the Oceanic Crust. V.E = 1:1

4-4-1-4. Out-of-Sequence Thrust Zone of Line 215

The out-of-sequence thrust zone (OOST) occurs landward of the imbricated thrust zone (ITZ) along the Muroto Transect (Fig. 4-14). Out-of-sequence thrust zones are caused by reactivation of older in-sequence thrusts or by the evolution of new thrust faults through a deformed thrust sheet (Morley, 1988).

On seismic Line 215, this section of the accretionary prism has ~2 km of thickness above the décollement at the frontal of the OOST zone. The zone thickens to the landward edge of OOST where it is ~4-5 km thick. Based on the interpretation of Line 215, the OOST system is highly thrusted and thickened by out-of-sequence thrusting. Moreover, the system has many splay faults, some of which branch from the décollement.

Based on the seismic interpretation, slope basins are present in the back of out-of-sequence thrust zone. The deepest point of the slope basin is determined ~450 m.

The brown section on figure 4-14 is interpreted as the out-of-sequence thrust system. The yellow section is interpreted as the slope basin. The red section is interpreted as subduction channel. The purple section is interpreted as the oceanic crust.

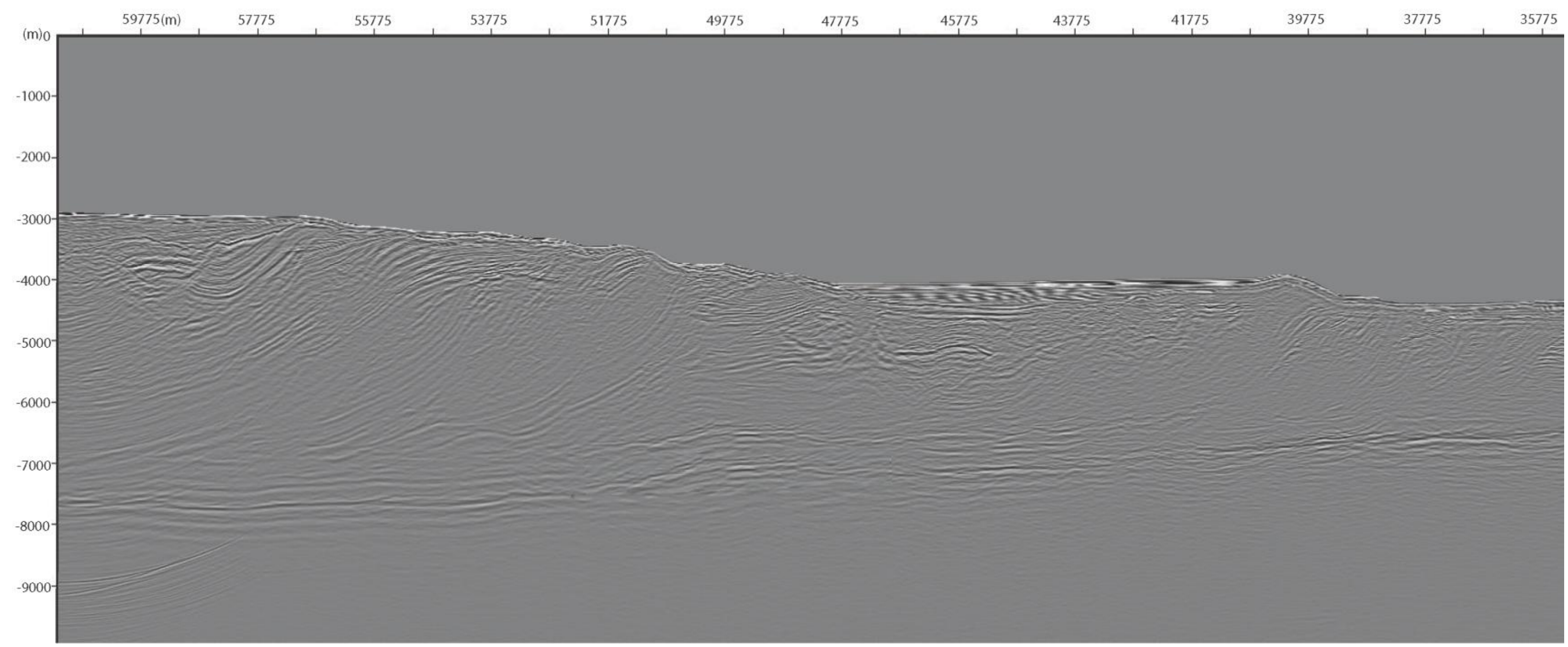

Figure 4-13. Non-interpreted seismic section of the OOST of the Line 215. V.E. = 1:1

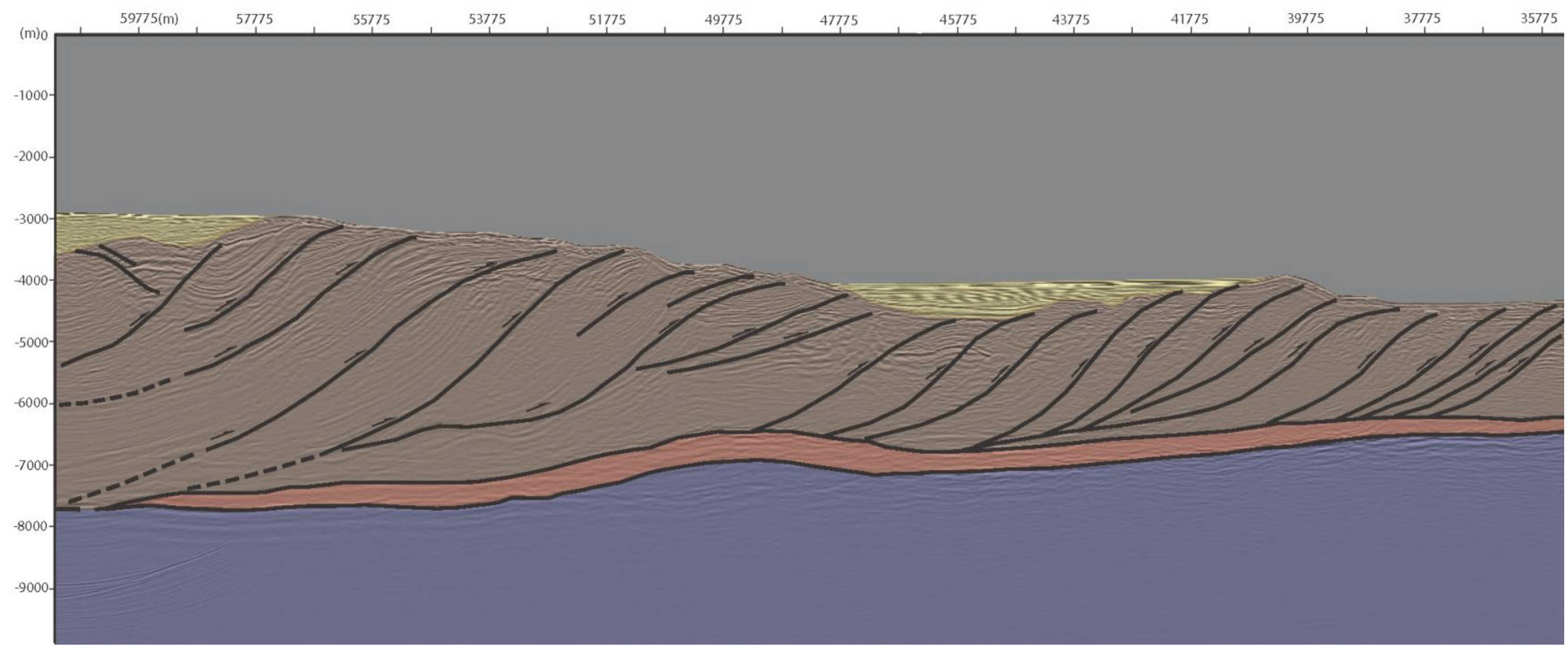

Figure 4-14. Interpreted seismic section of the OOST of the Line 215. The yellow colored part on the seismic slice illustrates slope basin. The brown colored part is shown all sequence of the OOST zone. The red colored part is the subduction channel. The channel shows between décollement and top of oceanic crust. The zone includes large thrust faults. The purple colored part is the oceanic crust. V.E. = 1:1

4-4-2. Line 260

4-4-2-1. Nankai Trough Trench Axial Zone of Line 260

Sediments above the basement reflector of the Nankai Trench contain turbidites overlying oceanic pelagic sediments (Shikoku Basin sequence). The pelagic sediment is nearly constant in thickness; however the overlying turbiditic trench sediments thin seaward. The Shikoku Basin sequence (Moore et al., 2001) is interpreted as the oceanic pelagic sequence above basement formed in the Shikoku trough prior to entering the subduction factory. This sequence is overlain by arc-derived turbiditic sequence deposited in the morphologic trench. The thickness of the wedge is ~500 m landward of the trench axial zone, and gradually decreases to ~100 m at the seaward edge of the trench wedge (Moore et al., 2001).

In this zone, the development of new faults is observed on the seismic section. Small, younger faults generally develop in the Unit III (Upper Shikoku Basin Facies) and IV (Lower Shikoku Basin Facies) which are right above the décollement. This is the indicator that the evolution of new faults begins near the décollement, and continues until the fault by reach the surface (Fig. 4-16).

A trench axial zone is interpreted based on the core samples from Sites 808 and 1174,. The light blue unit in figure 4-16 is Unit II-A (Axial Trench-Wedge Facies). The dark blue unit is Unit II-B (Outer Trench Facies). The yellow unit is Unit II-C (Trench to Basin Facies). The green unit is Unit III (Upper Shikoku Basin). The red unit is Unit IV (Lower Shikoku Basin). The purple unit is the oceanic crust.

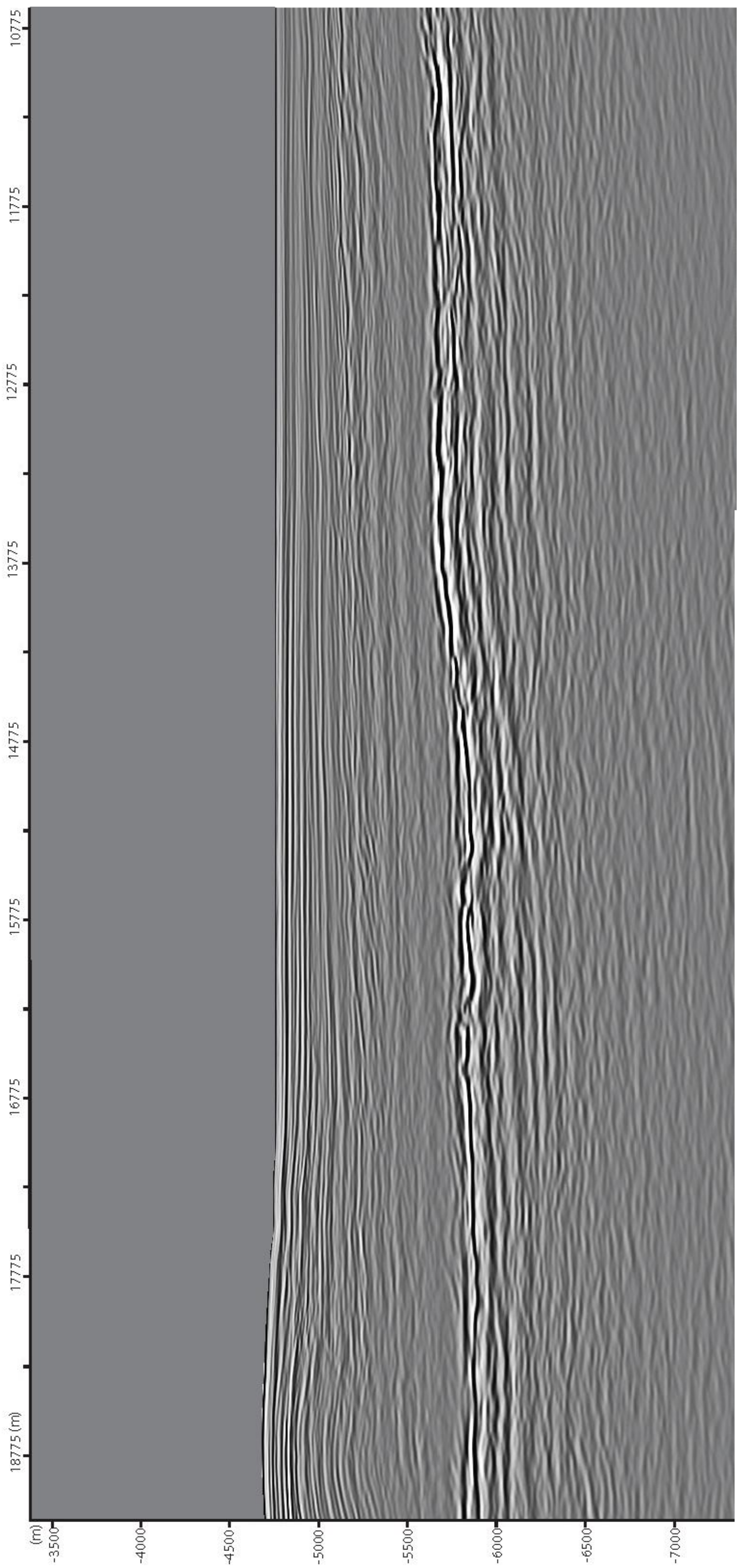

Figure 4-15. Non-interpreted seismic section of the axial-trench zone of the Line 260. V.E. = 1:1

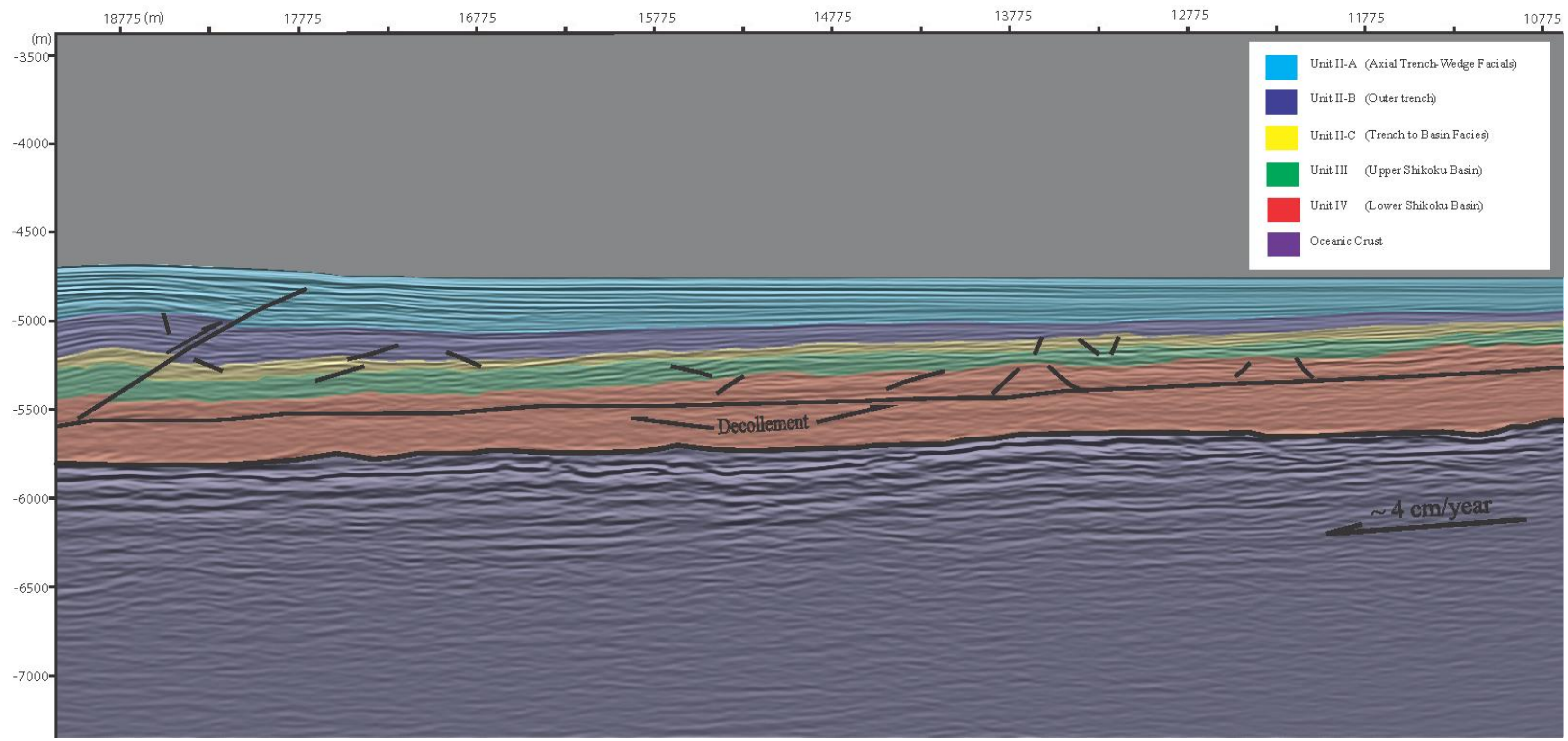

Figure 4-16. Interpreted seismic section of the axial-trench zone and proto-thrust zone of the Line 215. The interpretation of the sequence is done based on the Site 808 and 1174 from ODP Leg 190 and 196. The light blue unit represents Unit II-A (Axial Trench-Wedge Facies). The dark blue unit is Unit II-B (Out Trench Facies). The yellow unit is Unit II-C (Trench-Basin Facies). The green unit is Unit III (Upper Shikoku Basin). The red unit is Unit IV (Lower Shikoku Basin). The purple unit is the oceanic crust. V.E. = 1:1

4-4-2-2. Proto-thrust Zone (PTZ) of Line 260

Because of the subducting oceanic crust, the trench sediment and upper hemipelagic deposits which are overlying on the plate are stripped off and accreted to the overlying plate. The accretionary prism is subdivided into several structural features. One of those features which is located between the deformation front and frontal thrust, and is called the proto-thrust zone (PTZ) (Fig. 4-18).

This zone is characterized as an area where the initial deformation occurs and the décollement can first be seen on the seaward side of the trench. Because of more limited tectonic shortening, many small faults and some minor folding deformation are observed in this region. Moreover, based on this shortening, in addition to the landward increase in trench sediment thickness, structural thickening of the package by thrusting and folding begins in this zone (Morgan and Karig, 1995).

The proto-thrust zone is the zone where the new thrust faults develop. When the Trench Axial Zone is investigated, small-scale thrust faults which are close the décollement are observed. In this case, the fault development starts near the décollement area and it continues through the surface. Depending on the amount of upward progression, some of the faults in this zone are blind faults. Because the blind faults do not offset the surface, they are hard to observe (Dolan et al., 2003).

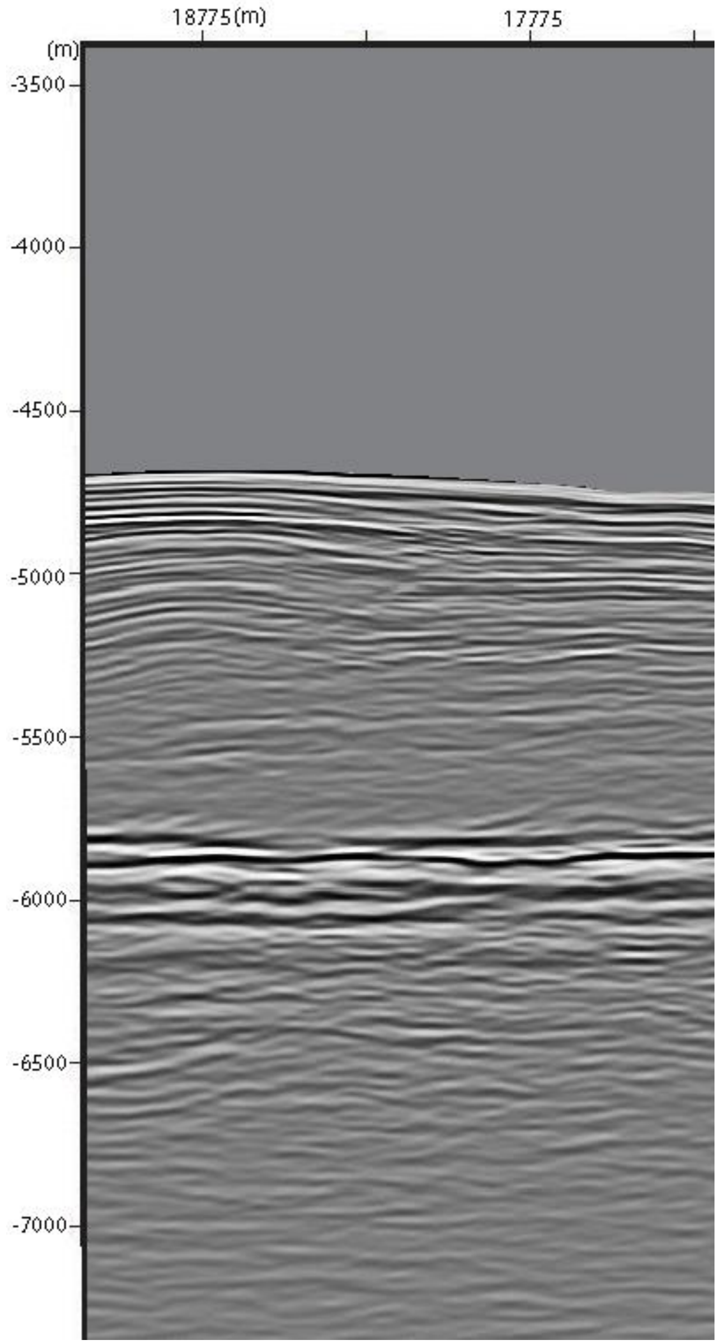

Figure 4-17. Non-interpreted seismic section of proto-thrust zone of the Line 260. V.E. = 1:1

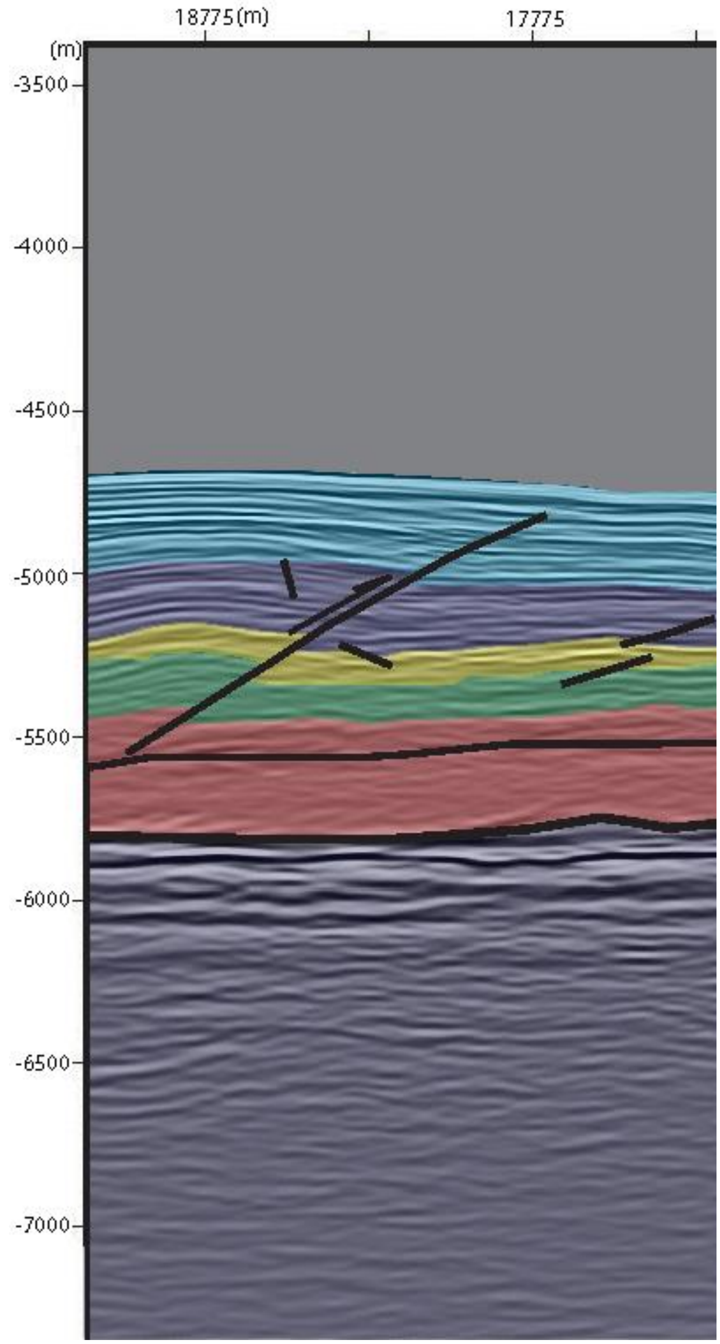

Figure 4-18. Interpreted seismic section of proto-thrust zone of the Line 260. The interpretation of the sequence is done based on the Site 808 and 1174 from ODP Leg 190 and 196. The light blue unit represents Unit II-A (Axial Trench-Wedge Facies). The dark blue unit is Unit II-B (Out Trench Facies). The yellow unit is Unit II-C (Trench- Basin Facies). The green unit is Unit III (Upper Shikoku Basin). The red unit is Unit IV (Lower Shikoku Basin). The purple unit is the Oceanic Crust. V.E. = 1:1

4-4-2-3. Imbricated Thrust Zone of Line 260

A well-formed imbricated thrust units occurs landward of the PTZ zone (ITZ) (Fig. 4-21). This zone is ~16 km wide and it consists of 13 thrust blocks, each of which is dipping ~30° landward. The thicknesses of the blocks vary between ~700-800 m. The most characteristic feature of these thrust packages is a hanging-wall anticline structure. This feature is observed through almost every one of the packages. Moreover, these thrust packages detach from the well-defined décollement which is developed ~200-300 m above the oceanic crust. On the seismic data, a well-developed Bottom-Sea-Reflector (BSR) can be observed along the imbricated thrust zone.

Along the ITZ of Line 260, anticlinal fault-bend folds are observed (Fig. 4-19). This structural feature develops because of that the hanging-wall of thrust fault moves over the fault surface and the sedimentary sequences of the hanging-wall are bent (Suppe, 1983).

Based on Sites 808 and 1174, the horizons of imbricated thrust zone of Line 260 are interpreted by considering the lithological units described in Chapter 3. This is because the region is geologically very young, and the stratigraphy is known by drilling. Based on the core data obtained from Sites 808 and 1174, most of the imbricated system of the Muroto Transect was developed during the Quaternary (Moore et al. 2001).

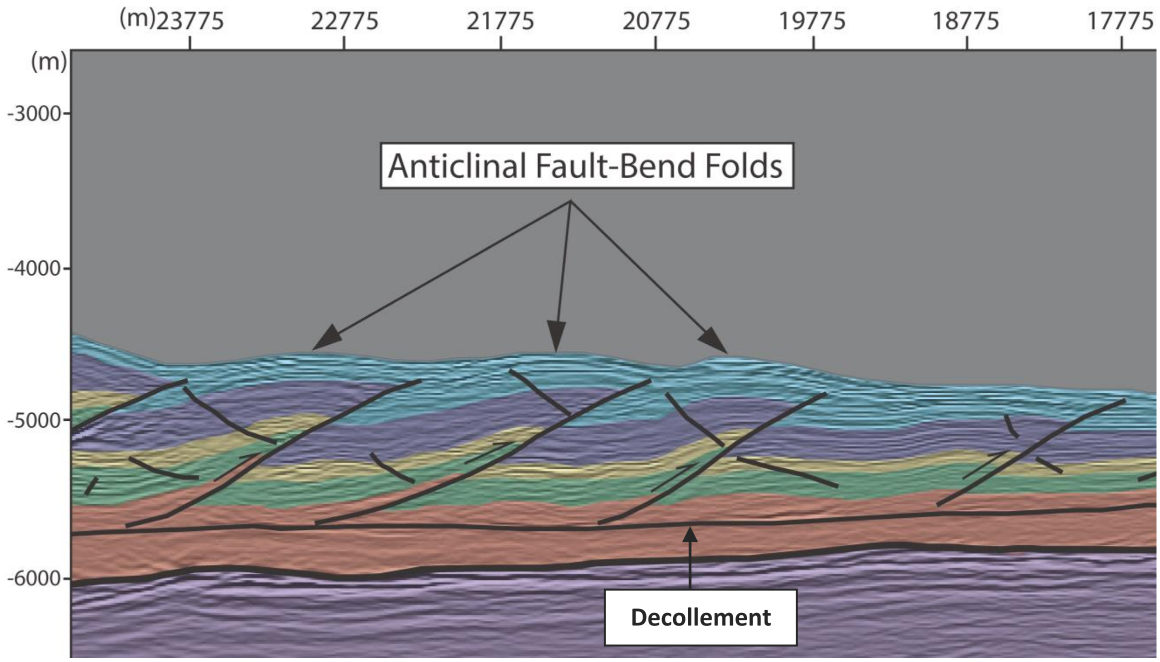

Figure 4-19. This seismic slice is taken from imbricated thrust zone of Line 260. Based on the fault interpretation, well-developed anticlinal fault-bend folds are observed on the seismic slice.

Therefore, the uppermost unit of the imbricated thrust zone which is colored light blue in figure 4-19 is Unit II-A (Axial Trench Wedge Facies). The unit consists of sandy, muddy sandy, and silty turbidites, and hemipelagic mud. The dark blue unit is Unit II-B which contains silt turbidites, hemipelagic mud interpreted as the Outer Trench Facies. The yellow colored unit is Unit II-C which underlies Unit II-B. This unit includes silty turbidites, volcanic ash and hemipelagic mud interpreted as Trench to Basin Facies. The next unit is the Unit III which is colored green. The unit consists of hemipelagic mudstone and abundant volcanic ash interpreted as Upper Shikoku Basin. Unit IV is present below Unit III, and it is colored red. This unit contains hemipelagic mudstone, rare siliceous claystone and rare calcareous claystone.

The unit, which is interpreted as lower Shikoku Basin, is divided by décollement. Along Line 260, the top of the décollement is observed at ~805 and ~920 mbsf and the bottom at ~840-950 mbsf (Fig. 4-21).

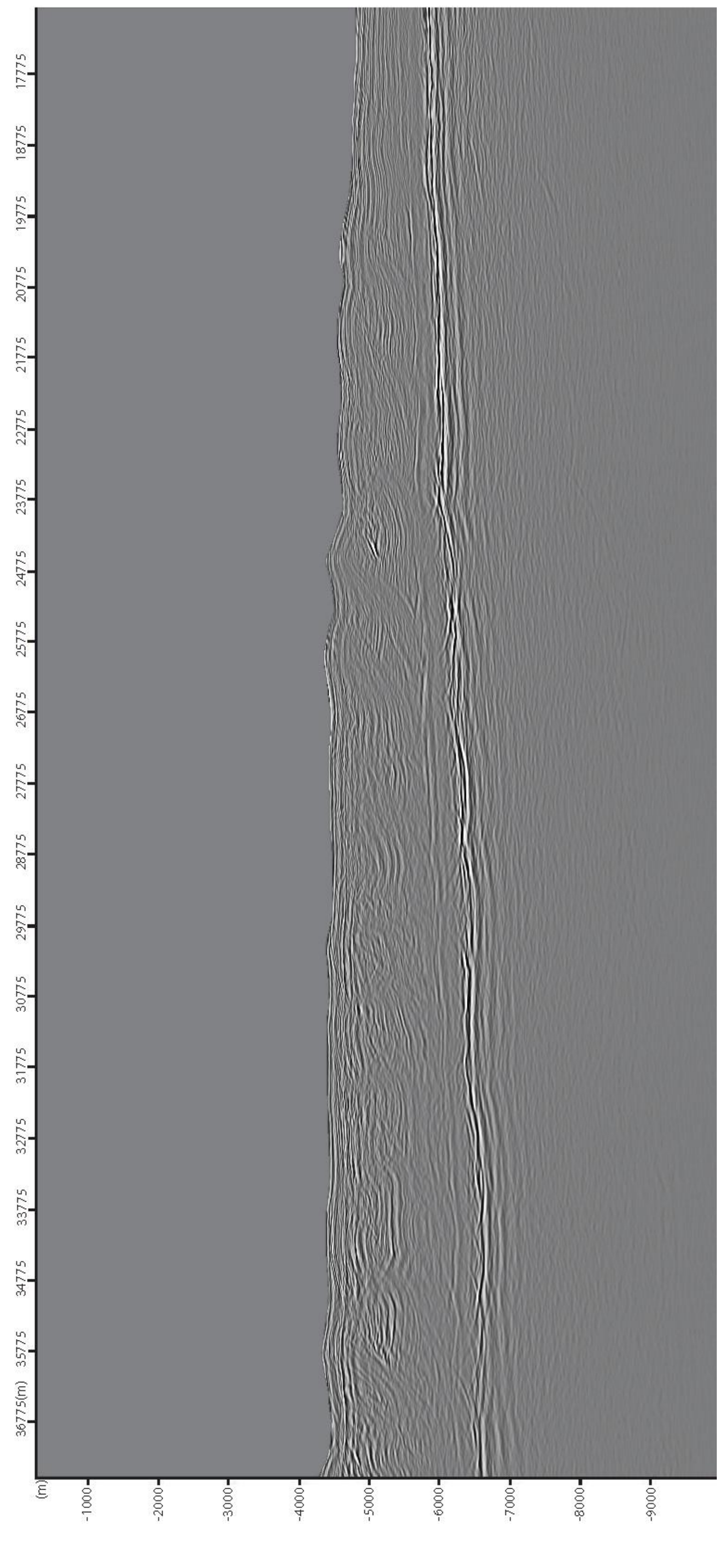

Figure 4-20. Non-Interpreted seismic section of the imbricated thrust zone of the Line 260. V.E. = 1:1

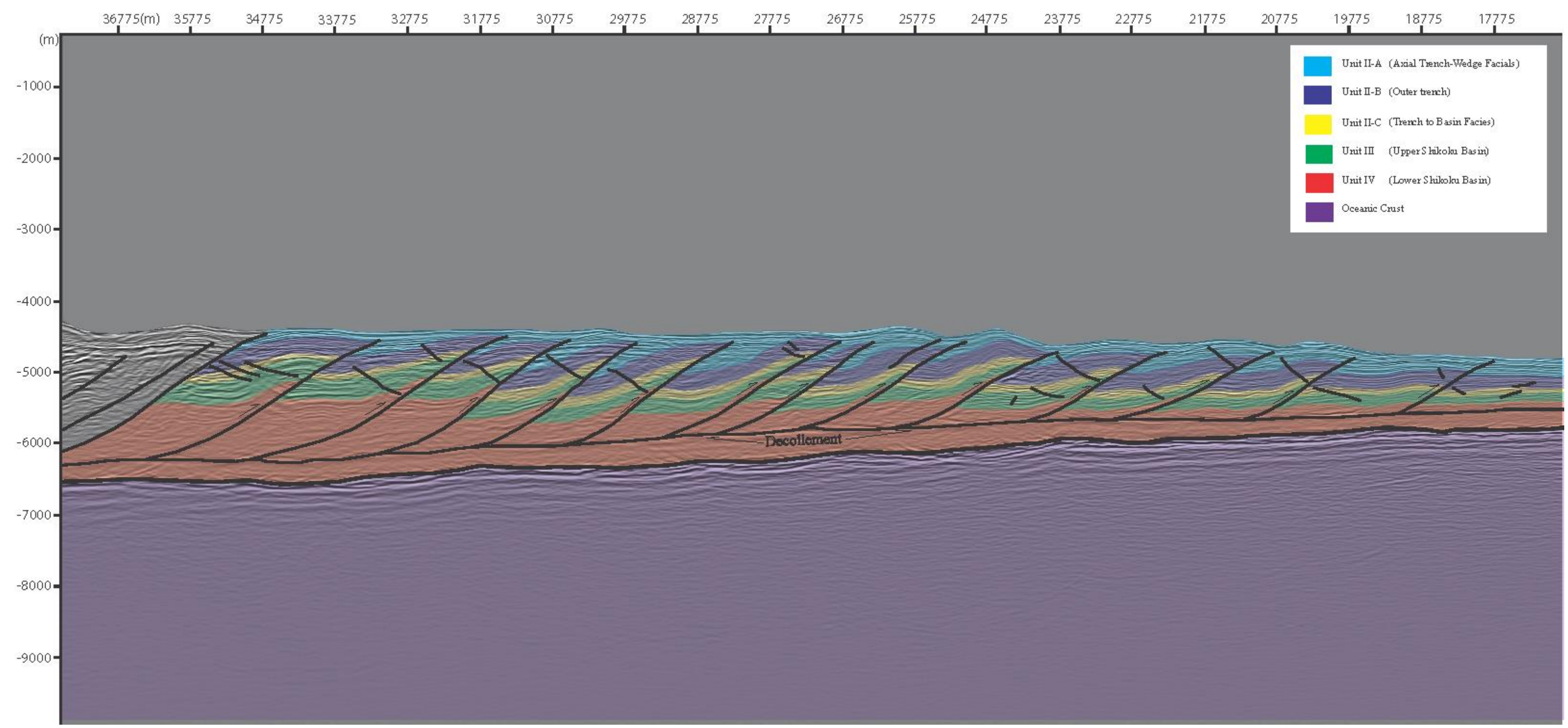

Figure 4-21. Interpreted seismic section of the imbricated thrust zone of the Line 260. The interpretation of the sequence is done based on the Site 808 and 1174 from ODP Leg 190 and 196. The light blue unit represents Unit II-A (Axial Trench-Wedge Facies). The dark blue unit is Unit II-B (Out Trench Facies). The yellow unit is Unit II-C (Trench- Basin Facies). The green unit is Unit III (Upper Shikoku Basin). The red unit is Unit IV (Lower Shikoku Basin). The purple unit is the Oceanic Crust. V.E = 1:1

4-4-2-4. Out-of-Sequence Thrust Zone of Line 260

The out-of-sequence thrust zone (OOST) occurs landward of ITZ along the Muroto Transect (Fig. 4-14). Out-of-sequence thrust zones are caused by reactivation of older in-sequence thrusts or by the evolution of new thrust faults through a deformed thrust sheet (Morley, 1988).

On seismic Line 260, this section of the accretionary prism has ~2 km of thickness above the décollement at the frontal of the OOST. The zone thickens to ~4-5 km at the landward edge of OOST zone. Based on the interpretation of Line 260, the OOST system is highly thrusted and thickened by out-of-sequence thrusting. Moreover, the system has many splay faults, some of which branch from the décollement.

Based on the seismic data, slope basins are present in the back of out-of-sequence thrust zone. On the seismic line, the deepest point of the slope basin is determined ~450 m. The subducted seamount is shown beneath the subduction channel. The height of seamount is ~1 km.

The brown section in figure 4-23 is interpreted as the out-of-sequence thrust system. The yellow section is interpreted as the slope basin. The red section is interpreted as subduction channel. The purple section is interpreted as the oceanic crust.

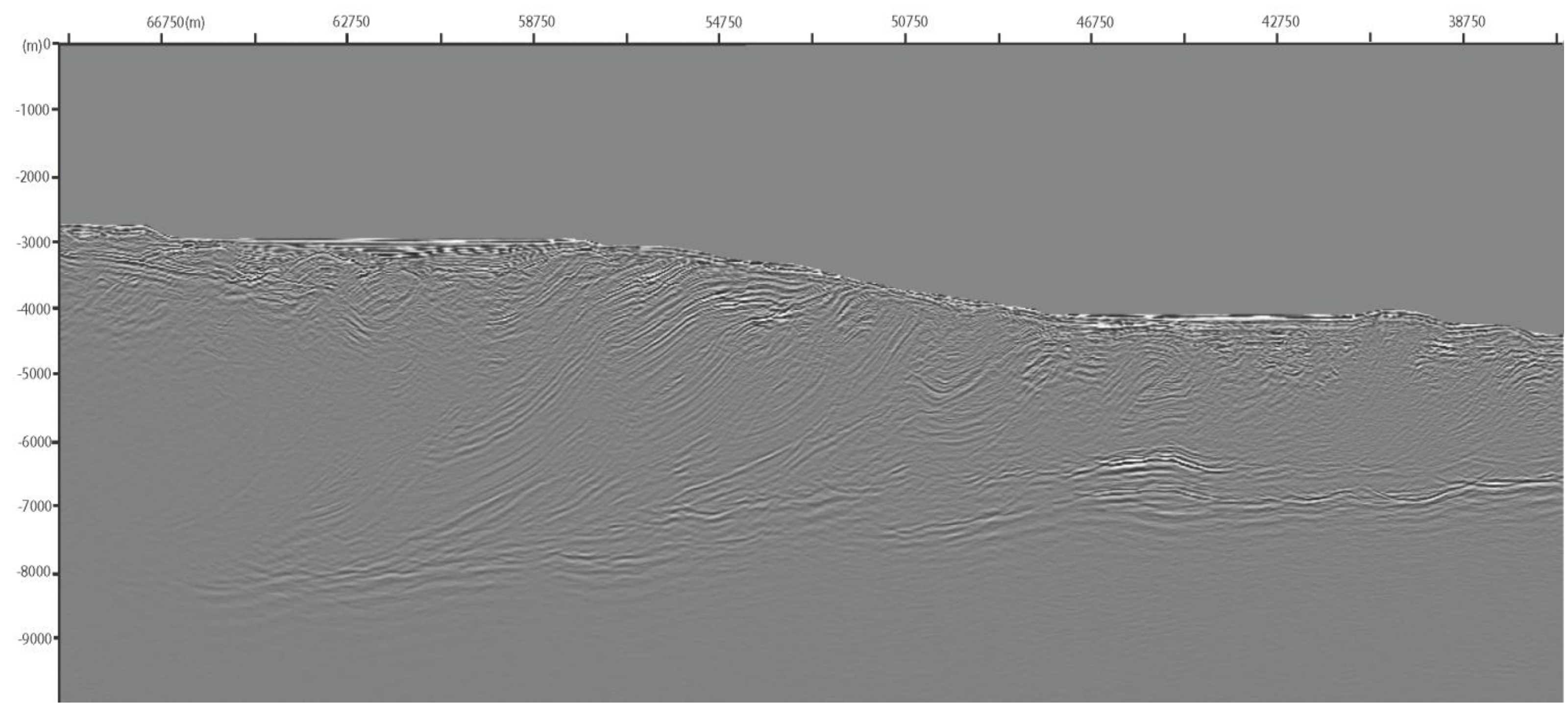

Figure 4-22. Non-interpreted seismic section of the OOST of the Line 260. V.E. = 1:1

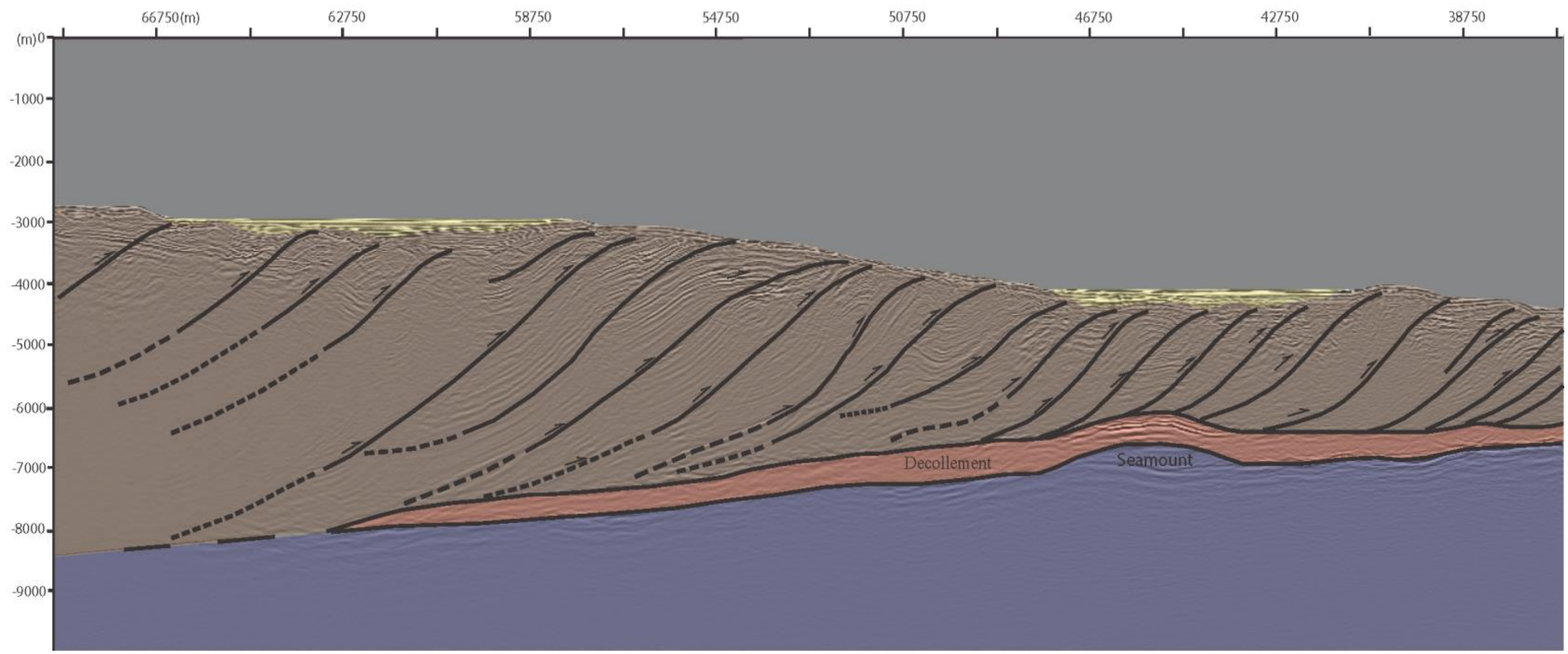

Figure 4-23. Interpreted seismic section of the OOST of the Line 260. The yellow colored part on the seismic slice illustrates slope basin. The brown colored part is shown all sequence of the OOST zone. The red colored part is the subduction channel. The channel shows between décollement and top of oceanic crust. The zone includes large thrust faults. The purple colored part is the oceanic crust. V.E. = 1:1

4-4-3. Line 284

4-4-3-1. Nankai Trough Trench Axial Zone of Line 284

Sediments above the basement reflector of the Nankai trench consist of turbidites overlying oceanic pelagic sediments (Shikoku Basin sequence). While the pelagic sediment are nearly constant in thickness, the overlying turbiditic trench sediments thin seaward. The Shikoku Basin sequence (Moore et al., 2001) is interpreted as the oceanic pelagic sequence above basement formed in the Shikoku trough prior to entering the subduction factory, which are overlain by arc-derived turbiditic sequence deposited in the morphologic trench. The thickness of the wedge is ~500 m landward of the trench axial zone, and gradually decreases to ~100 m through the seaward edge of the trench.

In the axial trench zone, the development of new faults is observed on the seismic section. The small faults generally develop in the Unit III (Upper Shikoku Basin Facies) and IV (Lower Shikoku Basin Facies), which are right above the décollement. This is the indicator that the evolution of new faults starts near the décollement and continues until reach the surface (Fig. 4-25).

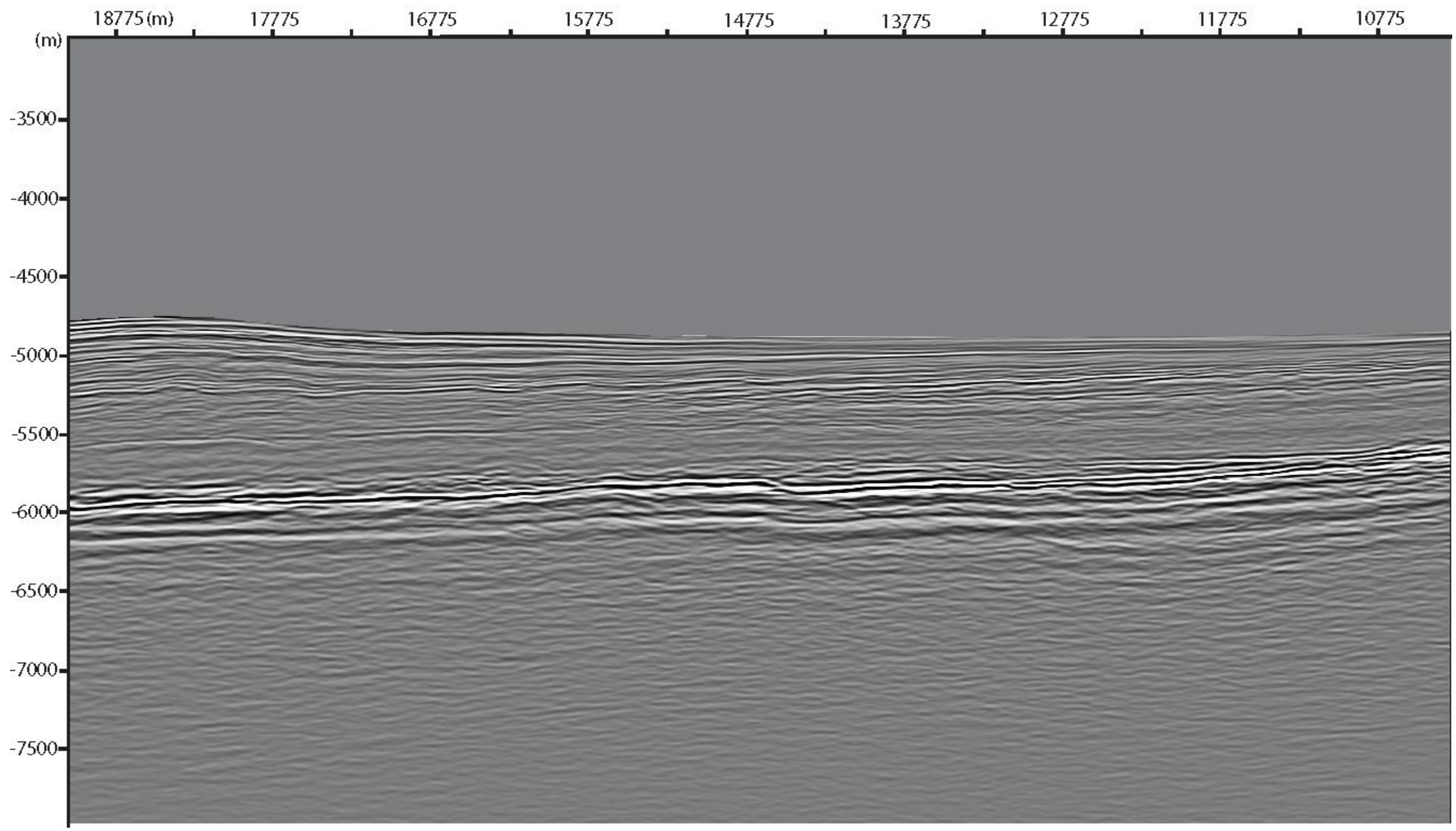

Figure 4-24. Non-interpreted seismic section of the axial-trench zone of the Line 284. V. E. = 1:1

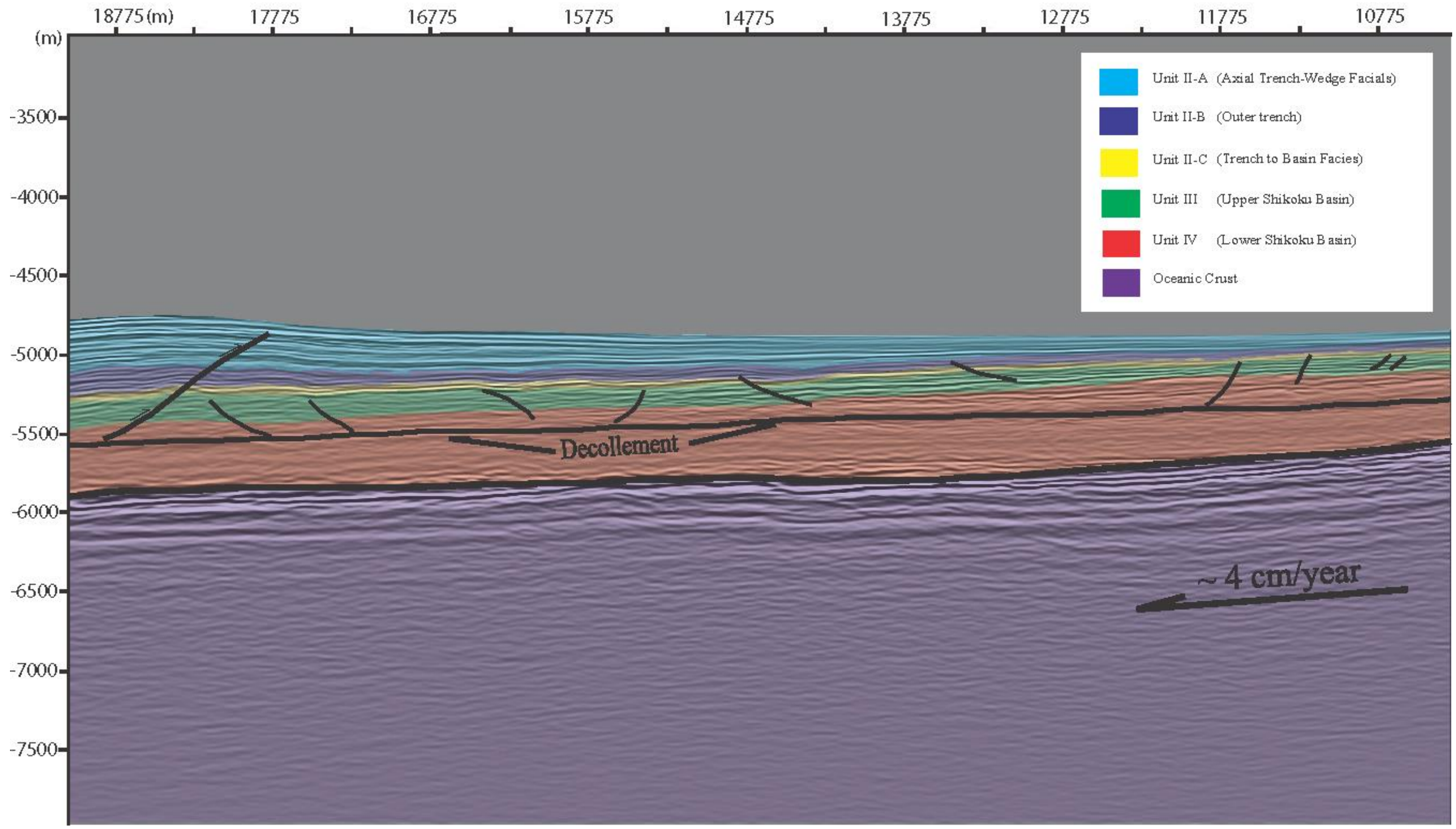

Figure 4-25. Interpreted seismic section of the Axial-Trench-Zone and Proto-Thrust-Zone of the Line 284. The interpretation of the sequence is done based on the Site 808 and 1174 from ODP Leg 190 and 196. The light blue unit represents Unit II-A (Axial Trench-Wedge Facies. Dark blue unit is Unit II-B (Out Trench Facies). Yellow unit is Unit II-C (Trench- Basin Facies). Green unit is Unit III (Upper Shikoku Basin). Red unit is Unit IV (Lower Shikoku Basin). Purple unit is the Oceanic Crust. V.E. = 1:1

4-4-3-2. Proto-thrust Zone (PTZ) of Line 284

Because of the subducting oceanic crust, the trench sediment and upper hemipelagic deposits which are lying on the plate are stripped off and accreted to the overlying plate. The accretionary prism is sub-divided into several structural features. One of the features is located between deformation front and frontal thrust, and is called Proto-Thrust Zone (PTZ) (Fig. 4-27).

This zone is characterized as an area where the initial deformation occurs and the décollement can first be seen on the seaward side of the trench. Because of more limited tectonic shortening, many small faults and some minor folding deformation are observed in this region. Moreover, based on this shortening, in addition to trench sediment thicknesses increasing landward, structural thickening of the package by thrusting and folding begins in this zone (Morgan and Karig, 1995).

The proto-thrust zone is the zone where the new thrust faults develop. When the trench axial zone is investigated, small-scale thrust faults which are close the décollement are observed. In this case, the fault development starts near the décollement area and it continues through the surface. Depending on the amount of upward progression, some of the faults in this zone are blind faults. Because the blind faults do not offset the surface, they are hard to observe (Dolan et al., 2003).

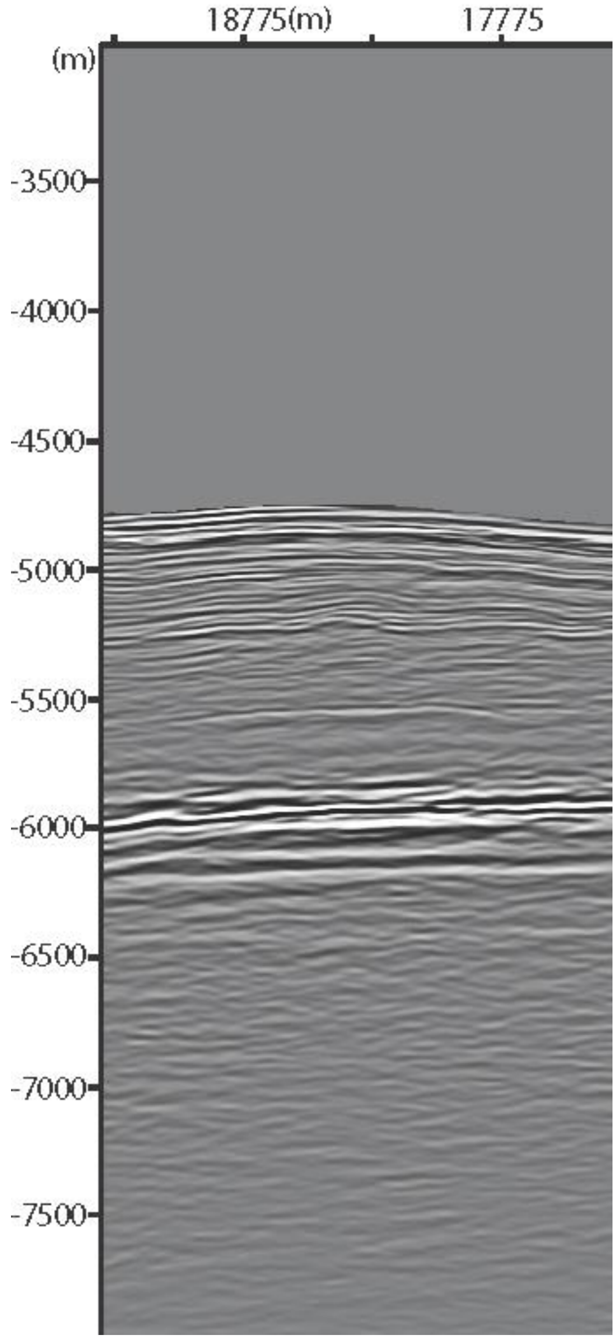

Figure 4-26. Non-interpreted seismic section of Proto-Thrust Zone of the Line 284. V.E. = 1:1

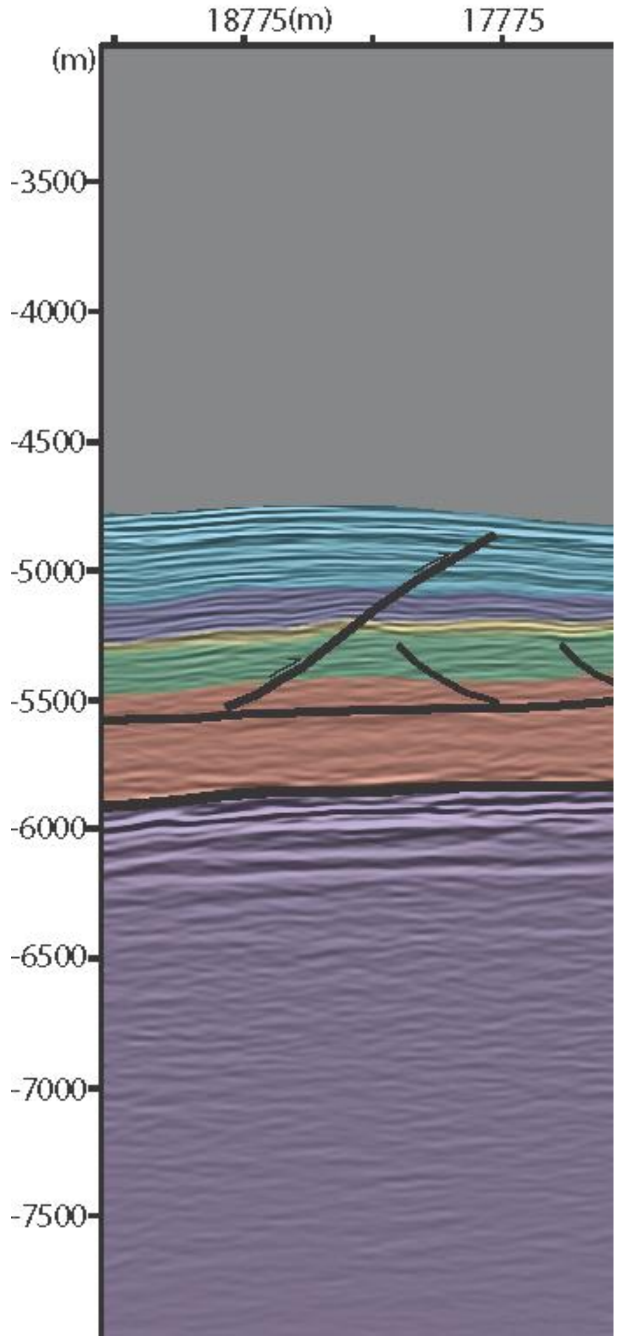

Figure 4-27. Interpreted seismic section of proto-thrust zone of the Line 284. The interpretation of the sequence is done based on the Site 808 and 1174 from ODP Leg 190 and 196. The light blue unit represents Unit II-A (Axial Trench-Wedge Facies). The dark blue unit is Unit II-B (Out Trench Facies). The yellow unit is Unit II-C (Trench- Basin Facies). The green unit is Unit III (Upper Shikoku Basin). The red unit is Unit IV (Lower Shikoku Basin). The purple unit is the Oceanic Crust. V.E. = 1:1

4-4-3-3. Imbricated Thrust Zone of Line 284

A zone, well-formed imbricated thrust faults (ITZ), occurs landward of the PTZ zone (Fig. 4-30). This zone is ~16 km wide and it consist of 13 thrust blocks, each one of which dips ~30° landward. The thicknesses of the blocks vary between ~700-800 m. The most characteristic feature of these thrust packages is a hanging-wall anticline structure. This feature is observed in almost every one of the packages. Moreover, these thrust packages detach from the well-defined décollement which is developed ~200-300 m above the oceanic crust. On the seismic data, a well-developed Bottom-Sea-Reflector (BSR) can be observed along the imbricated thrust zone.

According to Suppe (1983), because the fault surface is not planar, deformation occurs on at least one of the fault block when they slip past one another, and the rocks are not durable enough to fill the large gap. The layered rocks which are layered might fold because of the mechanism of riding over the bend in a fault. The mechanism of folding is called fault-bend fault. This type of mechanism is generally observed in thrust-fold belts and accretionary prisms (Tavani et al., 2006).

The anticlinal fault-bend folds are observed, within the ITZ of Line 284 (Fig. 4-28). This structural feature develops because of that the hanging-wall of thrust fault moves over the fault surface and the sedimentary sequences of the hanging-wall are bending (Suppe, 1983).

Based on Sites 808 and 1174, the horizons within the imbricated thrust zone on Line 284 are interpreted by considering the lithological units described in Chapter 3. This is because the region is very young geologically, and the stratigraphy is known by drilling. Based on the core data obtained from Sites 808 and 1174, most of the imbricated system of the Muroto Transect was developed throughout the Quaternary.

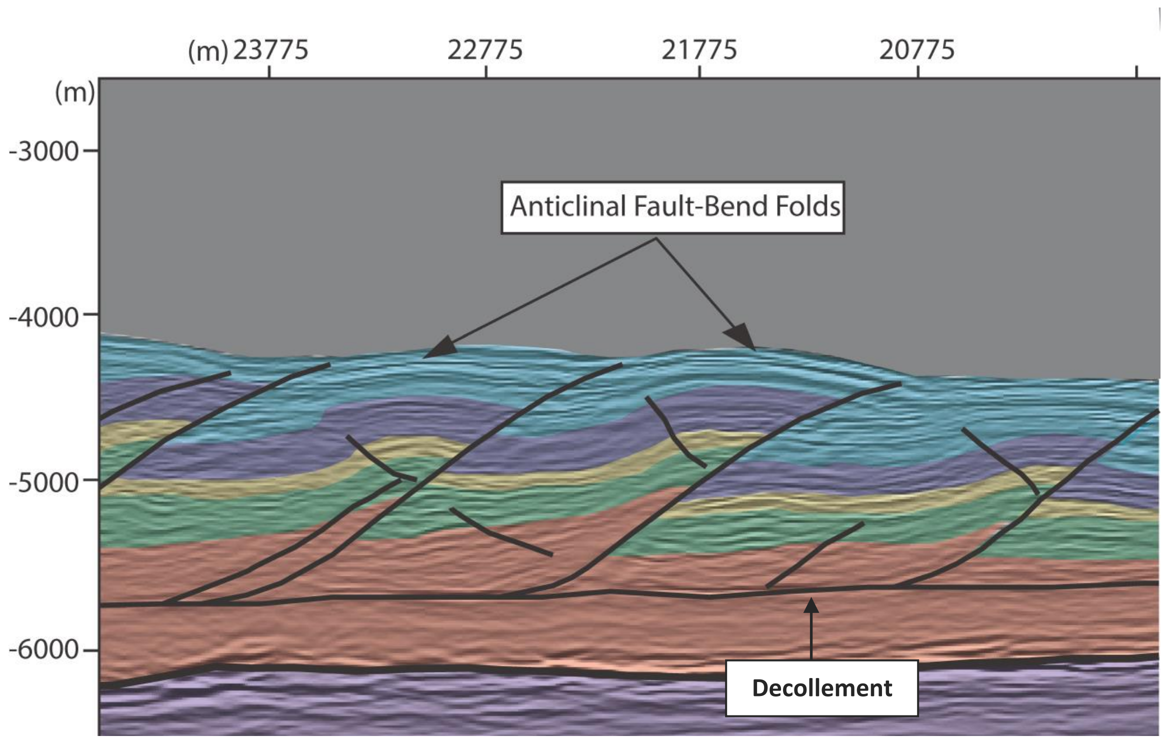

Figure 4-28. This seismic slice is gotten from imbricated thrust zone of Line 284. Based on the fault interpretation, well-developed anticlinal fault-bend folds are observed on the seismic slice.

Therefore, the uppermost unit of the imbricated thrust zone, which is colored light blue in figure 4-30 is called Unit II-A (Axial Trench Wedge Facies). The unit consists of sandy, muddy sandy, and silty turbidites, and hemipelagic mud. The second unit in the system, which is colored dark blue, is Unit II-B, which contains silty turbidites, hemipelagic mud interpreted as the Outer Trench Facies. Beneath Unit II-B is Unit II-C, which is colored yellow. This unit includes silty turbidites, volcanic ash, and hemipelagic mud interpreted as Trench to Basin Facies. Additionally, the next unit is Unit III which is illustrated green. The unit consists of hemipelagic mudstone and abundant volcanic ash interpreted as Upper Shikoku Basin. Below Unit III is Unit IV, which is colored red. The unit contains hemipelagic mudstone, rare siliceous claystone and rare calcareous claystone. The unit which is interpreted as lower Shikoku Basin is divided by the décollement surface. Along Line 284, the décollement occurs from ~805 to ~920 mbsf for top of the décollement and the bottom ~840-950 mbsf for bottom of the décollement along the Line 284 (Fig. 4-30).

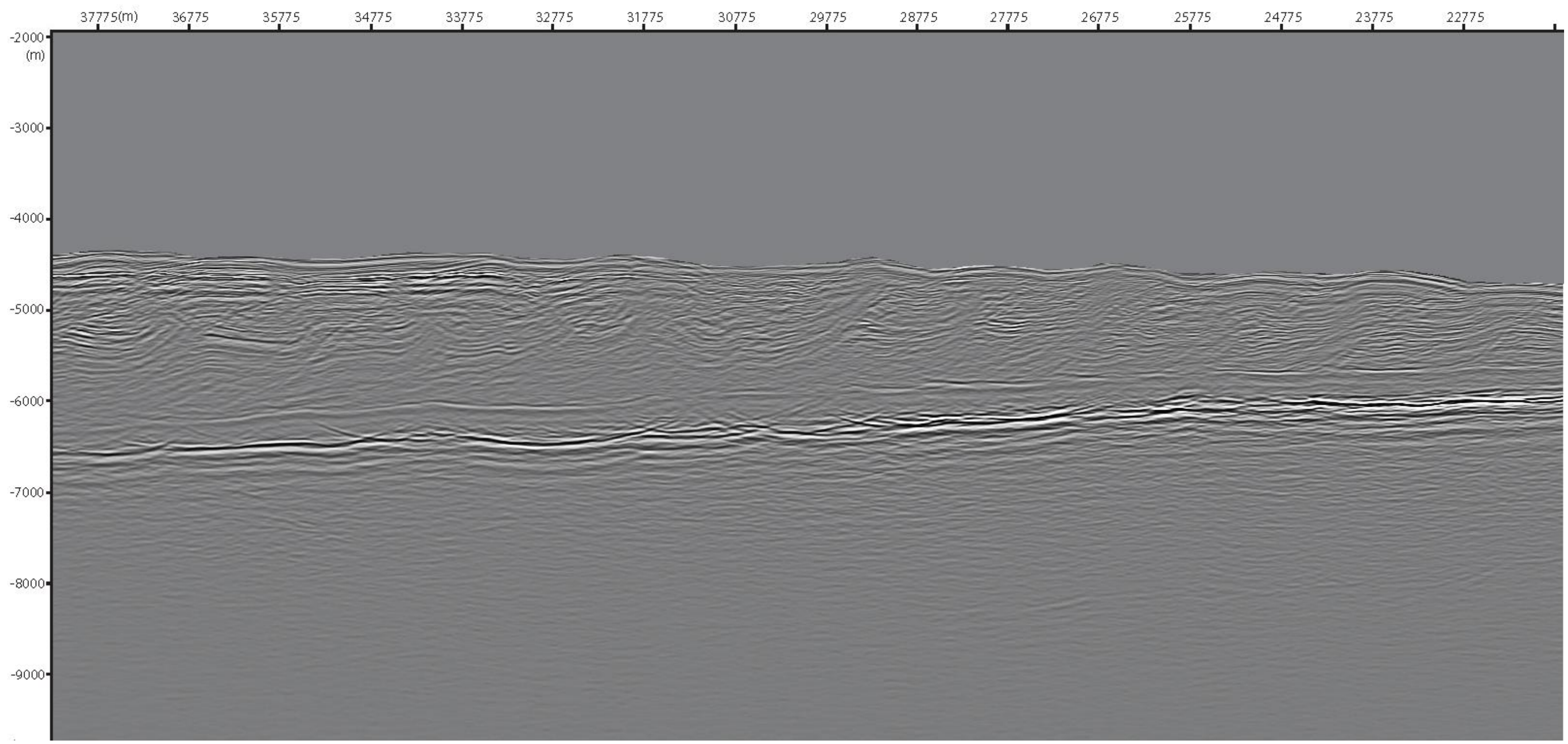

Figure 4-29. Non-Interpreted seismic section of the imbricated thrust zone of the Line 284. V.E. = 1:1

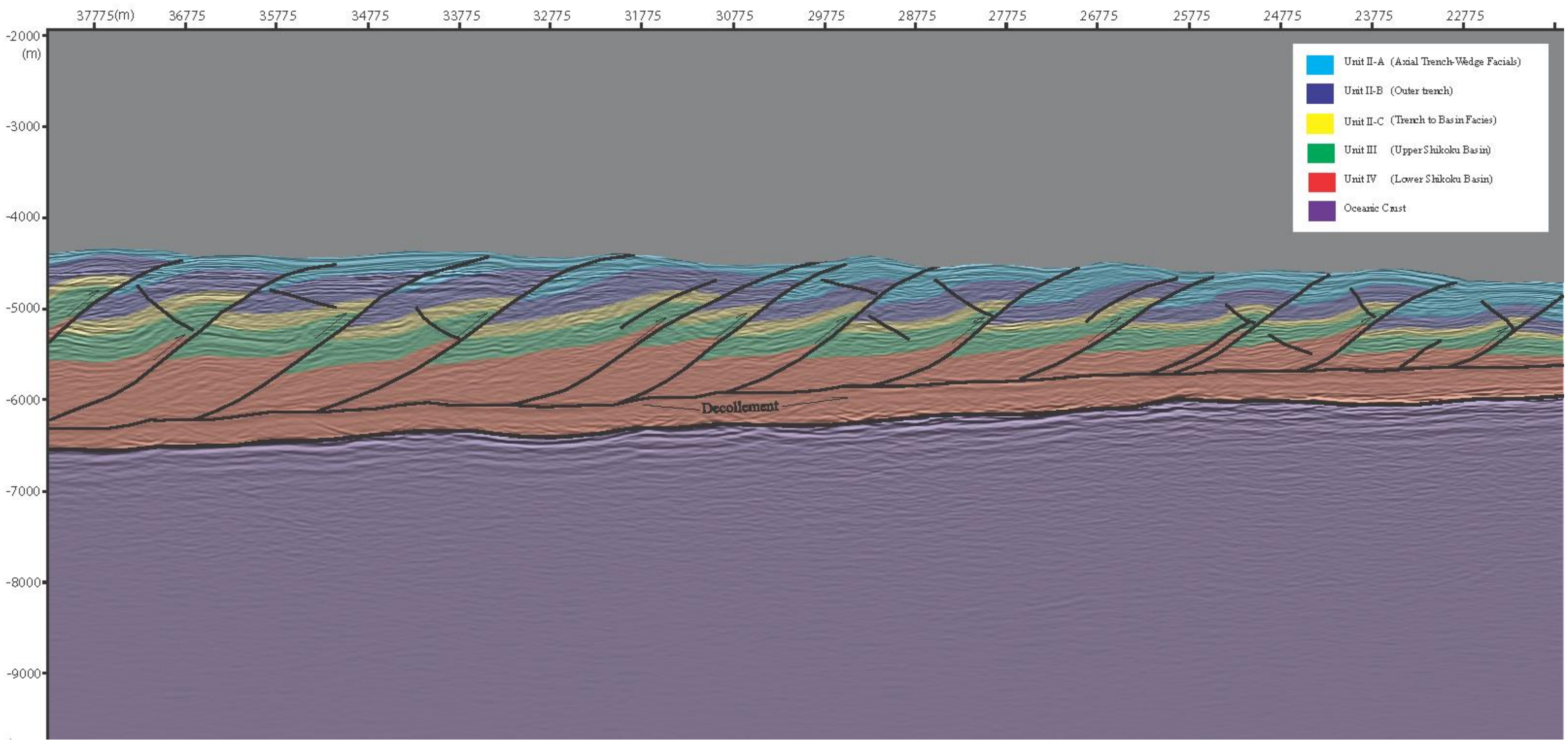

Figure 4-25. Interpreted seismic section of the imbricated thrust zone of the Line 284. The interpretation of the sequence is done based on the Site 808 and 1174 from ODP Leg 190 and 196. The light blue unit represents Unit II-A (Axial Trench-Wedge Facies. Dark blue unit is Unit II-B (Out Trench Facies). Yellow unit is Unit II-C (Trench- Basin Facies). Green unit is Unit III (Upper Shikoku Basin). Red unit is Unit IV (Lower Shikoku Basin). Purple unit is the Oceanic Crust. V.E. = 1:1

4-4-3-4. Out-of-Sequence Thrust Zone of Line 284

The out-of-sequence thrust zone (OOST) is landward of the imbricated thrust zone along the Muroto Transect (Fig. 4-14). Out-of-sequence thrust zones are caused by reactivation of older in-sequence thrusts or by the evolution of new thrust faults through a deformed thrust sheet (Morley, 1988).

On seismic Line 284, this section of the accretionary prism has ~2 km of thickness above the décollement at the frontal edge of the OOST. This thickens to ~4-5 km at the landward edge of OOST. Based on the interpretation of Line 284, the system is highly thrusted and thickened by out-of-sequence thrusting, superimposed on a prior history of in-sequence thrusting. The system has many splay faults, some of which branch from the décollement.

Based on the seismic data, slope basins were discovered in the back portion of the out-of-sequence thrust zone. On the seismic line, the deepest point of the slope basin is ~450 mbsf. The subducted seamount is shown beneath the subduction channel. The height of the seamount is ~1km.

The brown section on figure 4-32 is interpreted as the out-of-sequence thrust system. The yellow section is interpreted as the slope basin. The red section is interpreted as subduction channel. The purple section is interpreted as the oceanic crust.

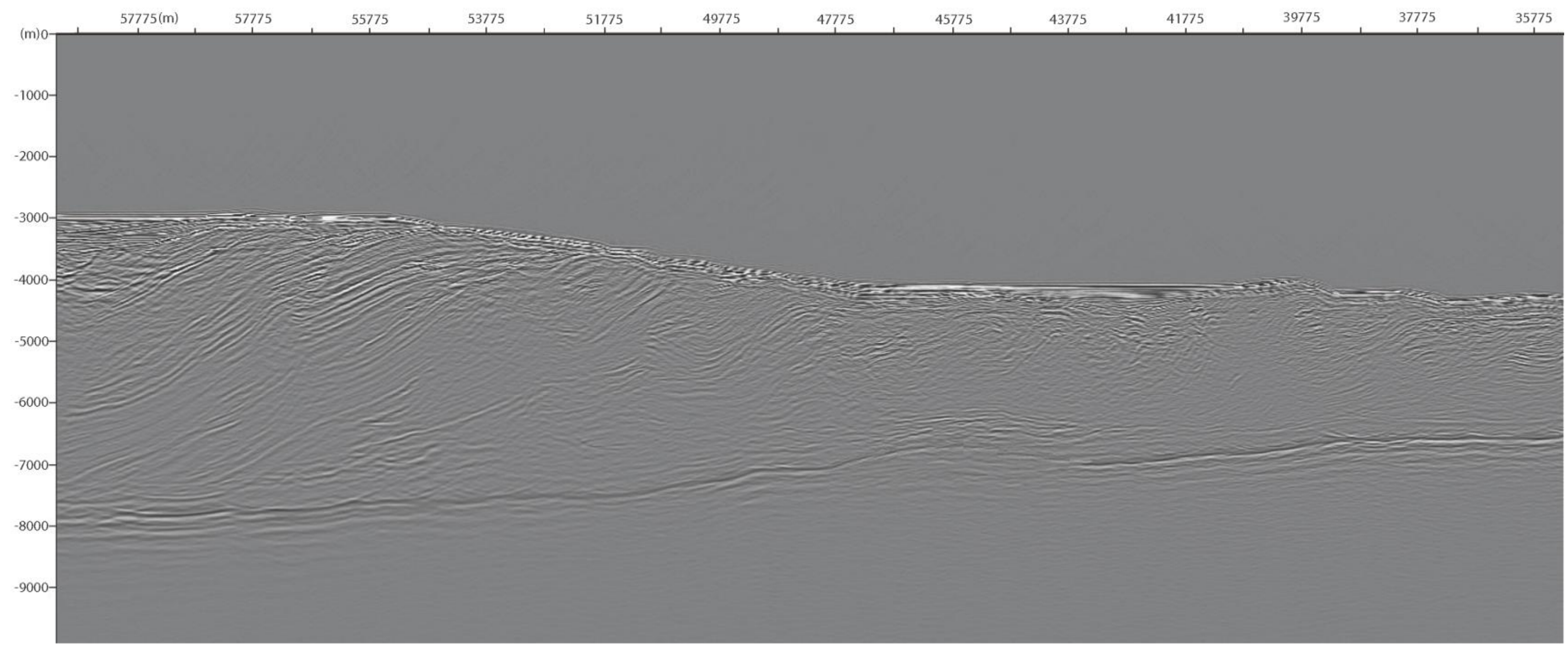

Figure 4-31. Non-interpreted seismic section of the OOST on Line 284. V.E.= 1:1

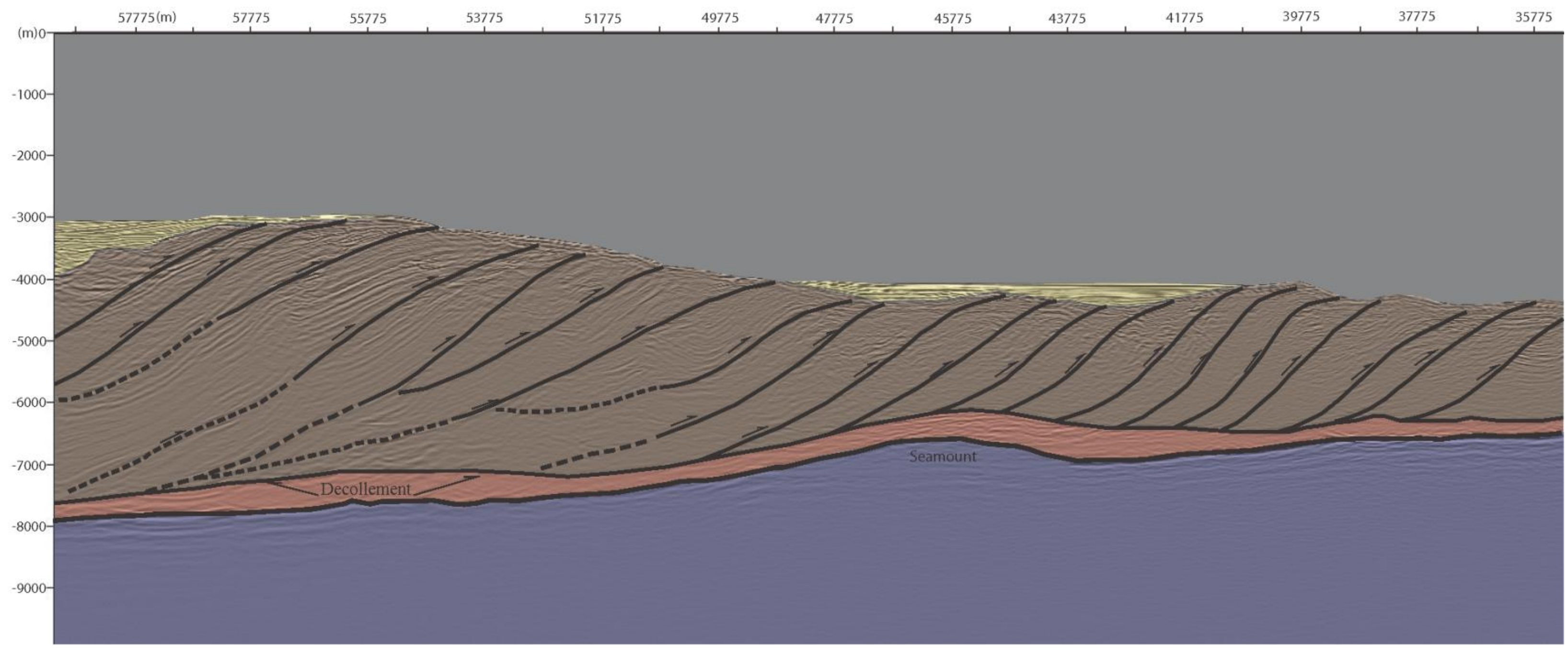

Figure 4-32. Interpreted seismic section of the OOST on Line 284. The yellow colored part on the seismic slice illustrates slope basin. The brown colored part is shown all sequence of the OOST's zone. The red colored part is the subduction channel. The channel shows between décollement and top of oceanic crust. The zone includes large thrust faults. The purple colored part is the oceanic crust. V.E. = 1:1

4-5. The Boundary of the ITZ and OOST

The imbricated thrust system and out-of-sequence thrust system are divided by the subducted seamount. While the seamount subducted into the accretionary prism, the fault which is a boundary between the imbricated thrust system and out-of-sequence thrust system, was reactivated due to the subducted seamount into the out-of-sequence thrust system. The 3D seismic volume and the slope angle bathymetry (Fig. 4-34) clearly illustrate the distinction between the imbricated thrust system and out-of-sequence thrust system.

The model (Fig. 4-33) describes the evolution of the Muroto Transect based on the subducted seamount. In figure 4-33 (A) the seamount starts to subduct into the accretionary prism. At this stage, the accretionary prism is in satiable condition. In figure 4-33 (B), the seamount continues to subduct into the prism. The present imbricated thrust system initiated to develop behind the subducted seamount in this stage. The previous thrust faults are reactivated in this stage. Finally, in figure 4-33 (C), the reactivated thrust fault cuts off the Quaternary sediment which are deposited above the accretionary prism. Then, the slope basin develops over the out-of-sequence system.

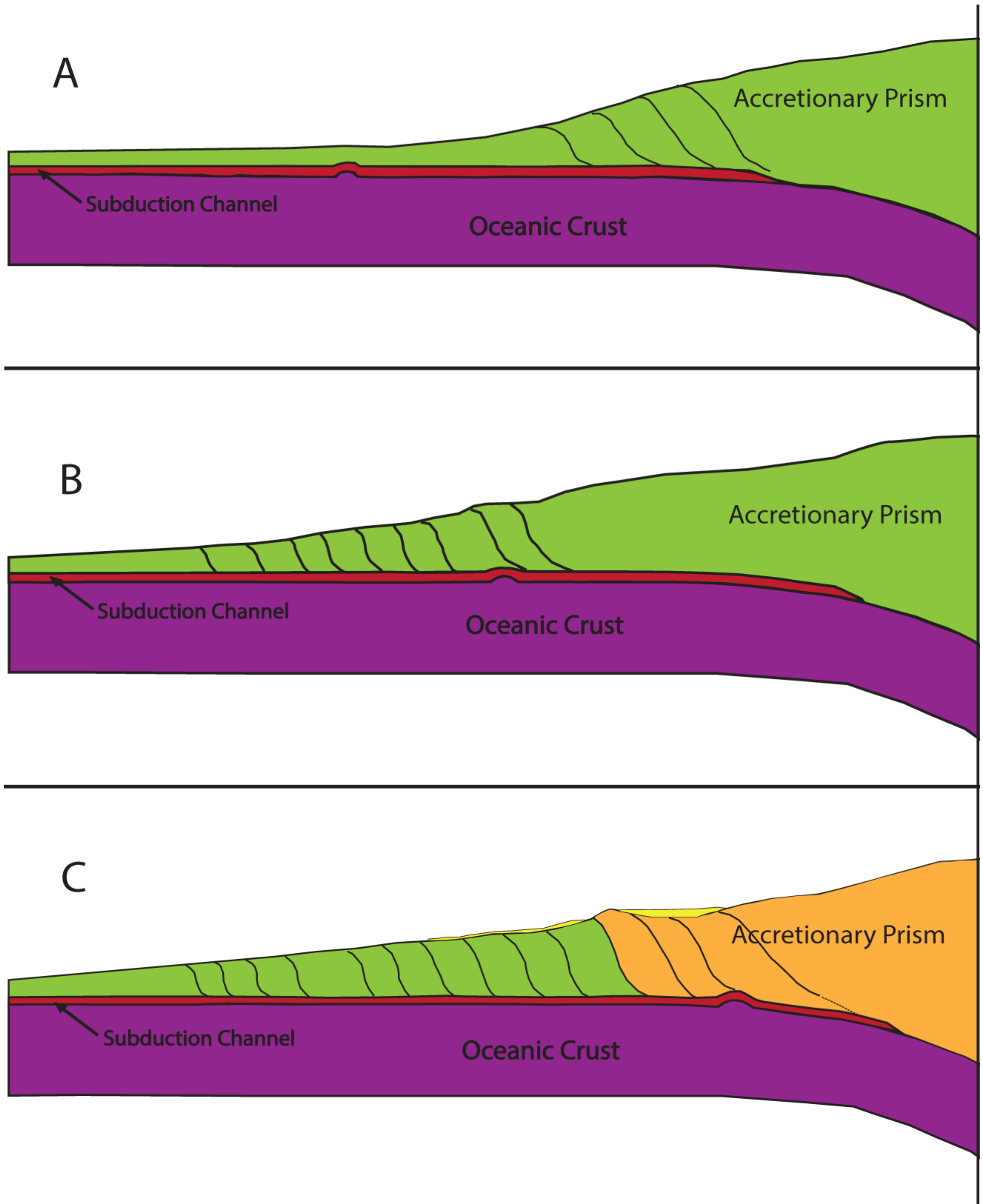

Figure 4-33. The modeling of the subducted seamount into the accretionary prism. Top figure (A) illustrates the accretionary prism before the seamount subducted. The middle figure (B) shows while the seamount subducted into the prism, and it reactivates the previous thrust faults. The bottom figure (C) represents the present condition of the accretionary prism. The green colored section is imbricated thrust system and the orange colored is the out-of-sequence thrust system.

On the seismic slices of the out-of-sequence thrust system, the reactivated thrust fault separated the out-of-sequence system from the imbricated thrust system (Fig 4-34 and 4-35). The fault started to grow and it cuts the Quaternary deposits when the seamount subducted into the out-of-sequence thrust system. Then, the slope basin developed over the system (Fig. 4-34 and 4-35).

Based on the seismic interpretation, the tips of the many large thrust faults reach the seafloor in the out-of-sequence thrust system (Fig. 4-36). This circumstance indicates that the faults are reactive in the out-of-sequence thrust zone.

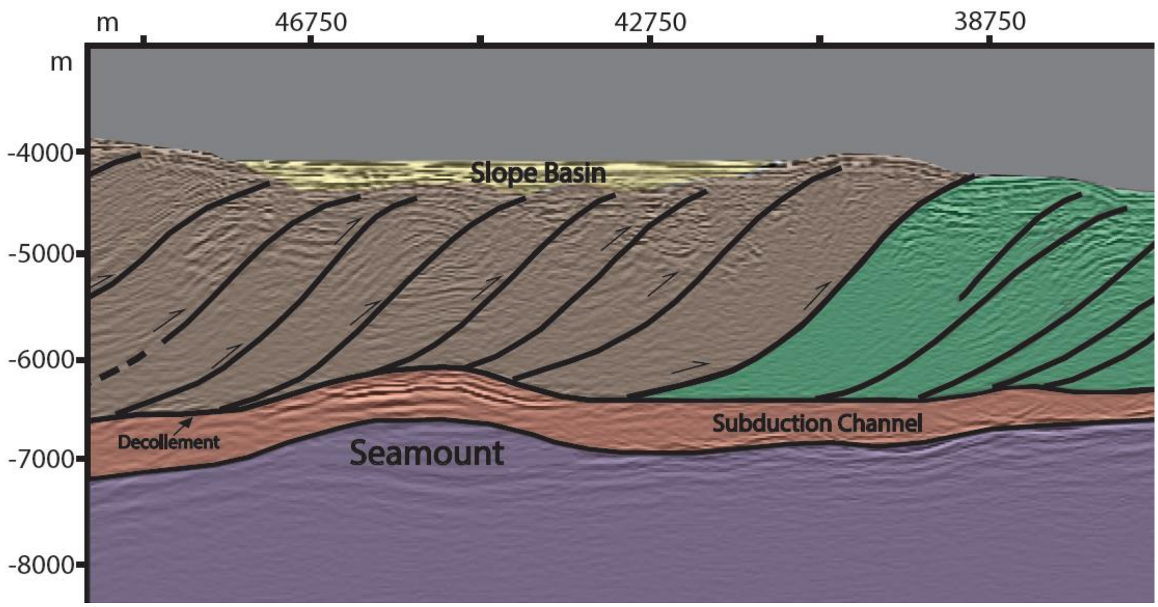

Figure 4-34. The boundary between the imbricated thrust system and out-of-sequence thrust system in seismic slice 260. The green colored part is the imbricated thrust system. The brown colored part is the out-of-sequence thrust system. The yellow colored part is the slope basin. The red colored part is the subduction channel. The purple colored part is the oceanic crust.

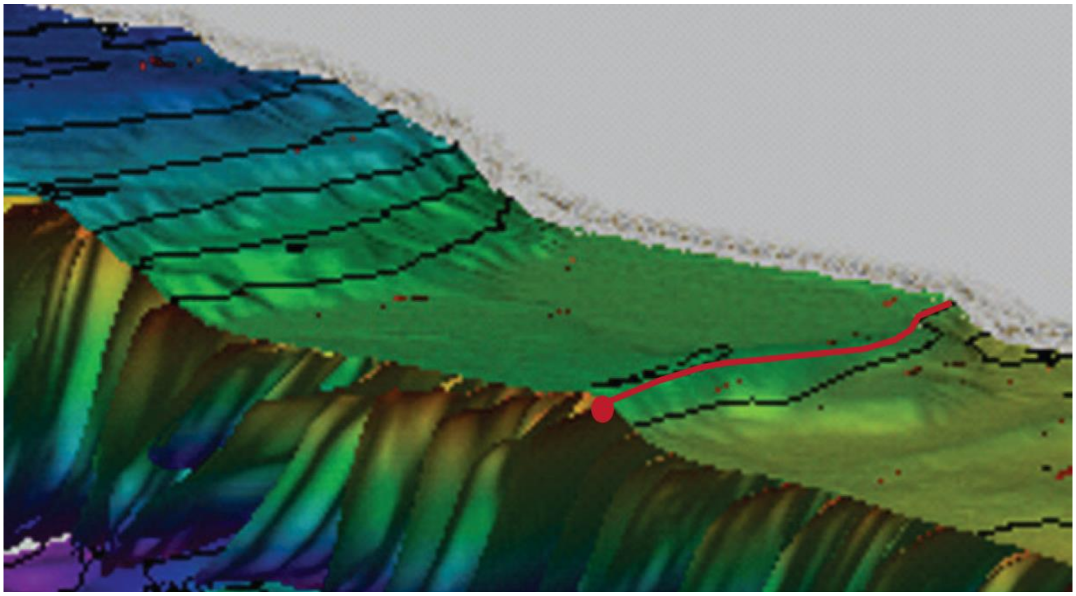

Figure 4-35. The 3-D illustration of the boundary between the imbricated thrust system and the out-of sequence thrust system. The red line shows the boundary on the bathymetry of the Muroto Transect. The red point shows the tip of the fault which is boundary between imbricated thrust system and out of-sequence system.

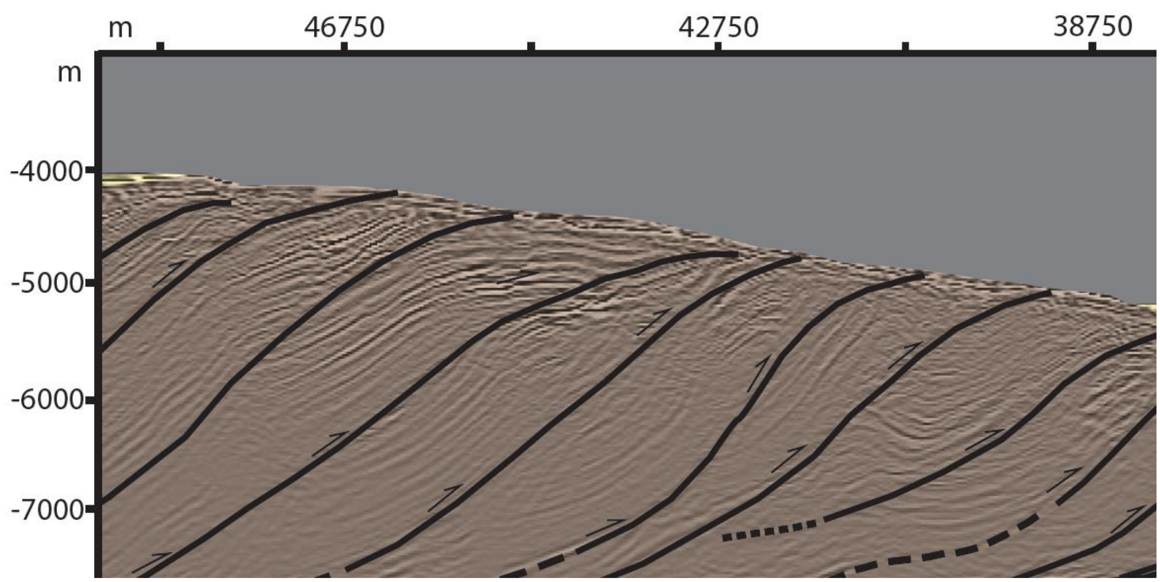

Figure 4-36. The large thrust faults in the out-of-sequence thrust system. The tips of the large thrust faults in the out-of-sequence reach the seafloor.

Chapter 5: Structural Restoration of the Muroto Transect

5-1. Structural Restoration of the Muroto Transect

Understanding the deformation distribution of the rock layers caused by tectonic forces is an important task for geologist from the purely scientific point of view; however it also can be used for economical gain in hydrocarbon, mining, and ground water exploration (Mansini, Bulnes, and Poblet, 2009). In order to determine the deformation in the rocks, some methods utilize strain markers such as fossils, fossil traces, and different types of particles. These methods use geometrical parameters which are obtained from lines on planes, producing strain ellipses and ellipsoids (Ramsay, 1967), the all-object-separation plot (Fry, 1979a), analysis of fibrous mineral overgrowths (Durney and Ramsay, 1973), and the R/4 method (Ramsay, 1967). These methods do not always give perfect results because the deformation cannot be commonly observed sufficiently due to inadequate strain markers (Mansini, Bulmes and Poblet, 2009). Instead of dealing with these methods which require rock samples from geological structures, predicting deformation models of the possible geological structures helps get rid of the drawback of these methods. In order to analyse the geological bodies, these methods utilize geological maps, cross-sections, seismic data, and 3-D geological surface. These methods include curvature analysis of the folded structures, forward modeling, restoration, and restoration plus forward modeling (Poblet and Bulnes, 2007).

Early structural restoration was applied to compressional system in order to determine the deformation state of the system (Dahlstrom, 1969). Fossen (2010) stated that the balanced cross-section method is conceivable for the structures if slip directions are in the plane of the cross-section. To determine the initial condition of the primary structures, the balanced cross-section is important.

The restoration of cross-sections helps to understand the link between deformed and undeformed states of the structures. Basically, the layers are reconstructed into their pre-deformational condition during the restoration process. Restoring the structural model can be helpful to confirm the result of geological and geophysical interpretation of the structural model.

The kinematic restoration method uses some concepts which are essential in order to obtain correct restoration results. According to Fossen (2010), the concepts are listed below ;

1. The interpretation must be reasonable for the geology of the region.
2. The strain must be dominantly a plane strain deformation.
3. The cross-section must be located along the tectonic movement or slip direction.
4. The applied algorithm must be acceptable for the given geologic and tectonic history of the region.
5. During the restoration, the gaps and overlaps must not be occurred or be kept at a minimal level.
6. After the restoration the horizontal layer must be in the restored state.
7. Depending to the other applications and experiences, the restoration model must be acceptable.

5-2. Application of Structural Restoration into the Muroto Transect

5-2-1. Method of Fault-Parallel Flow

Kinematic models are developed based on the geometry in order to determine the development of deformations in the rocks. For this purpose, many geometrical models are produced, and they are used in order to interpret faulted and folded regions (Suppe, 1983; Geiser et al., 1988). There are many algorithms available to solve the geometrically problematic terrains e.g.; fault-parallel flow (Egan et al., 1997), bed-parallel shear (Suppe, 1983), and inclined shear (Withjack and Peterson, 1993). Savage and Cooke (2003) stated that flexural-slip models are generally used in order to determine the geometrical deformation of the compressional terrain; however, this algorithm cannot be applied for all fault geometry.

I utilized the fault-parallel flow algorithm which was proposed by Egan et al. (1997) because the algorithm can provide the best result to analyze the tectonic deformation in my study area.

Egan et al. (1997) describes the working principle of the fault-parallel flow algorithm;

1. In the direction of the displacement, the algorithm rectifies the slip path based on all vertices in the hanging wall.
2. The vertices are displaced along the parallel line over the fault surfaces.

From the fault surface which is widened into the hanging wall, dip domain is delineated in order to adjust variations in fault dip. Along the process, the hanging wall is bounded by lines which are bisected depending on variations in fault dip (Tanner et al., 2003). The cut-off angles of lines and surface and also strain within lines and surface are altered by moving over a dip-domain boundary. A certain amount of simple shear which is parallel to the fault surface and displacement direction can fix changes of the cut-off angles of and strain within lines and surfaces (Tanner et al., 2003).

The algorithm gives the best result when it is applied for modeling hanging-wall movement on the faults which are parts of the fold and thrust belts. The deformation is assumed to develop between bed interfaces of the faults. The algorithm is applied to the anticlinal fault-bend fold structures (Fig. 5-1). The algorithm is appropriate for the horizons which are deformed by faults. The fault-parallel algorithm was created in order to kinematically deform the hanging-wall, and it aims to determine whether or not the deformation observed along the designed hanging-wall blocks is caused by fault-parallel shear (Egan et al., 1997). Based on Egan (1997), the method assumes that particular flow is parallel to the fault surface and parallel to the plane of cross-section. The algorithm can be used for extensional regions as well. The best advantage of the algorithm is that it does not have the obstacle in the Flextural Slip algorithm, which cannot be applied to simple ramp-flat-ramps with a dip less than 30°.

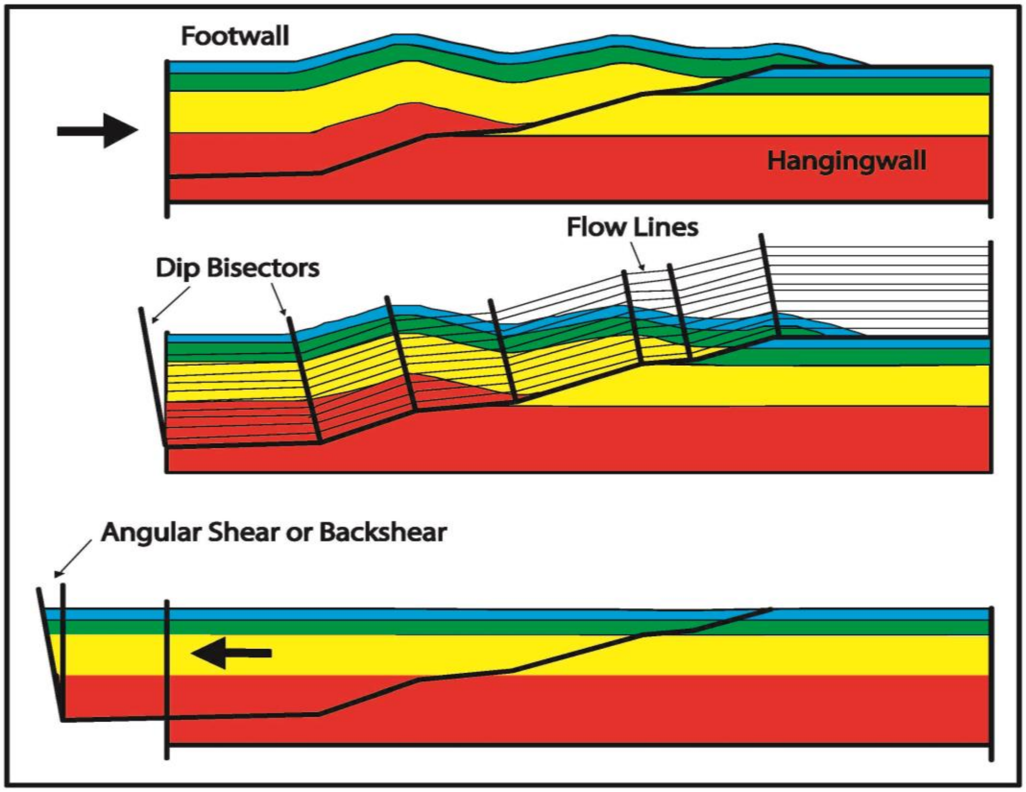

Figure 5-1. Schematic illustration of the fault-parallel flow algorithm (Adopted from Egan et al., 1997)

In order to do restoration of the thrust modeling and fold due to compression forces, the 2-D MOVE kinematic analysis software (Midland Valley Ltd) is utilized for the three lines of the Muroto Transect. The software includes the fault-parallel flow algorithm in which basically all points that are located over the surface of the hanging-wall move parallel to the surface of the footwall (Savage and Cooke, 2003). The algorithm reserves the area of the bed. Additionally, if back-shear is not observed on the hanging-wall, the beds are getting thinner through the forelimb of the fold (Fig. 5-2, 5-3, 5-4).

5-2-2. Application Result of Structural Restoration into the Muroto Transect

The restoration process is applied to the axial-trench zone, proto-thrust zone, and imbricated thrust zone of the Muroto Transect. For this application, Lines 215, 260, and 284 are chosen (Fig 5-2, 5-3, 5-4). The deformations of each line are restored by starting from the proto-thrust zone and it continues until at the end of the imbricated thrust zone. With this application, the shortening rate of the region from the trench axial zone to the out-of-sequence zone along the Muroto Transect is calculated based on these three lines. In Table 5-1, the results of the restoration are shown. During the restoration, the deformation areas are defined from the first proto-thrust fault to the end of the imbricated thrust zone.

Depending on the restoration result of the Muroto Transect, the deformation increases from southwest of the region to northeast along the imbricated thrust zone (ITZ) of the Muroto Transect. The total deformation along the Line 215, 260, and 284 are 20, 25.6, and 24.8 percent, respectively (Table 5-1).

Table 5-1. Measurement of the horizontal shorting along the Muroto Transect and calculated structural restoration results along the Muroto Transect.

Restored Lines of The Muroto Transect	Total Deformation Length (km)	Total Restored Length (km)	Ratio of Total Restored Length (%)
215	25	30	20
260	25	31.4	25.6
284	25	31.2	24.8

The crescent-shape of the Tosa Bae embayment, which is almost 20 km away from the Muroto Transect, can be seen using the general bathymetry of the Nankai Trough. The seamount, located on the subducting plate, generates the embayment at the edge of overriding plate (Pedley et al., 2010). The Tosa Bae embayment was developed due to subducting seamount (Bangs et al., 2006).

The shortening results show an increase in shortening from southwest to northeast along the Muroto Transect. This slightly variation of shortening from southwest to northeast is an indicator of the seamount which was subducted into the Tosa Bae embayment.

Additionally, based on these results, the largest amount of the fault slip is located at the northeast of the Muroto Transect. Therefore, we can suggest that when the seamount subducted into the accretionary prism, the existed imbricated thrust zone was not totally developed. On the other hand, the seamount which is shown in the seismic volume of the Muroto Transect does not have enough size to create an embayment on the Muroto Transect.

Based on the shortening results, the relationship between Muroto Seamount and the accretionary prism was investigated. The slightly variation in the restoration results of the imbricated thrust system of the Muroto Transect suggest that there is little to no effect of the subducting Muroto Seamount.

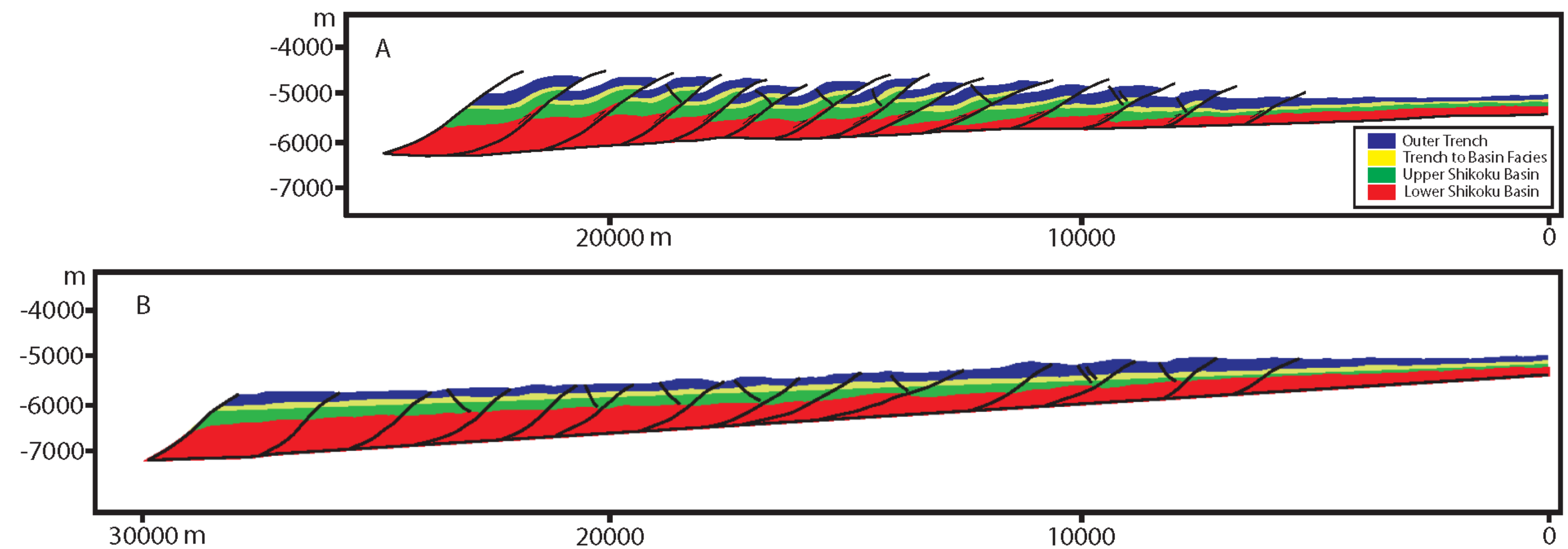

Figure 5-2. The application of the fault paralel flow on the line 215. A is the deformed section of the line 215 and B is the restorated section of the line 215.

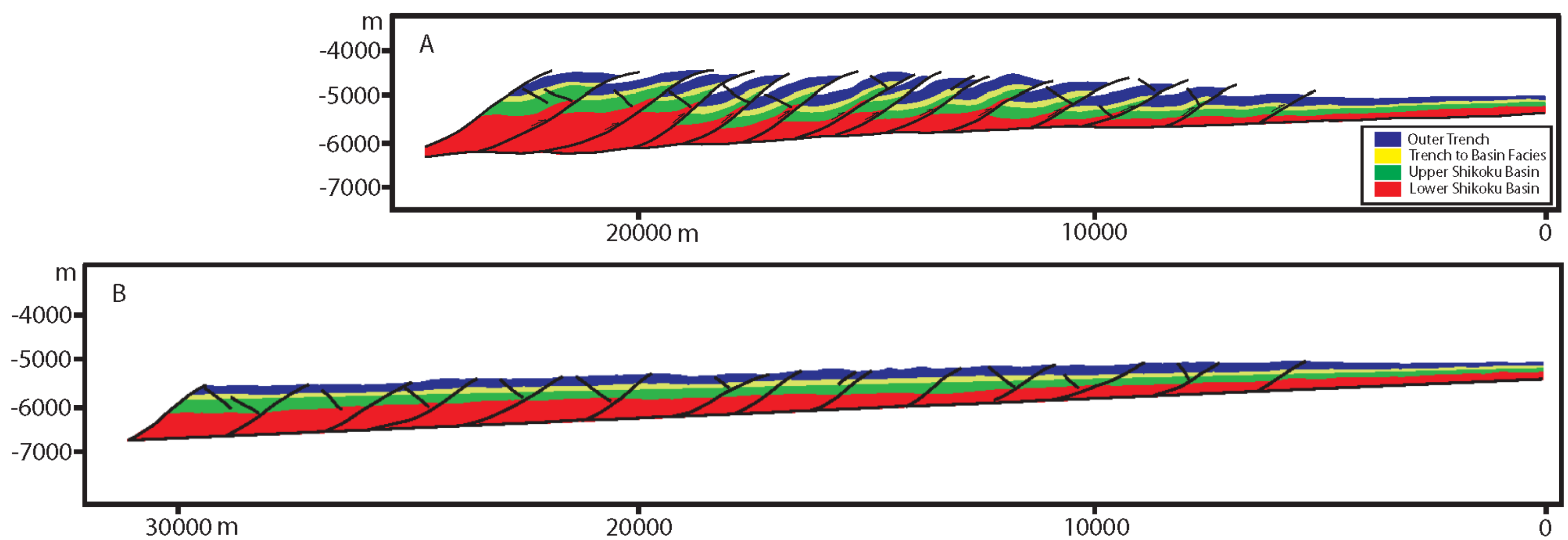

Figure 5-3. The application of the fault paralel flow on the line 260. A is the deformed section of the line 260 and B is the restorated section of the line 260.

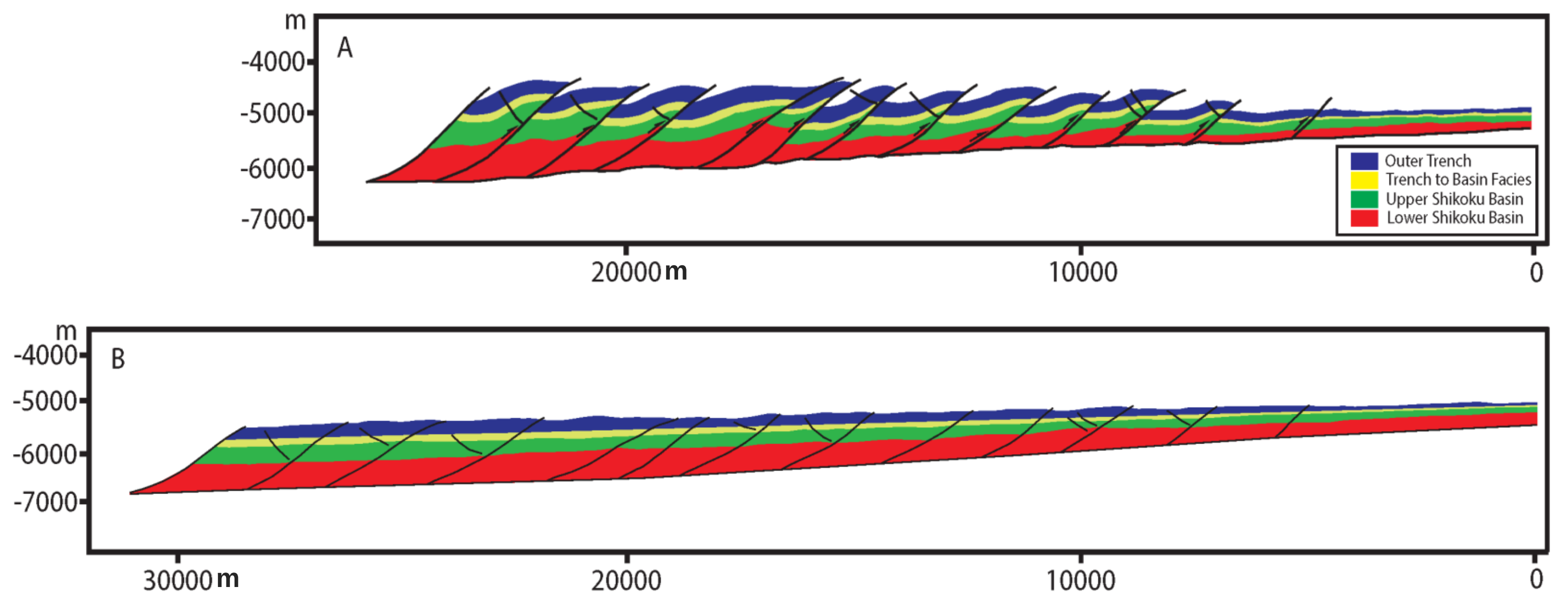

Figure 5-4. The application of the fault paralel flow on the line 284. A is the deformed section of the line 284 and B is the restorated section of the line 284.

Chapter 6: Application of the Coulomb Wedge Theory

6-1. Application of the Coulomb Wedge Theory

The Coulomb Wedge Theory plays an essential role in order to understanding the dynamics of the critical wedge mechanism. The development of an orogenic wedge can be summarized as being similar to the deformation of a ‘wedge of sand in front of the moving bulldozer’ (Elliott, 1976; Suppe, 1980; Davis et al., 1983; and Dahlen, 1990). According to this theory, the sand which is accumulated in the wedge is undergoing frictional sliding along its basal contact, similar to the subduction basal décollement. The sliding process continues until the well-developed triangular wedge is formed. The opening angle of the wedge ($\alpha+\beta$), which is called critical taper, is determined based on surface slope angle (α) and dip angle of the basal décollement (β) in the vertical plane (x,y) coordinate system (Fig. 6-1) (Davis et al., 1983). The critical taper is characterized by utilizing frictional and pore fluid pressure properties between wedge and basal décollement (Davis et al., 1983). Based on the wedge material, the critical taper of the wedge controls the angle of the taper. If any external impact (erosion and changing thickness of incoming material) or internal impact (change in material properties) lead to change the angle of taper, the wedge will become unstable, and shift to either a subcritical or supercritical state. Twiss and Moore (2007) defined the critical Coulomb Wedge mechanical model based on three assumptions;

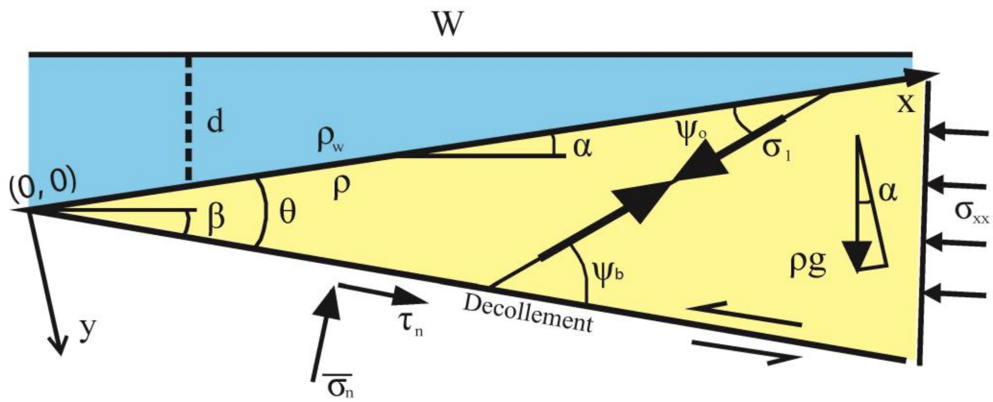

Figure 6-1. Schematic illustration of a critical wedge to show the coordinate systems (x,y), maximum compressive stres (σ_1), the critical taper (θ), angle of surface slope (α), dip of décollement (β), ψ_0 and ψ_b are the angles between $\sigma_1$and the x axis within the wedge and at the base of the wedge, water depth (d) and basal traction, ρ density of the wedge, and ρ_w is the density of sea water (adopted from Dahlen, 1983)

1) The basal décollement or crust should be predicted as a flat plane, and this plane is considered to be subducting into the landward crust with an angle β. The bathymetry of the wedge defines the surface slope and its seaward angle α.
2) The rocks in the thrust sheets are everywhere just at the critical stress for failure, as defined by the Coulomb fracture criterion, and thus stress everywhere in the thrust sheet is as large as possible before achieving failure (Twiss and Moore, 2007)
3) The acceleration of thrust wedge is taking into account the smallest values to be avoided. The driving forces that allow movement of wedges should be stabilized by the counter forces which consist of resisting forces based on the Newton's first law of motion.

Based on the measured rock density, the non-cohesion wedge can be described by four main parameters; these are internal and basal friction, and internal and basal pore pressure.

In this study, the two-dimensional seismic sections are used in order to investigate the physical parameters of the Muroto Transect and measure the critical wedge. The seismic sections, which are Lines 215, 260, 290, 315 and 350 are utilized to determine the slope angle (α), and dip angle of basal décollement (β). The wedge mechanism is also controlled by the gravitational force.

6-2. Surface Slope and Décollement Dip

According to the classical Coulomb Wedge Theory, the steeper slope is an indicator of stronger basal fault or a weaker wedge material for presuming stabile slip of the plate interface against constant resistance (Wang and Hu, 2006). Considering this prediction, the critical taper of the Muroto Transect is calculated with angle of surface slope and angle of décollement dip. The slope angle of the lines 215, 260, 290, 305, and 350 are determined depending on the bathymetry of the Muroto Transect (Fig. 6-2). The slope angle (α) are measured as 2.0°, 2.2°, 2.1°, 2.3°, and 2.4°, respectively (Table 6-1). The dip of the décollement (β) is defined from 3-D pre-stack depth migrated seismic volume. The dip of the décollement is determined 1.5° all the way of the décollement surface.

Table 6-1. The measured angle of surface slope (α), dip of décollement (β) and angle of the taper (α+β) for each line of the Muroto Transect.

Lines	215	260	290	305	350
Angle of Slope (α)	2.0°	2.2°	2.1°	2.3°	2.4°
Dip of Décollement (β)	1.5°	1.5°	1.5°	1.5°	1.5°
Taper (α+ β)	3.5°	3.7°	3.6°	3.8°	3.9°

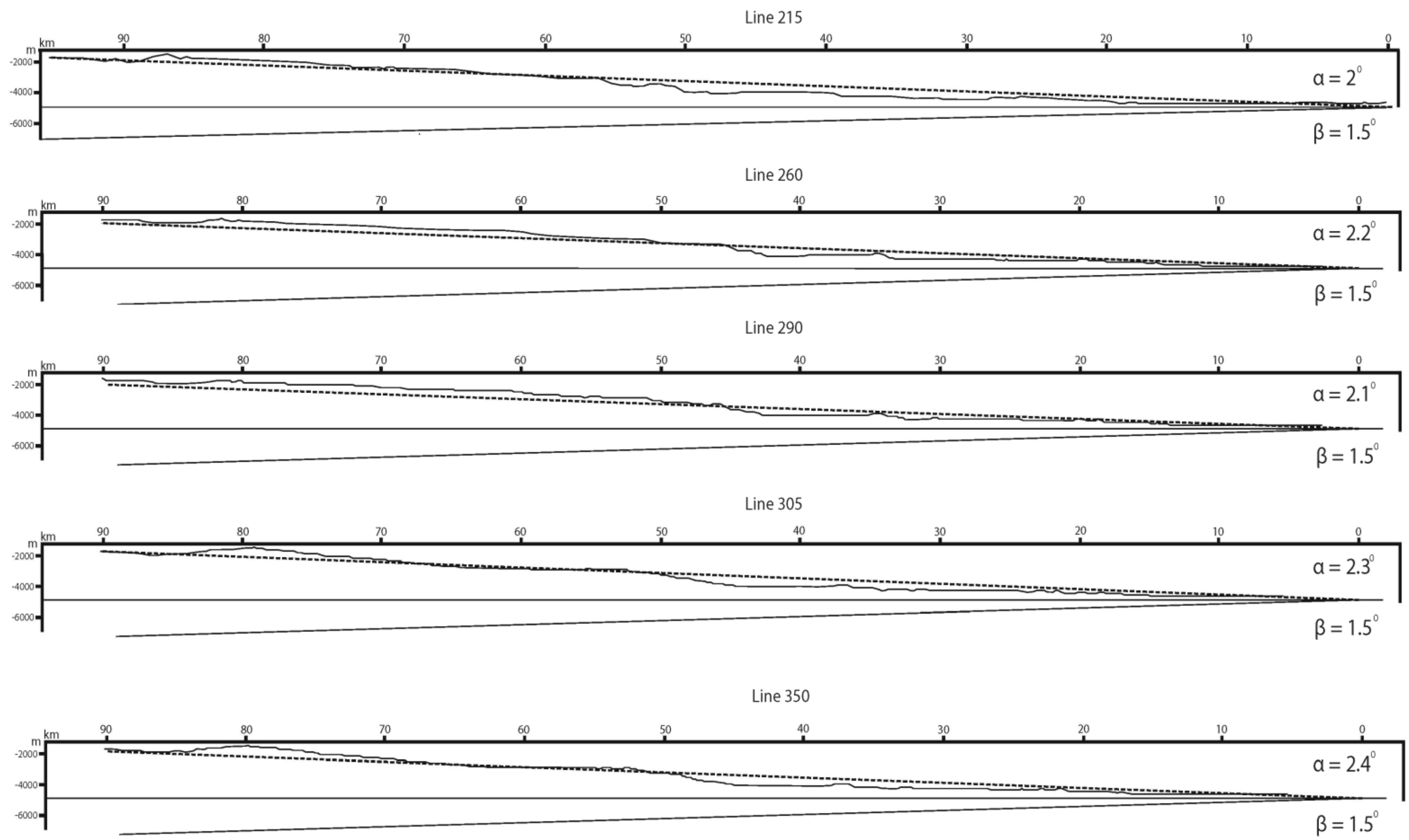

Figure 6-2. Based on the Coulomb Wedge Theory, the best fitting theoretical cohesive critical wedge compared with observed topography along the Muroto Transect. For this application, line 215, 260, 290, 305 and 350 are chosen.

6-3. Pore Pressure on the Muroto Transect

Porous sediments are deposited from the overriding continental plate onto the subducting oceanic plate and into the accretionary prism along the subduction zone (Skarberk and Saffer, 2009). The hydrologic and mechanical behavior of subduction complexes and the strength and sliding stability of faults are managed by the pore pressure (Skarberk and Saffer, 2009). The pore pressure between under-thrust sediments and down-going plate manipulates the shear strength of the décollement and critical taper of accretionary prism (Davis et al., 1983). Additionally, the upper margin of the seismogenic zone is likely affected by the dewatering rate of the wedge. Very low magnitude earthquakes, slow slip events, and episodic tremor and slip are observed because of high pore pressure (Ito and Obara, 2006; Kitajima and Saffer, 2012).

According to Skarberk and Saffer (2009), pore pressure can be obtained from two different ways. The first is to infer pore pressure using measured porosity. The second is to compute pore pressure using porosity which can be estimated from interval velocities of seismic reflections and also transform relating porosity to effective stress σ_z' (Pa). They estimate the pore pressure based on the vertical effective stress σ_z' (Pa) and fluid pressure P_f (Pa) by;

$$P_f = \sigma_z - \sigma_z' \quad (6\text{-}1)$$

where σ_z is the total vertical stress which is determined by downward integration of bulk density values from shipboard. Sharberk and Saffer (2009) proposed three ways to calculate pore pressure ratio:

1. Excess pore pressure; $P^* = P_f - P_h$,

2. The pore ratio; $\lambda = P_f / \sigma_z$

3. Modified pore pressure ratio defined;

$$\lambda^* = \frac{P_f - P_{hf}}{\sigma_m - P_{hf}} \qquad (6\text{-}2)$$

Laboratory consolidation tests and inversion of the porosity data help to calculate the effective stress. Sharberk and Saffer (2009) utilized the exponentially decreasing porosity ratio with depth in order to calculate the effective stress and the pore pressure ratio. Athy (1930) formulated the exponentially decreasing porosity,

$$\Phi = \Phi_0 \ \exp(-bz) \qquad (6\text{-}3)$$

where Φ_0 is the porosity of the seafloor material, b is the constant depending on the lithology and geological setting, and z is the depth (m). Sharberk and Saffer (2009) produced another formula for effective stress which is

$$\mathrm{Ln}\ \Phi - \Phi = \frac{-b\sigma_z'}{g(\rho_s - \rho_f)} + \ln \Phi_0 \ - \Phi_0 \qquad (6\text{-}4)$$

where, σ_z' is the vertical effective stress, g is gravitational acceleration, ρ_s is the density of the material, and ρ_f is the density of fluid in the wedge.

Sharberk and Saffer (2009) stated that porosity values can be inverted for effective stress where they are unknown. Hence, using this relation between porosity and effective stress, the pore pressure can be estimated.

In my study of the Muroto Transect, I used another porosity equation which is derived from compaction length Fruehn et al. (1997) produced an equation in order to calculate the porosity using compaction length of the wedge. Having the data from Site 1174, we already know the porosity variation with depth. By using the equation 6-5, the compaction length is calculated.

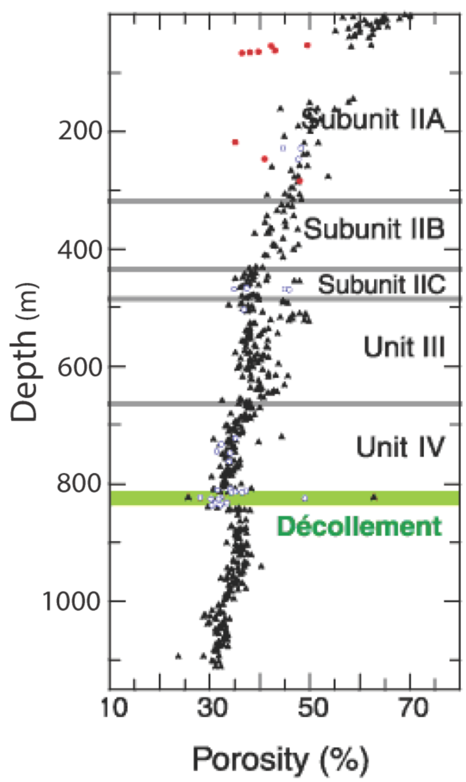

Figure 6-3. Measured porosity values from drilling Site 1174 (taken from Moore et al., 2001).

$$\Phi = \Phi_0 \ \exp(-z/c) \qquad (6\text{-}5)$$

where Φ_0 is the porosity of the seafloor materials, c is the compaction length of the wedge, and z is the depth (m). After the depth (z) is eliminated from equation, another porosity equation is produced (Kopp and Kukowski, 2006):

$$\Phi = \Phi_0 \exp [- ((1\text{-}\lambda)\rho d/(\rho_w - \rho)c)] \quad (6\text{-}6)$$

Using on this equation, the pore pressure ratio was determined along the toe of the Muroto Transect. Finally, the pore pressure ratio was determined to be 0.49 along the Muroto Transect.

6-4. Internal Friction and Internal Effective Basal Friction

The geometry of the conjugate pair of fore-thrust and back-thrust is used in order to determine the internal friction and internal effective basal friction of the Muroto Transect. The mechanical parameter can be calculated from pre-stack depth migrated seismic slices. This method was utilized by Kukowski et al. (2001), Kopp and Kukowski (2003), and Wang and Hu (2006).

The frontal faults are presumed to be fresh Coulomb fractures. The Coulomb failure criterion is fulfilled along two planes inclined at an angle of 45°- $\frac{\phi}{2}$ to the $\sigma_1$axis (Davis and von Huene, 1987). Therefore, the angle between the maximum compressional stress (σ_1) and the décollement is useful to find out the orientation of preferred slip lines (Davis and von Huene, 1987). By utilizing this relation, the internal friction and internal effective basal friction coefficients along the Muroto Transect are determined using lines 215, 260, 290, 305, and 350. First, I measure the dipping angle of frontal thrust fault (δ_f) and conjugate thrust fault (δ_b).

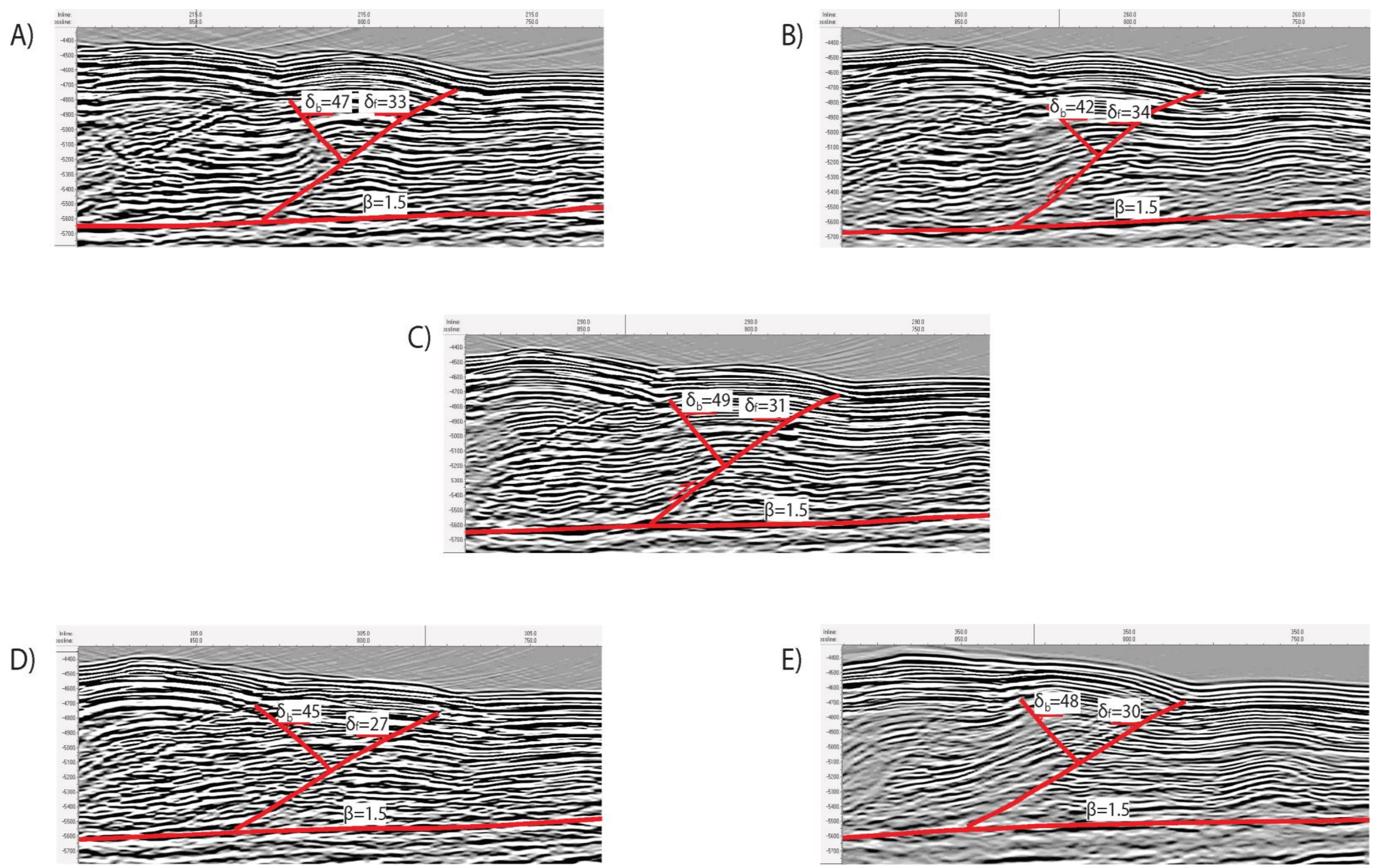

Figure 6-4. Detailed view of the deformation front and lower slope along the Muroto Transect. The structural analysis of the Muroto Transect is based on the geometry of the conjugate pair of fore-thrust and back thrust imaged in the depth migratedline 215, 260, 290, 305, and 350.

After that, the relative relation between dip angle of frontal thrust and conjugate thrust fault (δ_{frel} and δ_{brel}) and dip angle of décollement (β) were determined with equations 6-7 and 6-8 (Kopp and Kukowski, 2003).

$$\delta_{frel} = \delta_f - \beta \tag{6-7}$$

$$\delta_{brel} = \delta_b + \beta \tag{6-8}$$

Based on the relation of two plane inclined at the angle of 45°- $\frac{\phi}{2}$ to the $\sigma_1$axis, μ = tan ϕ equation gives the internal friction coefficients where ϕ is the angle of internal friction. Davis and von Huene (1987) proposed that the angle of internal friction (ϕ) can be calculated with equation 6-9.

$$\Phi = 90 - \delta_{frel} - \delta_{brel} \tag{6-9}$$

The internal friction coefficients (μ) of the wedge can be easily calculated using the angle of internal friction (ϕ) using the relationship below;

$$\mu = \tan(\phi) \tag{6-10}$$

For the assumption of low cohesion at the frontal part of the accretionary prism, the relation between dip of maximum compressive stress (ψ_b), and internal (μ) and basal (μ_b) friction coefficients is formulated (Kopp and Kukovski, 2003);

$$\psi_b = \frac{1}{2} \arcsin [\sin(\phi_{beff}) / \sin(\phi)] - \frac{1}{2} \phi_{beff} \tag{6-11}$$

From this equation, angle of effective basal friction (ϕ_{beff}) can be obtained, this information is used to calculate effective basal friction coefficient (μ_{beff}).

$$\mu_{beff} = \tan(\phi_{beff}) \tag{6-12}$$

The calculated effective basal friction coefficients for each seismic line are shown in Table 6-2. In order to estimate the strength ratio between basal detachment and internal parts of the accretionary wedge, the effective basal friction is divided by the internal basal friction (Kopp and Kukowski, 2003).

Depending on the result of effective basal friction coefficients and internal pore pressure for each line, the basal internal friction coefficients can be calculated. For the calculation, equation 6-12 is used.

6-5. Sediment Strength

The sediment strength is a crucial parameter in order to understand subduction mechanics along the wedge. Davis and von Huene (1987) stated that the parameter is important because it manipulates the stress condition where deformation is observed, coupling between converging lithospheric plates and variation of the compressing stress in the overriding plates. In this study, the relationship between angles of force and back thrust along the Muroto Transect is utilized to evaluate the front of the subduction zone of the Nankai Trough.

Table 6-2. Measured angles and defined principal stress orientations along five seismic lines along the Muroto Transect. The angle of the internal friction (ϕ), the internal effective friction (ϕ_{beff}), internal friction coefficient (μ), internal basal effective friction coefficient (μ_{beff}) and sedimentary strength (μ/μ_{beff}).

	ϕ	μ	ϕ_{beff}	μ_{beff}	μ/μ_{beff}
Line 215	14°	0.25	4.03°	0.07	3.57
Line 260	13°	0.23	3.43°	0.06	3.83
Line 290	13°	0.23	4.03°	0.07	3.28
Line 305	12°	0.21	3.83°	0.067	3.13
Line 350	10°	0.176	3.09°	0.054	3.26

Saffer et al. (2008) stated that the sediment strength along the subduction zone is controlled by the dehydration and rheology, which in turn manipulates sliding stability of the faults. According to Saffer et al. (2008), the increasing fluid pressure, which decreases the shear strength, is caused by the release of bound water into low permeability mudstones raising pore pressures. In addition, they indicated that the water migration from the sedimentary layer leads to increase the intrinsic strength of the dewatered sedimentary layers by increases in cohesion as cementation increases.

Many researchers have used the sediment strength in order to analyze accretionary prisms. Kopp and Kukowski (2006) investigated the Sunda Strain Transect and they determined the sediment strength of the transect. The sedimentary sequence along the Sunda Strain Transect is 2.3 times stronger than the detachment zone. Additionally, Davis and von Huene (1987) investigated the Aleutian Trench. Based on their investigation, the sedimentary blocks along the trench is 1.5 times stronger than the detachment zone. Finally, the overriding sedimentary sequence is 2.8 times stronger than the detachment zone at the toe of Markan Trench (Kukowski, 2001).

In order to obtain the sediment strength, the effective basal friction is first calculated based on the equation developed by Kukowski (2001):

$$\mu_{beff} = \sin (2\psi_b) / (1 / \sin \phi - \cos (2\psi_b)) \tag{6-16}$$

The effective basal friction is derived from dip of maximum compressive stress (ψ_b) and the angle of internal friction (ϕ). The sediment strength is calculated by obtaining the ratio between effective basal friction (μ_{beff}) and internal friction (μ).

$$\text{Sediment Strength} = \frac{\mu}{\mu_{beff}} \tag{6-17}$$

The ratios of sediment strength along the Muroto Transect are calculated using Lines 215, 260, 290, 305, and 350 (Table 6-2.). Along the Muroto Transect, the sediment strength is determined to be within the range of 3.13 and 3.83. The sedimentary strengths for lines 215, 260, 290, 305, and 350 are determined to be 3.57, 3.83, 3.28, 3.13, and 3.26 respectively. In the direction of northeast to southwest along Muroto Transect, the sediment strength slightly increases.

Based on the sediment strength at the Muroto Transect, the relation between sediments in the wedge and basal décollement is shown throughout the Muroto Transect. The sedimentary wedge at the southwest of the Muroto Transect is ~3.7 times stronger than the detachment zone, where as the sedimentary wedge at the northeast of the Muroto Transect is ~3.2 times stronger than the detachment zone.

6-6. Implication of Coulomb Wedge Theory

On the Muroto Transect, the angle of the surface slope is controlled by;

1. Internal Friction (μ)
2. Effective Basal Friction (μ_{beff})

Based on the calculation of these parameters, we can propose that the angles of surface slope changes have an influence on the internal friction and internal effective basal frictions of the wedge. When the angle of the surface slope increases, the effective basal friction must decrease and the internal friction must decrease along the wedge. Based on this assumption, I calculated the internal friction coefficients along the Muroto Transect in order to show the relation of angle of surface slope and effective basal and internal friction coefficients. According to the results, the internal friction coefficients of the northeastern part of the wedge are slightly lower than the coefficients of the southwestern part of the wedge. Additionally, angle of surface slope of the Muroto Transect slightly decrease from the southwestern part of the wedge to the northeastern part of the wedge. Moreover, the sediment strengths (μ/μ_{beff}) are calculated along the Muroto Transect. The results of the sediment strength along the Muroto Transect illustrate that when the sediment strength increases, the taper of the prism decreases.

Based on these observations, the seamount which is illustrated in the 3D pre-stack depth migrate data does not have an influence on the toe of the Muroto Transect. The imbricated thrust system of the Muroto Transect has developed after the seamount subducted into the accretionary prism. When the tapers of the prism are investigated on different part of the Muroto Transect, large differences along the Muroto Transect were not observed. Moreover, the effective basal friction and internal friction coefficients along the toe of the Muroto Transect do not have large differences.

Chapter 7: Conclusions

The relationship between Muroto Seamount and the accretionary prism is investigated. Detailed investigation over the imbricate system of the Muroto Transect suggests that there are few if any effects caused by the subducting Muroto Seamount. Based on the seismic interpretation, the contact between the seamount and the accretionary prism was illustrated below the interpreted subduction channel, and the imbricate thrust system detached from the décollement without any impact of the seamount in the down-going plate. Additionally, the impact of the seamount along the prism was investigated using structural restoration and Coulomb Wedge Theory. The results show that the present imbricate system has developed with no apparent inherited or lingering effect from the seamount subduction, as the seamount upper contact lie below the subduction channel as interpreted and wedge strength indicates very little change from the interpreted transect along strike outside the zone of seamount subduction.

Results of the study are summarized based on the structural restoration of the imbricated system and application of the Coulomb Wedge Theory along the Muroto Transect. There are two main components of shortening associated with subduction zones. The first is related to shortening achieved by the subduction of the oceanic lithosphere and removal of material from the Earth surface, a non-conservative process in terms of the surface layer or lithosphere. The second main component is structural shortening (or extension) due to faulting, folding, and strain accumulated in surface sediment on the down-going plate when transferred to the overriding plate. Restoration results are helpful in order to understand how the structural horizontal shortening developed along the Muroto Transect that does not account for the subduction component of shortening. The restoration results of horizontal shortening are calculated as 20, 25.6, and 24.8 % for lines 215, 260, and 284, respectively. When the seamount subducted into the wedge, a "crescent shape" occured along the wedge. The example of the crescent shape is observed about 20 km to northeast of the Muroto Transect which is called the Tosa Bae embayment. The shortening at the wedges gives us an idea about how the seamount subducted into the accretionary prism. The shortening should be highest where the seamount subducted at the edge of the wedge. However, the seaward horizontal shortening results along the Muroto Transect for different lines only slightly increase from southwestern to northeastern of Muroto Transect.

The implication of the Coulomb Wedge Theory along the Muroto Transect is consistent with the restoration results. The critical tapers of the Muroto Transect **(**$\alpha+\beta$) are determined as 3.5, 3.7, 3.6, 3.8, and 3.9 for lines 215, 260, 290, 305, and 350. Based on these results, the internal friction coefficients must be increased along the Muroto Transect. The internal friction and effective basal friction coefficient are calculated along the wedge. The internal friction coefficients (μ) are determined as 0.25, 0.23, 0.23 0.21, and 0.176 for lines 215, 260, 290, 305, and 350 respectively. Based on the results, the the coefficients of the northeastern part of the wedge are slightly lower than the coefficient of the southwestern part of the wedge. Additionally, the effective basal friction coefficients (μ_{beff}) are calculated as 0.07, 0.06, 0.07, 0.067, and 0.054 for lines 215, 260, 290, 305, and 350. The effective basal friction coefficients slightly decrease from the southwestern part of the Muroto Transect to the northeastern part of the Muroto Transect.

The results illustrate that the Muroto Transect has a weaker décollement zone where the thrust faults detached. The seamount which subducted in the Tosa Bae embayment has an effect on the northeastern part of the Muroto Transect. This is because the internal friction coefficients and effective basal friction slightly decrease, and tapers of the prism slightly increase in this part of the Muroto Transect. On the other hand, the seamount affects the out-of-sequence thrust system. The subducted seamount reactivated the frontal thrust fault of the out-of-sequence thrust system. Then, the fault cut the Quaternary deposits, and caused a slope basin to develop over the out-of-sequence thrust system. Moreover, the tips of the large thrust faults reach the seafloor in the out-of-sequence thrust system based on the seismic interpretation. This is because the subducted seamount reactivated the thrust faults and they reached to the seafloor.

To sum up, the effect of the seamount was not observed on the imbricated thrust system of the accretionary prism. On the other hand, its effect was observed on the out-of-sequence thrust system of the accretionary prism.

References

Amano, K. A. Z. U. O. (1991). Multiple collision tectonics of the South Fossa Magna in central Japan. *Modern Geology*, *15*(4), 315-329.

Ando, M. (1975). Source mechanisms and tectonic significance of historical earthquakes along the Nankai Trough, Japan. *Tectonophysics*, *27*(2), 119-140.

Arai, R., Iwasaki, T., Sato, H., Abe, S., & Hirata, N. (2009). Collision and subduction structure of the Izu–Bonin arc, central Japan, revealed by refraction/wide-angle reflection analysis. *Tectonophysics*, *475*(3), 438-453.

Athy, L. F. (1930). Density, porosity, and compaction of sedimentary rocks. *Association of American Petroleum Geologists Bulletin*, *14*(1), 1-24.

Bangs, N. L. B., Gulick, S. P. S., Shipley, T. H., Gulick, S. P. S., & Shipley, T. H. (2006). Seamount subduction erosion in the Nankai Trough and its potential impact on the seismogenic zone. *The Geological Society of America Bulletin*, *34*, 701–704. doi:10.1130/G22451.1

Brown, K. M., Saffer, D. M., & Bekins, B. A. (2001). Smectite diagenesis, pore-water freshening, and fluid flow at the toe of the Nankai wedge. *Earth and Planetary Science Letters*, *194*(1), 97-109.

Chamot-Rooke, N., Renard, V., & Le Pichon, X. (1987). Magnetic anomalies in the Shikoku Basin: a new interpretation. *Earth and Planetary Science Letters*, *83*(1), 214-228.

Dahlen, F. A. (1990). Critical taper model of fold-and-thrust belts and accretionary wedges. *Annual Review of Earth and Planetary Sciences*, *18*, 55.

Dahlstroom, C. D. A. (1969) Balanced cross-section. *Canadian Journal of Earth Science* 6, 743-757

Davis, D., Suppe, J., & Dahlen, F. A. (1983). Mechanics of fold-and-thrust belts and accretionary wedges. *Journal of Geophysical Research: Solid Earth (1978–2012)*, *88*(B2), 1153-1172.

Davis, D. M., & von Huene, R. (1987). Inferences on sediment strength and fault friction from structures at the Aleutian Trench. *Geology*, *15*(6), 517-522.

Deyhle, A., Kopf, A., & Pawlig, S. (2004). Cross-section through the frontal Japan Trench subduction zone: Geochemical evidence for fluid flow and fluid–rock interaction from DSDP and ODP pore waters and sediments. *Island Arc*, *13*(1), 271-288.

Dolan, J. F., Christofferson, S. A., & Shaw, J. H. (2003). Recognition of paleoearthquakes on the Puente Hills blind thrust fault, California. *Science*,*300*(5616), 115-118.

Durney, D.W., Ramsay, J.G., (1973). Incremental strains measured by syntectonic crystal growths. *In: de Jong, K.A., Scholten, R.(Eds.), Gravity and Tectonics.* Wiley, New *York, pp. 67 – 96.*

Egan, S. S., Buddin, T. S., Kane, S. J., & Williams, G. D. (1997). Three-dimensional modelling and visualisation in structural geology: New techniques for the restoration and balancing of volumes. In *Proceedings of the 1996 Geoscience Information Group Conference on*.

Elliott, D. (1976). The energy balance and deformation mechanisms of thrust sheets. *Philosophical Transactions of the Royal Society of London. Series A, Mathematical and Physical Sciences*, *283*(1312), 289-312.

Expedition 333 Scientists (2012). Expedition 333 summary. In Henry, P., Kanamatsu, T., Moe, K., and the Expedition 333 Scientists, *Proceeding IODP, 333: Tokyo (Integrated Ocean Drilling Program Management International, Inc.). doi:10.2204/iodp.proc.333.101.2012*

Fergusson, C. L. (2003). Provenance of Miocene-Pleistocene turbidite sands and sandstoness, Nankai Trough, Ocean Drilling Program Leg 190. *Proceedings of the Ocean Drilling Program, Scientific Results, 190/196 p:1-28.*

Fossen, H. (2010). *Structural Geology*. Cambridge University Press.

Fruehn, J. , White, R. S. and Minshull, T. A. (1997), Internal deformation and compaction of the Makran accretionary wedge. *Terra Nova, 9: 101–104. doi: 10.1046/j.1365-3121.1997.d01-13.x*

Fry, N. (1989). Random point distributions and strain measurement in rocks. *Tectonophysics v: 60 p:89-105.*

Geiser, P. A. (1988). The role of kinematics in the construction and analysis of geological cross sections in deformed terranes. *Geometries and mechanisms of thrusting: Geological Society of America Special Paper, 222,* 47-76.

Gulick, S. P. S., Bangs, N. L. B., Shipley, T. H., Nakamura, Y., Moore, G., & Kuramoto, S. (2004). Three-dimensional architecture of the Nankai accretionary prism's imbricate thrust zone off Cape Muroto, Japan: Prism reconstruction via en echelon thrust propagation. *Journal of Geophysical Research: Solid Earth (1978–2012)*, *109*(B2) p: 1-12.

Ito, M. (1987). Middle to Late Miocene foredeep basin successions in an arc-arc collision zone, northern Tanzawa Mountains, central Honshu, Japan. *Sedimentary Geology*, *54*(1), 61-91.

Ito, Y., & Obara, K. (2006). Very low frequency earthquakes within accretionary prisms are very low stress-drop earthquakes. *Geophysical Research Letters*, *33*(9), p: 1-4 *doi: 10.1029/2006GL025883*

Kamata, H., & Kodama, K. (1994). Tectonics of an arc-arc junction: an example from Kyushu Island at the junction of the Southwest Japan Arc and the Ryukyu Arc. *Tectonophysics*, *233*(1), 69-81.

Kano, K. (1991). *Stratigraphy and Geologic History of the Cenozoic of Japan* (Vol. 274). Geological Survey of Japan.

Kitajima, H., & Saffer, D. M. (2012). Elevated pore pressure and anomalously low stress in regions of low frequency earthquakes along the Nankai Trough subduction megathrust. *Geophysical Research Letters, 39(23),*1-5*. doi:10.1029/2012GL053793*

Kobayashi, K. (1984). Subsidence of the Shikoku back-arc basin.*Tectonophysics*, *102*(1), 105-117.

Kobayashi, K. (1995). Role of subducted lithospheric slab in uplift and subsidence of the northwestern Pacific margins. *Marine Geology*, *127*(1), 119-144.

Kopp, H., & Kukowski, N. (2003). Backstop geometry and accretionary mechanics of the Sunda margin. *Tectonics*, *22(6),* 1-16*. doi: 10.1029/2002TC001420*

Kouketsu, Y., & Enami, M. (2011). Calculated stabilities of sodic phases in the Sambagawa metapelites and their implications. *Journal of Metamorphic Geology*, *29*(3), 301-316.

Kukowski, N., Schillhorn, T., Huhn, K., von Rad, U., Husen, S., & Flueh, E. R. (2001). Morphotectonics and mechanics of the central Makran accretionary wedge off Pakistan. *Marine Geology*, *173*(1), 1-19.

Lee, G. H., Kim, H. J., Han, S. J., & Kim, D. C. (2001). Seismic stratigraphy of the deep Ulleung Basin in the East Sea (Japan Sea) back-arc basin. *Marine and Petroleum Geology*, *18*(5), 615-634.

Lee, G. H., Yoon, Y., Nam, B. H., Lim, H., Kim, Y. S., Kim, H. J., & Lee, K. (2011). Structural evolution of the southwestern margin of the Ulleung Basin, East Sea (Japan Sea) and tectonic implications.*Tectonophysics*, *502*(3), 293-307.

Masini, M., Bulnes, M., & Poblet, J. (2010). Structural analysis and deformation architecture of a fault-propagation fold in the southern Cantabrian Mountains, NW Iberian Peninsula. *Trabajos de geología*, *30*, 55-62.

Maruyama, S., Isozaki, Y., Kimura, G., & Terabayashi, M. (1997). Paleogeographic maps of the Japanese Islands: Plate tectonic synthesis from 750 Ma to the present. *Island Arc*, *6*(1), 121-142.

Mikada, H., K. Becker, J.C. Moore, A. Klaus, and Et Al. (2002). Site 808. *Proceedings of the Ocean Drilling Program, Initial Reports* 196, 15-16.

Miller, M. S., Kennett, B. L. N., & Lister, G. S. (2004). Imaging changes in morphology, geometry, and physical properties of the subducting Pacific plate along the Izu–Bonin–Mariana arc. *Earth and Planetary Science Letters*, *224*(3), 363-370.

Moore, J. C. (1989). Tectonics and hydrogeology of accretionary prisms: Role of the decollement zone. *Journal of Structural Geology*,*11*(1), 95-106.

Moore, G. F, & Klaus, A. (2001). Site 1174. *In Proceedings of the Ocean Drilling Program, Initial Reports, 190,* 1-149.

Morgan, J. K., & Karig, D. E. (1995). Décollement processes at the Nankai accretionary margin, southeast Japan: Propagation, deformation, and dewatering. *Journal of Geophysical Research: Solid Earth (1978–2012)*, *100*(B8), 15221-15231.

Morley, C. K. (1988). Out-of-sequence thrusts. *Tectonics*, *7*(3), 539-561.

Nanayama, F., Satake, K., Furukawa, R., Shimokawa, K., Atwater, B. F., Shigeno, K., & Yamaki, S. (2003). Unusually large earthquakes inferred from tsunami deposits along the Kuril trench. *Nature*, *424*(6949), 660-663.

Needham, D. T., & Mackenzie, J. S. (1988). Structural evolution of the Shimanto Belt accretionary complex in the area of the Gokase River, Kyushu, SW Japan. *Journal of the Geological Society*, *145*(1), 85-94.

Niitsuma, N. (1988). Neogene tectonic evolution of southwest Japan. *Modern Geology*, *12*(1-4), 497-532.

Niitsuma, N. (1989). Collision tectonics in the Fossa Magma, Central Japan. *Modern Geology 14*, 3-18.

Niitsuma, N. (1996). The Trench-Trench-Trench type triple Junction and Tectonic Evolution of Japan. *Geoscience Report of Shizuoka University*, *23*, 1–8.

Niitsuma, N. (2004). Japan Trench and tectonics of the Japanese Island Arcs. *The Island Arc*, *13*, 306–317.

Ohmori, K., Taira, A., Tokuyama, H., Sakaguchi, A., Okamura, M., & Aihara, A. (1997). Paleothermal structure of the Shimanto accretionary prism, Shikoku, Japan: Role of an out-of-sequence thrust. *Geology*,*25*(4), 327-330.

Okino, K., Shimakawa, Y., & Nagaoka, S. (1994). Evolution of the Shikoku basin. *Journal of Geomagnetism and Geoelectricity*, *46*(6), 463-479.

Park, J. O., Tsuru, T., Kaneda, Y., Kono, Y., Kodaira, S., Takahashi, N., & Kinoshita, H. (1999). A subducting seamount beneath the Nankai accretionary prism off Shikoku, southwestern Japan. *Geophysical Research Letters*, *26*(7), 931-934.

Party, S. S. (1975). Site 297. *Initial Reports of the Deep Sea Drilling Project*, *31*, 275-316.

Party, S. S. (1991). Site 808. In *Proceeding Ocean Drilling Program Initial Report* (Vol. 131, pp. 71-269)

Pedley, K. L., Barnes, P. M., Pettinga, J. R., & Lewis, K. B. (2010). Sea floor structural geomorphic evolution of the accretionary frontal wedge in response to seamount subduction , Poverty Indentation , New Zealand. *Marine Geology*, *270*, 119–138. doi:10.1016/j.margeo.2009.11.006

Poblet, J. and Bulnes, M., (2007). Predicting strain using forward modeling of restorred cross-sections: Application to rollover anticlines over listric normal fault. *Journal of Structural Geology* v.29 p. 1960-1970.

Ramsay J. G. (1967). Folding and Fracturing of Rock. *McGraw-Hill*, New York.

Sacks, I.S., Suyehiro, K., Acton, G.D., et al. (2000). Leg 186 summary. *Proceedings of the Ocean Drilling Program, Initial Reports Volume 186*, 1-37

Savage, H. M., & Cooke, M. L. (2003). Can flat-ramp-flat fault geometry be inferred from fold shape?: A comparison of kinematic and mechanical folds. *Journal of Structural Geology*, *25*(12), 2023-2034.

Seno, T., Stein, S., & Gripp, A. E. (1993). A model for the motion of the Philippine Sea Plate consistent with NUVEL-1 and geological data. *Journal of Geophysical Research: Solid Earth (1978–2012)*, *98*(B10), 17941-17948.

Skarbek, R. M., & Saffer, D. M. (2009). Pore pressure development beneath the décollement at the Nankai subduction zone: Implications for plate boundary fault strength and sediment dewatering. *Journal of Geophysical Research: Solid Earth (1978–2012)*, *114*(B7), 1-20. doi: 10.1029/2008JB006205

Soh, W., Taira, A., & Tokuyama, H. (1988). A trench fan in the Izu-Ogasawara Trench on the Boso Trench triple junction, Japan. *Marine geology*, *82*(3), 235-249.

Suppe, J. (1983). Geometry and kinematics of fault-bend folding. *American Journal of science*, *283*(7), 684-721.

Taira, A. (1988). The Shimanto belt in Shikoku, Japan-evolution of Cretaceous to Miocene accretionary prism. *Modern Geology*, *12*, 25-46

Taira, A., & Ashi, J. (1993). Sedimentary facies evolution of the Nankai forearc and its implications for the growth of the Shimanto accretionary prism. In Hill, IA, Taira. A., Firth, JV, et al., *Proceedings of the Ocean Drilling Program, Scientific Results 131*, 331-341.

Tamaki, K. (1992). Tectonic synthesis and implications of Japan Sea ODP drilling. In *Proceeding. Ocean Drilling Program, Scientific Results. 127*, 1333-1348. College Station.

Tanner, D. C.; Behrmann, J. H.; and Dresmann H., (2003). Three-dimensional retrodeformation of the central nappe, Northern Calcaneous Alps. *Journal of Structural Geology. 25*, 737-748

Taylor, B. (1992). Rifting and the volcanic-tectonic evolution of the Izu-Bonin-Mariana arc. In *Proceeding Ocean Drilling Program Scientific Results*. *126*, 627-651.

Tavani, S., Storti, F., & Salvini, F. (2006). Double-edge fault-propagation folding: geometry and kinematics. *Journal of Structural Geology*, *28*(1), 19-35.

Tsuji, T., Tokuyama, H., Pisani, P. C., & Moore, G. (2008). Effective stress and pore pressure in the Nankai accretionary prism off the Muroto Peninsula, southwestern Japan. *Journal of Geophysical Research*, *113*, 1-19. doi: 10.1029/2007JB005002

Twiss R.J. & Moores, E.M. (2007). Structural Geology, 736 pp. New York: WH Freeman.

Underwood, M. B., Orr, R., Pickering, K. T., & Taira, A. (1993). Provenance and dispersal patterns of sediments in the turbidite wedge of Nankai Trough. *In Proceedings of the Ocean Drilling Program Leg 131*. *131*, 15-34.

Utsunomiya, A., Jahn, B. M., Okamoto, K., Ota, T., & Shinjoe, H. (2011). Intra-oceanic island arc origin for Iratsu eclogites of the Sanbagawa belt, central Shikoku, southwest Japan. *Chemical Geology*, *280*(1), 97-114.

Wang, K., & Hu, Y. (2006). Accretionary prisms in subduction earthquake cycles: The theory of dynamic Coulomb wedge. *Journal of Geophysical Research: Solid Earth (1978–2012)*, *111*(B6).

Wibberley, C., Shimamoto, T., (2003). Internal structure and permeability of major strike-slip fault zones: the Median Tectonic Line in Mie Prefecture, Southwest Japan. *Journal of Structural Geology 25*(1), 59–78.

Withjack, M. O., & Peterson, E. T. (1993). Prediction of normal-fault geometries--a sensitivity analysis. *Association of American Petroleum Geologists Bulletin*, *77*(11), 1860-1873.

Yamamoto, S., Nakajima, J., Hasegawa, A., & Maruyama, S. (2009). Izu-Bonin arc subduction under the Honshu island, Japan: Evidence from geological and seismological aspect. *Gondwana Research*, *16*(3), 572-580.